universiteit hasselt
KNOWLEDGE IN ACTION

2015 | Faculty of Engineering Technology

DOCTORAL DISSERTATION

Impedance based biosensor platform design and applications

Doctoral dissertation submitted to obtain the degree of
Doctor of Engineering Technology, to be defended by

Stijn Duchateau

Promoter: Prof. Dr Ward De Ceuninck | UHasselt
Co-promoters: Prof. Dr Ronald Thoelen | UHasselt
Prof. Dr Patrick Wagner | UHasselt

D/2015/2451/6

universiteit hasselt | imec
IMO - IMOMEC
INSTITUUT VOOR MATERIAALONDERZOEK

Table of contents

Acknowledgements

“We must find time to stop and thank the people who make a difference in our lives.”

John F. Kennedy

First I would like to express my gratitude towards Prof. Dr. Ward De Ceuninck. Ward, thanks for giving me the opportunity and much needed guidance during these last six years. This project has thought me that all basic research starts with an idea which, if sufficiently nurtured and monitored, can evolve to interesting new developments and technological advances.

Prof. Dr. Ronald Thoelen, we started our ‘XIOS’ career together. I vividly remember the first year at the institute in which you helped me to set the first steps in the world of research. The lively Friday night ‘Chouffe’ moments, the Christmas parties and other numerous ‘networking’ events made you a close friend and mentor.

Prof. Dr. Patrick Wagner, thanks for your time, fruitful discussions and help with abstracts and papers. Your funny ideas and thoughts helped me to persevere and overcome the most critical reviewer comments.

Mom, dad, I don't know how to express my gratitude, you guys always believed in me, supported me, and helped me to realize my crazy projects. Thanks for always being there and helping me become the person I am today.

Wouter, my partner in crime, over the years we had many fun moments together. The festivals, trips and other unforgettable moments made you above all a friend. Thanks little brother.

Tiene, thanks for the support and patience’s during these last few months. I know, sometimes, I was a bit distracted and preoccupied, with writing this dissertation, but your love and support helped me through the hard moments and helped me see it through.

My karate family, Aimé you thought me to persevere, endure and to make the best of myself. Frank, for helping me train and run our club. My students for their effortless training discipline.

Jeroen and Diether, thanks for the interesting discussions about failed measurements, theories and life. Marloes your help correcting this dissertation is greatly appreciated.

Thijs, we started this journey eleven years ago as bachelor students. The projects, the discussions about electronics, our Erasmus getaway to Vigo made you one of my closest and most valued friends.

I would like to thank everybody from the EMAP and BIOS group for their technical and biological support, interesting lunch breaks, parties and other special moments that made every day at the office an enjoyment. Jan, Jhonny and Lieven for their help, expertise and technical support.

The boardgamers and my friends for the entertaining afternoons, trips and support. Your friendship gave me the much needed distraction, loads of joy and happiness in my life.

My family for a life time of support and happy moments.

Last I would like to thank my grandparents, for their love, support and life lessons. The dinners on Sunday, card sessions and other memorable moments thought me the most important things in life.

Abstract

Early disease detection could help to adjust patient treatment to their specific needs. For example, one hour prior to a heart attack the body releases an elevated level of the protein CRP. If a special sensor, sensitive to this protein, is incorporated in a wearable device, such as a wrist watch, the attack could be detected and the patient could go to the hospital and receive the appropriate treatment.

Biosensors are analytical devices, which can specifically respond to an analyte, interpret the concentration and transform it to a measurable electrical signal. Currently, a lot of research is focused on tailoring the recognition layers for specific enzymes, cells, DNA or antibodies. Recent work in this field has led to synthetic sensors able to mimic a biological detection. These molecular imprinted polymers (MIP) offer significant advantages over biological layers, including robustness and long shelf life, making them ideal for integration with commercial devices.

However, the readout of these biomimetic layers still needs some research. One of the methods suited for this readout is Electrochemical impedance spectroscopy. This powerful, non-invasive measurement technique is a well-established method in the field of biological research. Although impedance analyzers are readily available, a combination of high cost, large form factor and lack of a user-friendly operating method makes them unsuited for home use or smart device integration. This work focusses on the portability of electrochemical impedance readout devices through miniaturization, multiplexing of multiple channels and advanced signal processing.

First chapter discusses the typical layout, the working principles of a biosensor and its fields of application. The **second** chapter elaborates on different design principles, measurement setups and methods for electrochemical impedance spectroscopy as well as giving some basic measurement considerations.

The **third** chapter focuses on the developed devices. First the adaptions made to a commercially available impedance chip are discussed. The experiences and problems encountered, during a systems performance test, are then used to design the BioZ°. This eight-channel device is custom made to operate on biological relevant frequencies while still having a large impedance measurement range. Subsequently this system is expanded with a multiplexer making it possible to measure up to ninety six channels quasi-simultaneously. To further

increase the measurement speed two different arbitrary wave forms, based on the NI USB-6251 DAQ platform are presented. The first waveform is composed from a number of identical sine waves while the second method adapts the waveform to have a constant signal to noise ratio. Lastly a fourth design focused on mobility is presented. For this purpose the commercially available Arduino DUE board is adapted to perform standalone impedance measurements while storing the data to an SD-card.

The fourth chapter validates these setups in three different biological applications. First the adapted 5933 board is tested in a wet cell DNA hybridization and denaturation setup. Next the BioZ° is used to detect the molecules histamine and nicotine on a molecular imprinted polymer. After extension with the impediplexer the BioZ° is tested in a proliferation setup. In order to find the optimal starting concentrations for drug testing, three different cell lines (CHO,BV2, HEK) are seeded, in different concentrations on a nineteen six well plate with gold electrodes at the bottom. Subsequently the effects of different stimulators and growth inhibitors is tested on these different cell lines. Next the arbitrary wave setup is tested on a wet cell and a MIP layer sensitive to the Ara h 1 molecule. Lastly the Arduino DUE is used to monitor the wet cell over time.

The impedance methods presented in this work could ultimately lead to the development of smart devices able to interact with biological sensors sensitive to diverse disease pathogens.

Nederlandse samenvatting

Als ziektes gedetecteerd konden worden bij het uitbreken van de eerste symptomen, dan zou een specifiekere behandeling mogelijk worden. Bijvoorbeeld, één uur voor het krijgen van een hartaanval geeft het lichaam een verhoogde concentratie van het molecule CRP vrij. Als een sensor, gevoelig voor dit proteïne, wordt toegevoegd aan een draagbaar toestel, zoals een polshorloge, dan zou de patiënt gewaarschuwd kunnen worden waardoor hij tijdig naar het ziekenhuis kan gaan en de nodige zorg ontvangen.

Biosensoren zijn toestellen die specifiek reageren op een bepaald analyt, de aanwezige concentratie interpreteren en dit vertalen naar een meetbaar elektrisch signaal. Momenteel is er veel onderzoek gewijd aan het ontwikkelen van nieuwe herkeningslagen gevoelig aan enzymen, cellen, DNA en antilichamen. Dit onderzoek leidde recent nog tot de ontwikkeling van een synthetische sensor die, na bestempeling, een biologisch detectie kan reproduceren. Deze sensorlagen hebben enkele belangrijke voordelen ten opzichte van de klassieke biologische laag. Ze zijn robuust en hebben een lange houdbaarheidsdatum hierdoor zijn ze dan ook perfect geschikt voor integratie in commercieel bruikbare toestellen.

De uitlezing van deze lagen is echter nog niet optimaal en vergt nog verder onderzoek. Een mogelijke manier, om deze lagen uit te lezen, is elektrochemische impedantie spectroscopie. Deze krachtige, niet invasieve meettechniek is alom aanvaard binnen het biologisch onderzoek en leent zich perfect voor de integratie in slimme toestellen. Op de huidige markt zijn er al tal van impedantie analyzers te verkrijgen helaas zijn deze vooral bedoeld voor labo metingen. Ze hebben dan ook vaak grote afmetingen, een beperkte user interface en een hoog kostenplaatje. Deze scriptie beschrijft de ontwikkeling van vier verschillende impedantie analyzers, bruikbaar voor miniaturisatie, een zesennegentig kanaalsmultiplexer en twee verschillende uitleesmethoden.

Het eerste hoofdstuk geeft een introductie over de werkingsprincipes, de verschillende herkeningslagen, uitleesmethoden en commercieel verkrijgbare toestellen. Het tweede hoofdstuk beschrijft de verschillende meet- opstellingen en methoden voor elektrochemische impedantie spectroscopie en geeft enkele belangrijke meet tips.

Het derde hoofdstuk focust op de ontwikkelde toestellen. Eerst worden de aanpassingen aan een commercieel verkrijgbare impedantiechip besproken. De

ervaringen en problemen met deze chip zijn gebruikt voor de ontwikkeling van de BioZ°. Dit acht kanaalsmeettoestel is zo ontwikkeld om de hoogste gevoeligheid te hebben op biologisch relevante frequenties. Voorts werd dit systeem uitgebreid met een zesennegentig kanaalsmultiplexer voor de quasi-simultane uitlezing van een well plaat. Vervolgens worden er twee 'arbitrary wave' meetmethoden, gebaseerd op de NI USB-6251 DAQ kaart, besproken. De eerste golfvorm is een samenstelling van verschillende identieke sinussen, de tweede methode voert eerst een kalibratie uit en past vervolgens het signaal aan om een constante signaalruis verhouding te hebben. Het laatste design is gefocust op mobiliteit, hiervoor is het commercieel verkrijgbare Arduino DUE board zo aangepast om standalone metingen uit te voeren en op te slaan op een SD-kaart.

Het vierde hoofdstuk bespreekt de validatie van de meetopstellingen tijdens drie verschillende biologische applicaties. Eerst wordt het aangepaste AD5933 bord, op een natte cel bruikbaar voor de hybridisatie en denaturatie van DNA, getest. Vervolgens wordt het gebruik van de BioZ° voor de detectie van histamine en nicotine op een moleculair bedrukt polymeer besproken. Door dit systeem verder uit te breiden met een multiplexer kon de BioZ° ook ingezet worden in een proliferatie experiment. Eerst werden de optimale startcondities voor een drug test bepaald. Hiervoor werden verschillende concentraties BV2, CHO en HEK cellen in een wellplaat gegroeid. Deze concentraties werden daarna gebruikt om de effecten te bepalen van verschillende groei inhibitoren en promotoren. Vervolgens werd de arbitrary wave methode, op een natte cel en een MIP laag, gevoelig voor het Ara h 1 molecule, getest. In het laatste experiment werd de arduino DUE gebruikt uitlezen van een natte cel.

De impedantie methoden voorgesteld in dit werk kunnen leiden tot de ontwikkeling van slimme toestellen die in staat zijn om op basis van een biologische detectie verscheidene ziekte symptomen te herkennen.

Chapter 1

Introduction to biosensors

Early detection and prevention of diseases is the aim of many scientific studies [4-8]. The increased knowledge about pathogens makes it possible to develop specific biomarkers which can react to elevated concentrations of specific molecules or mutations in the human body [9]. These advances, in combination with the growing market for wearables such as smart- watches, glasses, scales, activity trackers, etc. [10-12] leave scientists to dream of a real-time home monitoring systems. Such a system might, in future applications, even be able to detect biomarkers such as such as the protein C-reactive protein (CRP). The concentration of this molecule, can indicate inflammation of internal organs or even signal cardiovascular problems in advance issues [13]. If for example a smart-watch, able to communicate and interpret data from a sensor specific to this biomarker, would be developed, many cardiac attacks could be prevented. Such systems should have a fast reaction time, be highly sensitive and specific to CRP and have a long of shelf life, to be truly usable in common day use. A first step towards these applications is the development of standalone easy to operate measurement devices.

Unknowingly, people have been using animals as biosensors for over decades. For examples rats, dogs and even dolphins have been trained successfully to detect explosives. They specifically react to the specific sent of an agent warning the environment of a potential thread. One could say that the animal does as a biological recognition and transduces it to a understandable signal. The readout mechanism would be the guards response. Apopo [14, 15] is one of these organizations that have been training rats to detect landmines. The great advantages of using these animals to detect explosive compounds is their fast breeding time, their specificity, and that they are reusable after a positive detection. However, there are a few disadvantages; their sensing capabilities are not constant and training is time consuming. Recently [16-18], a lot of scientific effort has been put in the development of sensors for volatile components to

supplement and eventually replace these animals. Key characteristics of such devices are high specificity, reusability, long operating time, portability and low cost.

This trend can also be found in general sensor design. Size and cost get reduced while the dynamic detection range, specificity and speed rise. This is especially true for bio-sensing systems. Some commercially available biosensor-based devices are the glucose sensors, heart rate monitors, blood pressure meters, thermometers and off course the well-known pregnancy test [19-24]. This chapter focuses on bio-sensing systems, their components, most used techniques, their advantages, disadvantages and explains the aim of the study.

1.1 Biosensors

The birth of modern biosensors started in 1916 when a first paper about the immobilization of proteins was published. Forty years later Clark, also known as the father of biosensors, made a huge discovery. He developed an oxygen electrode which was modified with enzymes. In 1962 he described a method to make electrochemical sensors intelligent by simply adding enzyme transducers as membrane enclosed sandwiches. To demonstrate his finding, he made the first amperometric glycose oxidase electrode [37] that could detect the amount of oxygen present in a liquid. The output of this system was directly proportional to the glucose concentration. Later on, Updike and Hicks described a technique to make the first working glucose sensor [38]. During the seventies, a company called ‘Yellow spring instruments’ developed the first commercial glucose sensor [39]. Over the years, these devices further enhanced their specificity and resolution with some notable advances including the use thermal and optic sensing techniques. Today, these glucose sensors have evolved to compact, user friendly devices. many other sensing techniques, based on these general principles have since been developed. The most famous one being based on antibody-antigen binding [40] developed in the 1980’s.

A biosensor is composed of 4 unique building blocks: a sensing element, a transducer, a signal processor and an output are the basic building blocks for every sensor system (**Figure 1-1**). The sensing element is capable of converting a physical event in a detectable signal. Before processing, this signal needs to be converted to the systems input range. This happens at the transducer layer. The processing element analyses the data and creates a response which can be visualized at the output of the system.

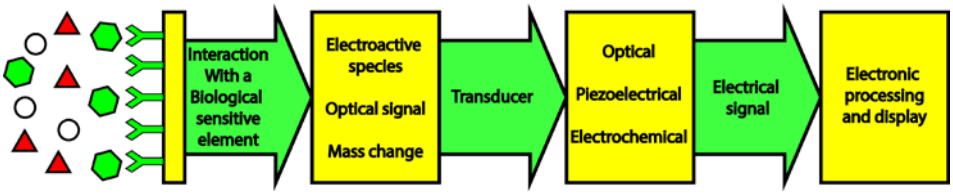

Figure 1-1 Basic biosensor layout [25]

Biosensor systems follow this general system approach. In the ideal case the sensing element will respond to a specific analyte. DNA fragments, cells, enzymes, membrane receptors or antibodies can all be immobilized [26-36] on the sensor surface for these purposes. The reaction to the analyte can be a chemical change, small current, heat release or other response. The transducer converts, filters and, in some cases, amplifies the signal so it can be processed in the signal processing unit. In this unit the signal will be converted to an understandable output.

The birth of modern biosensors started in 1916 when a first paper about the immobilization of proteins was published. Forty years later Clark, also known as the father of biosensors, made a huge discovery. He developed an oxygen electrode which was modified with enzymes. In 1962 he described a method to make electrochemical sensors intelligent by simply adding enzyme transducers as membrane enclosed sandwiches. To demonstrate his finding, he made the first amperometric glycose oxidase electrode [37] that could detect the amount of oxygen present in a liquid. The output of this system was directly proportional to the glucose concentration. Later on, Updike and Hicks described a technique to make the first working glucose sensor [38]. During the seventies, a company called 'Yellow spring instruments' developed the first commercial glucose sensor[39]. Over the years, these devices further enhanced their specificity and resolution with some notable advances including the use thermal and optic sensing techniques. Today, these glucose sensors have evolved to compact, user friendly devices. many other sensing techniques, based on these general principles have since been developed. The most famous one being based on antibody-antigen binding [40] developed in the 1980's.

1.2 Sensing elements

A sensitive and specific detection of the analyte always starts at the sensing element. There are recognition elements, each with a specific advantage to detect certain analyte changes. As previously stated, the **first** commercial biosensors were based on an enzymatic interaction. These enzyme electrode sensors use enzymes as biological recognition elements. They tend to be more specific and offer a faster response due to shorter diffusion paths than cell based sensors. However, their production cost is higher due to problems with isolating the enzyme. After this isolation they can become unstable and the addition of a cofactor is often needed for the detection of substances [41].

The **second group** of sensors are the immunosensors. These sensors use antibodies (Abs) as sensing element. The most famous example of such a sensor is the ELISA (Enzyme-Linked Immunosorbent Assay) test where the interaction of the Abs, and a reagent cause a color change upon substance detection.

A **third** important group of biosensors are the DNA sensors. Their 2 stranded DNA polymer chain has relatively weak hydrogen bindings, which can be broken and restored. The detection principle is based on the difference in time, temperature or impedance response between the hybridization or denaturation of target and control samples.

A **fourth** group are the microbial sensors, these can be used to test microbial cells, plant and animal tissues. Here a micro-organism, which has the ability to interact with the target is bound to the sensor surface. The advantage of such sensors, in comparison to enzymatic sensors are the many enzymes and co-factors that co-exist in the cells which give them the natural ability to consume and hence detect a large number of chemicals.

All these sensors however share some common problems. The biological layers, used for detection have a rather limited shelf life. Production cost can be high and living samples are often needed for the acquisition of the biological molecules. They can degrade after exposure to various measurement conditions, such as temperature or analyte changes. Fortunately the advances in polymer chemistry have provided an outcome for this problem. Molecular imprinted polymers (MIPs) can be tailored to mimic molecular recognition occurring in natural receptors. They are stable in many environments, relatively low-cost and have a long shelf life. Other promising detection elements such as aptamers, nanobodies and CNT can further increase the sensitivity and usability of biosensors.

Table 1-1 Comparison of the different sensing elements [42]

	Analyte	Imuno	DNA	Microbial	Biomimetic
Test	Glucose sensor	ELISA	Genome micro arrays	Sterility test	MIP
Price	$15	$350	$395	$200	Few dollar
Detection Time	Seconds	Days	Days	7-14 days	Seconds

1.3 Transducers and electronic readout

The second element of a biosensor system is the transducer. This component enables the translation of the binding event in the recognition layer. This translation can be done in a number of ways:

Calorimetric sensors detect temperature changes caused by chemical binding events. The accuracy of such sensors relies on the heat generated by such a binding event and the sensitivity of the temperature sensor. The most commonly used thermal biosensors are based on enzymatic receptors, e.g. glucose and esterase [43, 44], though research is conducted towards thermal MIP-based sensors [45]. The temperature sensor can use either thermistors, which rely on resistive changes for e.g. Pt100 sensors. Thermocouples who take advantage of the Seebeck effect or resistance temperature detector where a high-purity conducting metal is wound into a coil and whose resistance changes in function of temperature.

Optical techniques such as Raman spectroscopy, SPR, SAR, optical waveguide light mode spectroscopy, use either absorption, transmission or reflection for target detection [46]. Absorbance spectroscopy measures the amount of light absorbed by a sample at a given wavelength and is one of the most versatile and widely used techniques in chemistry and life sciences. Transmission spectroscopy is highly interrelated to absorbance spectroscopy. This technique can be used for solid, liquid and gas sampling. Here, instead of measuring the amount of light absorbed by the sample, the light transmitted by the sample is compared to the radiated light from the UV-light source. The resulting spectrum

depends on the path-length or sample thickness the setup is similar to the one used for absorption. Reflectance spectroscopy is the study of light as a function of wavelength that has been reflected or scattered from a solid, liquid or gas. As photons enter a sample, some are reflected, some will pass through and some will be absorbed. The detector measures the amount of reflected and scattered photons to determine target detection.

Mass sensitive sensors use piezoelectric crystals such as quartz. When mechanical stressed these crystals produce a small electrical signal. If instead an electrical signal would be applied the crystal will start to vibrate at it is natural frequency. If the mass of the sensor would change, for e.g. a binding event on the crystals surface, a frequency shift would, according to the Sauerbrey equation [47], occur. This very sensitive technique is label free and can be readout electrically.

The last group, **electrochemical transducers** covers a number of different readout techniques. Potentiometric sensors measure the potential difference between a working and reference electrode. The measured potential is directly dependent on the solution's analyte concentration. The most known example of this technique is the glucose sensor, where a simple voltmeter is used to measure the release of ions caused by the interaction of analyte, enzymes and the working electrode. Voltametric sensors on the other hand apply a time-dependent potential to a electrochemical cell. The current flowing through the cell is measured as a function of the applied potential. Amperometric biosensors produce a current after a constant voltage is applied. Their response time, dynamic range and sensitivity is similar to the potentiometric sensors. The most known amperiometric sensor is the Clark oxygen electrode. Electrochemical impedance spectroscopy (EIS) monitors impedances changes at different discrete frequencies. This readout technique can be used to retrieve physical information about the sample under test and can be fine-tuned for use in many biosensor applications. This technique is the cornerstone of the presented research and will be explained more in depth in the following chapter.

1.4 Biosensors on the consumer market

Although many devices based on the discussed principles have been developed, only a few are commercially available. Their size, price and need for specialized operating personal make them, in most cases not suited for home use.

In the 1970's, Ames developed a Reflectance Meter which used Dextrostix test strips to check the glucose level of patients. These strips changed their color proportional to the sugar level in the blood sample. The meter performed an optical readout excluding external factors such as the light source or user

interpretation which was a huge improvement for diabetics. With the advances in enzyme-based sensors these first sensors where replaced with more sophisticated devices using a amperometric readout. These developments ultimately led to the first miniature glucose monitor devices which were battery powered and had a LCD display like the devices shown in **Figure 1-2**.

Figure 1-2 Miniature glucose sensors [48]

At present time more and more people are aware of their physical wellbeing. The quest of having a fit and healthy body made room for a whole new market of e-health devices. The introduction of wearable technology which was easy to operate and had relevant body information added to the introduction on the consumer market. Today it is possible to interconnect a scale that not only gives information about the body weight, but also uses impedance spectroscopy to sense the body composition with a heart-rate sensor or with an activity sensor and use a dedicated software program to analyze your personal progress [3, 49] (**Figure 1-3**). It is even possible to share this information on social media which makes these wearables even more of an accessory.

Figure 1-3 Wearables available on the consumer market [1-3]

Even though these wearables are a good step towards complete at home health monitoring systems, there is still a big gap between these gadgets, intended for fitness monitoring and a system able to sense biological relevant events. At current state the devices intended for these applications are still complex, have a large form factor and are high cost. Impedance spectroscopy is one of the techniques which offers a lot of promise to make compact user friendly devices. It combines the advantages of electrochemical readout with the possibility to analyze the properties of a complete bio-measurement cell. However, the devices found at today's market [50-52] are bulky, often need multiplexers and signal attenuators, to perform non-invasive biological measurements. Recent advances in impedimetric readout techniques include the development of miniature, multichannel devices to enhance the field applicability of biosensors. Most of these systems are targeted for a specific type of biosensor or a specific application. Examples include an analyzer fine-tuned for quartz crystal resonating sensors [53] and device based on the Analog Devices AD5933 chip, specifically targeted towards applications in functional textiles [54].

1.5 The aim of this study

Biosensor research is still an emerging field of research. When looking at the scientific output related to biosensors, as illustrated in **Figure 1-4** in red, one can see a steady increase in the number of publications (source: Science Direct, search term: biosensor). Although most research currently conducted is focused on the development of new sensor layers and detection mechanisms, the valorization of impedance based biosensor devices is gaining more and more interest as can be seen in the blue bars in **Figure 1-4** (source: Science Direct, search term: (point-of-care OR embedded OR consumer) AND biosensor AND impedance). The healthcare sector on the other hand, is continuously searching for new ways to detect disease symptoms early on, to optimize patient treatment. If more easy to operate readout devices would become available to the general practitioner, or in the ideal case incorporated in smart devices, diseases could be detected as the first symptoms start to show.

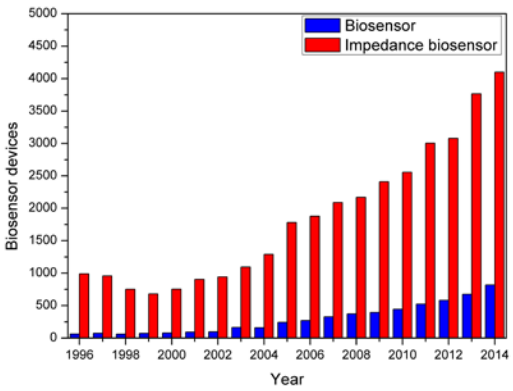

Figure 1-4 Number of biosensor and impedance based biosensor devices publications per year

In previous work conducted by the BIOSensor group of IMO, the proof of concept for biosenors, sensitive to DNA attachment on CVD diamond and MIPs for the detection of L-nictone, using impedance spectroscopy was established [55-58]. The aim of this work is to further optimize the impedance readout method for the development of universal biosensor readout equipment. This equipment should also be able to measure multiple samples at the same time without influencing the working principle of the biosensors. Settings such as the applied potential, measurement time, the frequency and impedance range should be investigated to have the highest relevant resolution, in the sensor's detection range, while still respecting the standards applicable for biological measurements.

This work presents the optimization of four different impedance measurement setups, their readout and connection methods. These designs are intended for point-of-care applications with a minimal amount of external equipment, small form factor and at a reasonable cost. The **first design** is focused on expanding the AD5933 development platforms measurement and frequency range. The problems encountered during the design were used to develop a multichannel, miniature, USB-controlled biosensor readout device, the BioZ°. To expand the number of measurement channels a multiplex circuit was developed to interface with a commercial 96 well plate. The readout of such a plate took about twelve minutes which is fast enough for cell proliferation measurements but to slow for fast changing systems. A new readout method using an arbitrary wave was proposed to reduce this measurement time. The **fourth** setup focuses on mobility, for this purpose an µ-controller circuit was adapted to do standalone impedances measurements. Aside from explaining the critical designs steps taken in device development, performance and applicability are evaluated. To do so, biosensors measurements were performed in specialized measurement setups such as a wet cell, a NIP/MIP sample and a proliferation setup. Furthermore, the software to control the devices and analyze the measurements is thoroughly explained and a future outlook and conclusion is given.

Chapter 2

EIS Basics and measurement principles

In the 1800's, Georg Ohm conducted the first impedance measurement. He used a load and a voltaic cell to determine the impedance of a circuit. This experiment ultimately led to the formulation of Ohm's law. While originally only resistors were considered, Faraday and Henry showed that other inventions such as the capacitor and coil have an effect on the current when a potential is applied. However, it was not until Maxwell invented the ballistic bridge that the effects of these components on an alternating current became clear.

The first commercial instruments using these principles where build by companies such as Elliot Bros. and Cambridge Instruments. These first devices used a wheatstone bridge, which had to be balanced with a box of known resistance standards. In 1915 General radio Co., brought the first ac boxes to the market. These devices are based on the same resistor setup as the first devices but had an input connection to connect an external standard of resistance, capacitance or inductance. After World War II, the electronics industry boomed and the first complete impedance measurement devices came to the market. These devices still need a lot of user interaction and their use is limited both in frequency range as in impedance range.

Today there are many measurement devices on the market, each with a specific scope. Industrial applications include, among others corrosion detection, coating evaluation and component analysis [59-64]. These devices often have a large form factor, need specialized operating personnel and are high-cost. The most known impedance analyzer for home use are the body analyzers, these are user friendly, relatively low cost, but lack the resolution and accuracy of the devices intended for laboratory use. A fine example of a device intended for clinical use that also penetrated the consumer market is the heart rate monitor. This device,

which performs impedance cardiography (ICG), gives information about the dynamics of blood flow in clinical applications while giving useful information about the heart rate to athletes.

These examples show the importance of impedance as a measurement technique. This chapter elaborates on the basic principles and common pitfalls specific to impedance spectroscopy. First, an overview is given of the EIS basics, modeling and components. Secondly, signal considerations, different measurement setups and measurement methods are discussed. The last sections give some suggestions and tips about the connection methods and error prevention.

2.1 Impedance spectroscopy

As mentioned above, Ohm's experiments show that if a direct current voltage (D.C.) is connected to a conductor and a conductive path to ground is available, a current will start to flow. While this is a well-known relationship, its use is limited to only one circuit element, the ideal resistor. An ideal resistor has several simplifying properties:

- Its resistance is frequency independent
- Ohm's Law is always applicable
- There is no AC phase shift between the voltage and current

However, the real world contains circuit elements that exhibit much more complex behavior. To characterize these elements a more general circuit parameter, impedance, is applied. Like resistance, impedance is a measure of the ability of a circuit to resist the flow of electrical current, but unlike resistance, it is not limited by the simplifying properties listed above.

EIS is usually measured by applying an electrochemical cell and measuring the current response through the cell. For an sinusoidal excitation voltage the response would be an AC current signal. This signal can be analyzed as a sum of sinusoidal functions (a Fourier series).

In a linear or pseudo-linear complex system, the current response to a sinusoidal voltage will be a sinusoid at the same frequency but shifted in phase (**Figure 2-1**). This means that, for most experiments, only a small excitation signal can be used since most cells have a pseudo linear behavior. Linearity is described in more detail in the following section.

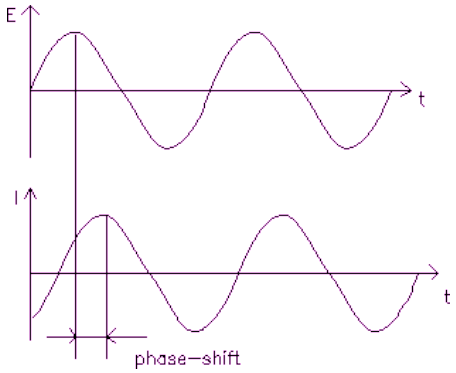

Figure 2-1 Voltage and current sinewave

During frequency sweeps, from a few Hz up to a few MHz, both magnitude (|Z|, [Ω]) and phase (φ, [°]) change with frequency due to the lagging effect of voltage and current to capacitors and inductors. Kennely described this interaction in 1893 [65] for the polar notation of Z in following formula (2-1.

$$\boldsymbol{Z = |Z| \angle\theta = |Z|e^{j\theta}} \qquad \textit{(2-1)}$$

It is also possible to represent the impedance as its real and imaginary component. The relation between the two forms is shown in **Figure 2-2** where Z is a vector under angle φ in respect to the real (Re) an imaginary (Im) axis. The standard rules for complex numbers as seen in **formula (2-2) and (2-3)** apply for the conversion between the polar and Cartesian notation.

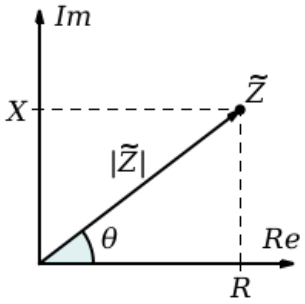

Figure 2-2 Complex impedance plane

$$Re = |Z| \cos\theta \text{ and } X = |Z| \sin\theta \quad (2\text{-}2)$$

$$|Z| = \sqrt{Re^2 x^2} \text{ and } \theta = tan^{-1}\frac{X}{R} \quad (2\text{-}3)$$

The most common representation of impedance is the Bode-diagram. Here the magnitude of the impedance is logarithmically plotted against the log-frequency. The phase is linearly plotted with a log-frequency axis. This bode plot is also useful for getting an indication of the equivalent electrical circuit of the sample under test.

2.2 Impedance modeling

This approach could give extra information about the composition, possible defects or abnormalities of the sample. To calculate this equivalent circuit, it is essential to know the effects of basic electrical components, their properties at different frequencies, and the interaction between them in different configurations. **Table 2-1** lists the most common circuit elements and their frequency response used when fitting impedance data from biosensor surfaces.

Table 2-1 Most common circuit elements

Equivalent element	Impedance
R	R
C	$1/j\omega C$
L	$j\omega L$
W (infinite Warburg)	$1/Y_0\sqrt{(j\omega)}$
O (finite Warburg)	$Tanh(B\sqrt{(j\omega)})/Y_0\sqrt{(j\omega)}$
Q (CPE)	$1/Y_0(j\omega)^a$

2.2.1. Basic components

If a circuit would only use ideal resistors, no frequency dependency would be observed. Such circuits can be recognized in a Bode plot when a constant value for the magnitude of Z and a constant phase of 0 ° is shown.

If only inductors (L, [H]) would be used, the Bode diagram would start with a low magnitude value and a phase of 0 °. At higher frequencies, |Z| and φ would rise until equilibrium at φ = 90 ° is reached. This effect is explained in Lenz law which states that ‘an induced electromotive force always gives a rises to a

current opposite to the original change in flux [66]. Most biological samples will not show this response, however cabling loops and crosstalk could still induce this effect and give a biased measurement response.

A third component is a capacitor(C, [F]) which, instead of countering the current flow, will store energy. In it is simplest form, a capacitor comprises two conductors separated by a dielectric. This property influences most circuit designs since most practical circuits have one or more signal wires in parallel separated by air. At high frequencies this will cause small stray capacitances which will alter the measurement signal. In a Bode plot an ideal C can be recognized with a high initial impedance and a phase of 90 °, at higher frequencies the impedance and phase will reach 0°.

A forth impedance component is called the Warburg impedance. This occurs when a substance in a fluid moves from a region with high concentration to a region with low concentration. The impedance of this diffusion depends on the frequency of the potential perturbation. At high frequencies, the Warburg impedance is small since diffusing reactants do not have to move very far. At low frequencies, the reactants have to diffuse farther increasing the Warburg impedance.

The capacitive effect in sensors often does not have an ideal capacitor behavior. Instead, they act like a constant phase element (CPE). As seen in Table **2-1** the basic formula for this CPE resembles the capacitor formula but adds an exponent α, which is less than 1. The "double layer capacitance" on real cells often behaves like a CPE. While several theories such as surface roughness, "leaking capacitor" and non-uniform current distribution have been proposed, it is probably best to treat α as an empirical constant with no physical basis.

2.2.2. Equivalent circuits

However, actual circuits do not correspond to one of these simple elements but combine them. For example, a coated metal behaves as a resistor in series with a capacitor [64]. As for biosensor systems, they can be interpreted as a simplified Randles cell (**Figure 2-3(a)**). This circuit includes an electrolyte resistance, which is often a significant factor in the impedance of an electrochemical cell and a double layer capacitor in parallel with a charge-transfer resistance.

The model describes the translation from electron to ion conduction, resulting in a non-uniform distribution of charges. At this solid to liquid interface, ions from the solution will attach to the biased biosensor layer, behaving as an electrode with a typical separation of 0.5 to 10 nm. During measurements, this layer will

behave as a CPE element. The electrochemical reactions at the interface form the charge-transfer resistance and the electrolyte resistance depends on the ionic concentration, type of ions, temperature, and the geometry.

An ideal Bode plot of such a circuit has a high |Z| plateau and a φ of 0 ° at low frequencies. In this region the magnitude corresponds to the series resistance added with the polarization resistance. The double layer capacitance has no effect in this region since the reactance equals infinity and thus acts as an open circuit. With a rising frequency the value of the reactance changes and the impedance of the parallel circuit will drop. Here the phase will first rise and, in the ideal case reach 90 ° before dropping back to 0 °. When the phase reaches zero, the circuits impedance will match the series resistance because the reactance of the parallel circuit equals zero and thus act as a short (**Figure 2-3(b)).**

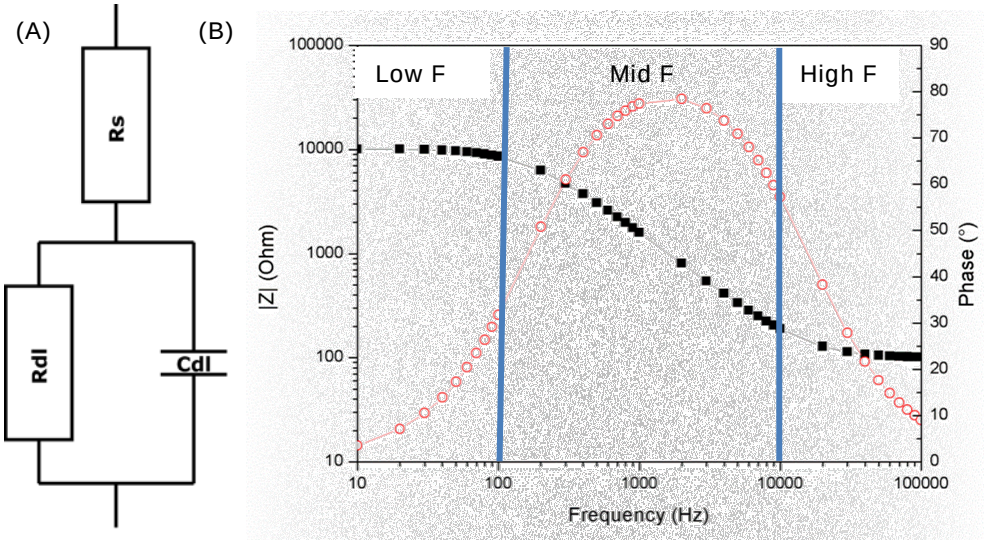

Figure 2-3 (a) Randles circuit (b) Bode plot Randles circuit

A 2nd way to graphically represent measured impedance is the Nyquist plot (**Figure 2-4**). This plot shows both the amplitude and phase angle in a single graph. It is mainly used as an stability assessment for closed loop circuits. The Nyquist Plot for a simplified Randles cell is always a semicircle. The solution resistance can found by reading the real axis value at the high frequency intercept. This is the intercept near the origin of the plot. The real axis value at the other (low frequency) intercept is the sum of the charge-transfer resistance and the solution resistance. The diameter of the semicircle is therefore equal to

the Charge-transfer resistance. The low frequency data is found at right and high frequency data at the left. However it is impossible to get detailed frequency information from the graph.

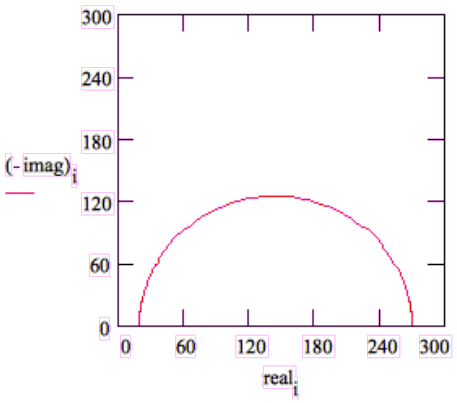

Figure 2-4 Nyquist plot

2.3 Linearity of Electrochemistry Systems

In circuit theory a distinction is made between linear and non-linear systems. For ease of use during analysis it is better to use a linear system. The following definition of a linear system is taken from Signals and Systems by Oppenheim and Willsky:'*A linear system ... is one that possesses the important property of superposition: If the input consists of the weighted sum of several signals, then the output is simply the superposition, that is, the weighted sum, of the responses of the system to each of the signals. Mathematically, let y1(t) be the response of a continuous time system to x1(t) ant let y2(t) be the output corresponding to the input x2(t).*'

Then the system is linear if:

1) The response to x1(t) + x2(t) is y1(t) + y2(t)

2) The response to ax1(t) is ay1(t) ...

Most electrochemical impedance spectrum measurements use a potential to stimulate the sample. Electrochemical cells however do not react linear, a doubling of the voltage will not necessarily double the resulting current. But when analyzing a small enough portion of a cell's current versus voltage curve,

it appears to be linear **Figure 2-5**. In order to stay in this linear part of the curve the maximum applied potential in EIS measurements is limited to 1 to 100 mV.

However, in some applications the non-linear response can be used. Linear systems should not generate harmonics, so the presence or absence of significant harmonic response allows one to determine the systems linearity.

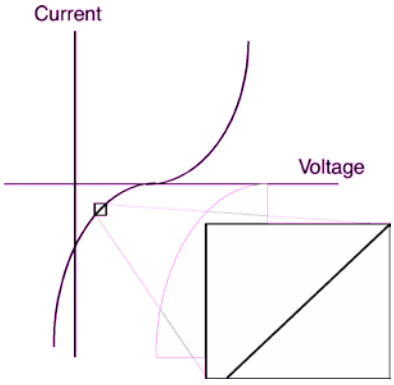

Figure 2-5 a cell's current vs voltage curve

2.4 Impedance measurement techniques

There are many different impedance spectroscopy measurement techniques, each of which has it is own advantages and disadvantages. However none of these setups includes all measurement capabilities so it is important to make a trade off. To select the right setup it is key to consider such factors as frequency coverage, measurement range, accuracy, ease of operation, connections and cost.

2.4.1. Bridge method

The first method uses the wheatstone bridge. In a balanced setup three components (L, C and R (displayed as Z)) in the range of the sample under test are placed at the ends of the bridge. When the system is balanced, no current flows through the detector. The value of the impedance can sequentially be calculated from the relationship between the individual components. To double the sensitivity of the measurement, two identical samples can be placed diagonally in the bridge. The main advantages of this technique are its high accuracy, wide frequency coverage (when using different types of bridges) and low cost. The need for manual calibration, long measurement times and narrow single instrument frequency coverage makes it less useful for standalone measurements. It can be used for frequencies up to 300 MHz.

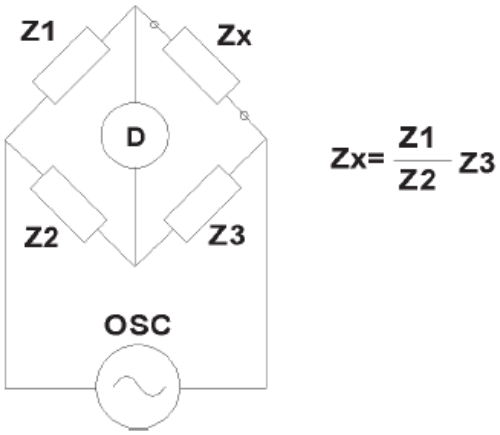

Figure 2-6 Bridge method [67]

2.4.2. Resonant method

A second method is to use a tunable capacitor, oscillator and a voltage meter to make a resonant circuit. The unknown impedance values are obtained from the test frequency, C value, and Q value measured directly using a voltmeter placed across the tuning capacitor. The setup can placed either in a direct, series and parallel connections to wider the measurement range. The good Q accuracy even up to high Q values makes it a good method for frequencies from 10 KHz up to 70 MHz. Its low accuracy for low impedances and the need for tuning makes it less practical in most measurement setups. The use of a gyrator circuit

combined with programmable resistors could make the technique more accessible for automated use.

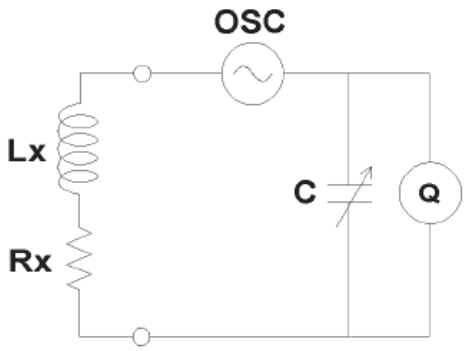

Figure 2-7 Resonant method [67]

2.4.3. I-V method

In the I-V method the unknown impedance is calculated from the voltage, current ratio. A known small valued resistor is used to measure the current caused by a known voltage. To prevent the effect caused by this resistor, a transformer can be placed in the circuit. However, this limits the applicable frequency range. The useable frequency range starts at 10 KHz and goes up to 100 MHz. One of the greatest advantages is its versatility which makes it suitable for probe-type tests. A second advantage is the possibility to ground the setup However, the method is less suited for measurements over a large impedance change due to large voltage differences which might occur over the sample.

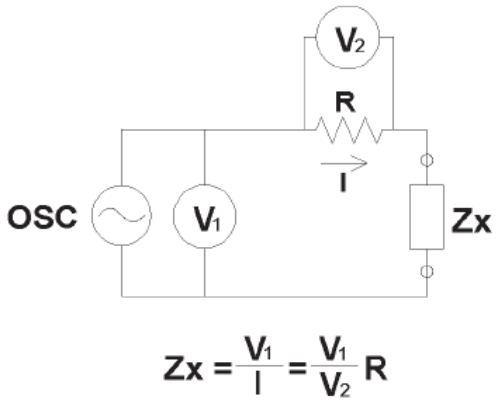

Figure 2-8 I-V method [67]

2.4.4. RF I-V method

The RF I-V method uses the same principles as the I-V method. The setup consists out of an impedance-matched measurement circuit an a precision coaxial test port for operation at higher frequencies. The impedance of the sample under test is derived from the measured voltage and current values. There are two different setups one for low and one for high impedances. This technique has a high accuracy and wide impedance range.

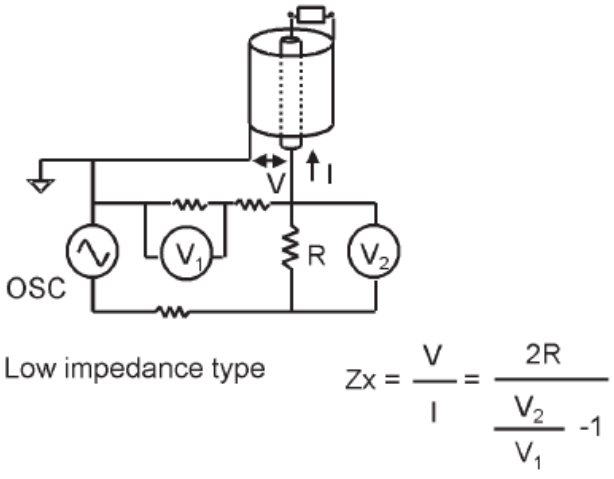

Figure 2-9 RF I-V method [67]

2.4.5. Network analysis method

In the network analysis method the reflection coefficient is obtained by measuring the ratio of an incident signal to the reflected signal. A directional coupler or bridge is used to detect the reflected signal and a network analyzer is used to supply and measure the signals. One of the greatest advantages is the high frequency range, good accuracy for impedances close to the characteristic impedance. Disadvantages are the purchase price, need for recalibration and narrow measurement range (above 300 KHz).

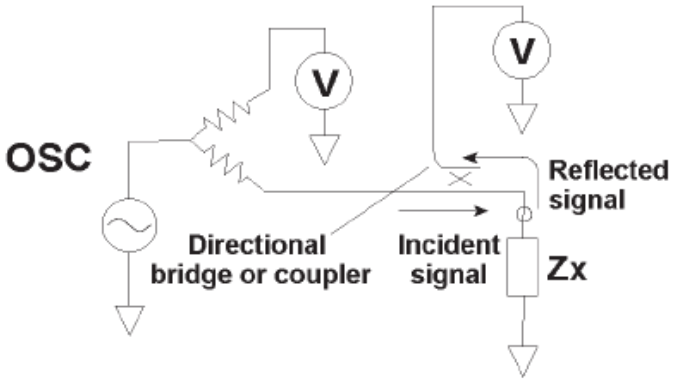

Figure 2-10 Network analysis method [67]

2.4.6. Auto-balancing bridge method

The most famous method is the auto-balancing bridge method which is usable for a broad frequency band with excellent accuracy over a wide impedance range. As with the I-V method it is possible to ground the device, making it useful for most measurement setups. The circuit uses an amplifier (opamp) circuit with a known resistor as feedback resistor (Rr). The test sample is placed between the output of the DAC and the inverting amplifier. The voltage at the output of the DAC and the resulting voltage at the output of the opamp are measured. The ratio between the two voltages and the feedback resistor can be used to calculate the impedance value. This method is the building block of all homemade setups described in this thesis and will be explained more in depth in chapter three.

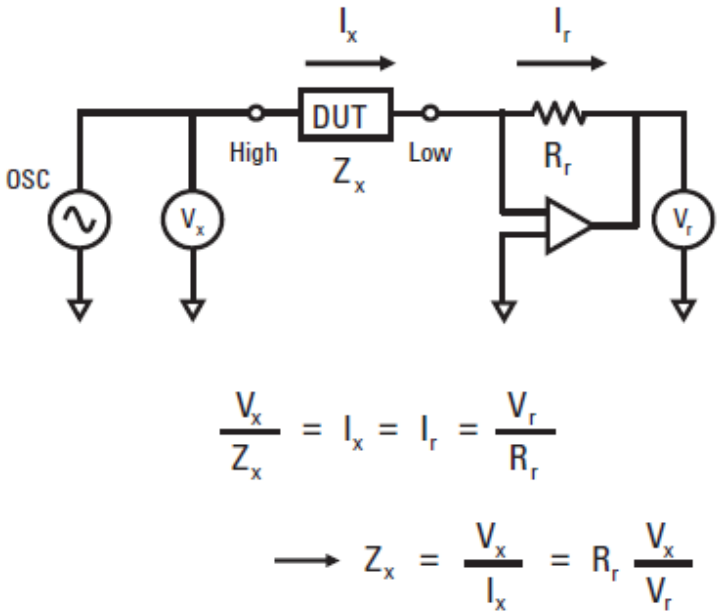

Figure 2-11 Auto-balancing bridge method

2.4.7. Conclusion

Table 2-2 Overview different impedance measurement techniques

	Advantages	Disadvantages	F range
Bridge method	* High accuracy * Wide F range * low-cost	* Balancing needed	DC to 300 MHZ
Resonant method	* Good Q accuracy	* Needs tuning * Low |Z| accuracy	10 KHZ to 70 MHz
I-V method	* Groundable	* Limited F range	10 KHZ to 100 MHz
RF I-V method	* High accuracy * Wide |Z| range at high F's	* Limited F range	1 MHz to 3 GHz
Network analysis	* Large f range * Good accuracy	* Calibration for each F * Narrow f range	< 300 KHz
Auto balancing bridge method	* Wide F range * High accuracy * Groundable	* High F's not available	20 Hz to 110 MHz

2.5 Signal dependent measurement methods:

There are two main methods used in EIS measurements. The first method will control the current sent injected in the sample. The voltage over the sample depends on its impedance. In these applications, it is very important to limit the maximum used voltage since this could, in some applications, lead to destruction of the sample. In a voltage controlled setup the current through the sample varies according to its impedance. When measuring low impedances this technique might lead to impermissible high current values. In these setups it is essential to limit the maximum current output of the device. Both methods can be implemented in different ways. The most popular ones will be explained in dept.

2.5.1. Sweep

This method is the most popular and easiest screening method. Here, each frequency is sequentially placed, with a fixed potential at the output of the DAC. After the signal is reconverted in the ADC the |Z| can be calculated in a few different ways. One way to calculate the amplitude is to measure the RMS value of the signal and simply use Ohm's law to know the value of the impedance. The phase can be calculated using a zero detection algorithm. This algorithm calculates the time between the zero crossing of the generated and measured signal using the sample clock. The technique is very accessible, only a small microprocessor, a DAC and ADC is necessary to build a basic setup. Another way is to use a Fourier transform, here the magnitude of the signal, at a certain frequency is used to calculate the impedance and phase value. This method does require a stronger processor to calculate the values. This technique however has one disadvantage; when measuring a lot of frequencies the measurement time adds up, especially at low frequencies this might cause a problem.

2.5.2. Arbitrary wave form

A possible way to speed up measurements is the use of an arbitrary wave form. The Fourier expansion theorem states that an ideal square wave form with an amplitude of 1 can be composed from a number integer harmonic frequency components **formula (2-4)** shows this interaction.

$$S_n(x) = \frac{A_0}{2} + \sum_{n=1}^{N} A_n * \sin\left(\frac{2\pi n x}{P} + \emptyset_n\right), for\ integer\ N \geq 1 \qquad (2\text{-}4)$$

If this theory would be applied to generate one arbitrary signal composed with all signals of interested the measurement time would drastically improve. Since performing a Fourier transform on a pure sine-wave generates a single frequency response. The amplitude of this signal at a given frequency could be used to calculate the impedance response. If instead of one sine-wave multiple waves are added together, just as with the Fourier expansion theorem, the frequency response of the signal would show multiple discrete values. These could be used to calculate the impedances values at each of these frequencies. When using this technique some design rules need to be kept in mind. Since the wave is a composition of multiple single waveforms the total voltage value differs from its original value. The underlying principles can be compared to those of an amplitude modulated (A.M.) signal in the radio frequent (R.F.) field where a carrier signal is mixed with a data signal with a different frequency and smaller amplitude. The first two pictures of **Figure 2-12**. show the singular signals before addition. In the third part both are added and a basic A.M. modulated wave is generated. If the maximum amplitude of the carrier and data signal would occur at the same time the total amplitude of the signal would be at it its peak. In all other cases the value lies between this peak value and zero. The same is true for an arbitrary wave but instead of two frequencies many more are mixed together.

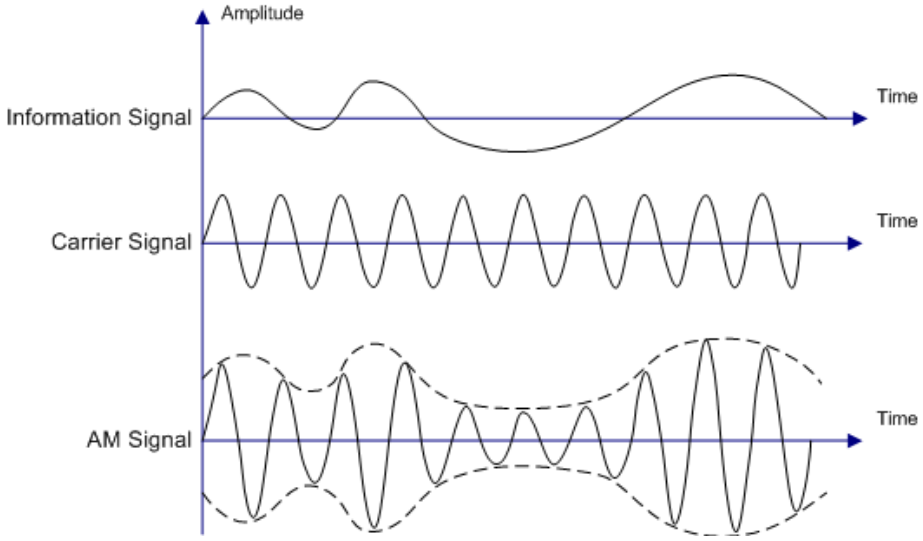

Figure 2-12 Arbitrary wave composition

2.6 Electrode configuration

The used measurement setup and method will determine a large portion of the measurement range. A third limiting factor is the connection between the DUT and the measurement device.

2.6.1. Two electrode setup

The most known connection method uses two measurement cables. Here the DUT is connected directly between the in- and output of the apparatus. This is a good option for most measurements since only one input and one output are needed and cabling is restricted to the bare minimum. However, if the sample under test has a small impedance value or if the samples contact resistance is high, then erroneous measurements might occur. If the sample has only a small impedance, the connected voltage will be divided between the DUT and the cable which is connected in series. In case of a high contact resistance, the measured impedance will be the sum of the contact resistance and the sample resistance. Both faults will cause a significant error. Since the result of such a measurement falls in the range of most devices it is virtually impossible to detect them.

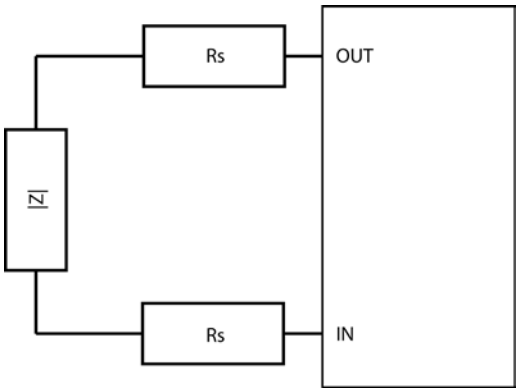

Figure 2-13 Two electrode setup

2.6.2. Four electrode setup

The four electrode setup solves these problems. Instead of using one in- output pair a second pair is added. The first pair connects and measures the current to the sample. The second measures the voltage. The simplest way to calculate the impedance is to calculate the complex ratio between voltage and current. A practical voltage meter has an input impedance in the mega-ohm range which means no current will flow through the second cable pair and the cable resistance will not influence the measurement. Since in a series circuit the current is constant through all elements, the measured current is equal to that of the sample under test giving a relative easy calculation of |Z|. Although this method guaranties correct impedance measurements, budget restrictions, wiring and in-output constrains limit the use of this setup.

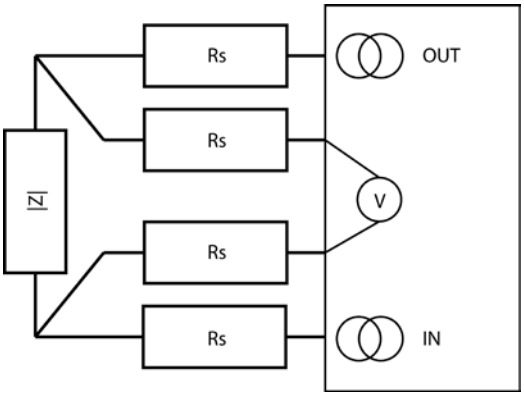

Figure 2-14 Four electrode setup

2.6.3. Three electrode setup

An alternative is the three electrode setup. It uses the same principles as the four electrode setup. Two wires will be used to sense and connect the current. The voltage meter is connected at one side of the DUT and its 2nd electrode is directly connected at the current output. This reduces the wiring problem but does not decrease the required number of measurement in-outputs. Secondly, a small error occurs because of the wiring resistance between the current output and the DUT.

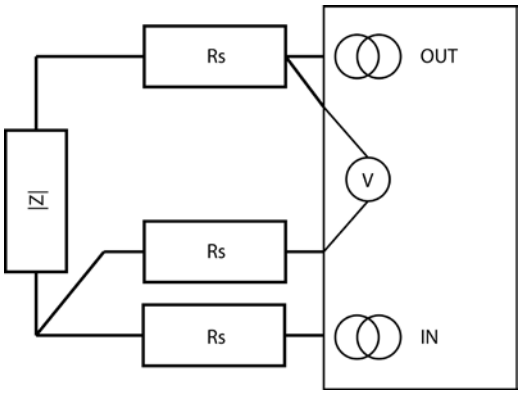

Figure 2-15 Three electrode setup

In practice most devices will either use the two- or four electrode setup. When choosing between the two considerations need to be made. If the DUT under test has a magnitude at least 100 times higher than the cable resistance, the contact resistance is low and cost is a factor. The two electrode setup will be the method of choice. If the accuracy needs to be very high even for low impedances or if the contact resistance is high, cabling and required input is of lesser concern then the four electrode setup would be an excellent choice.

2.7 General considerations:

There are some considerations to keep in mind when designing instrumentation. To have the best possible measurement results and to ensure the repeatability of a measurement it is key to control the environmental temperature. As state in the first paragraph Impedance spectroscopy, the impedance is directly related to the temperature. An uncontrolled environment could lead to misinterpretation of measurement data. Possible solutions are the use of an oven or to use a PID system to control the temperature.

A way to reduce random noise on a measured value is to stretch the measurement time. Over time, random noise has an average value of zero. By stretching the measurement time, this random noise error will reduce with the square root of the A/D operating time. Averaging the measured value over multiple samples has the same effect on the noise. Yet, the gain in accuracy needs to be weighed against the prolonged measurement time.

As explained in paragraph 2.3 linearity of electrochemistry Systems, small signals ensure the linear response of a system. A second signal consideration is the sample under test. If biological tissue, living cells or organism are measured, some general rules need to be uphold. Websters manual on Medical Instrumentation Application and Design [68] and EIC standard 891-04-62 [69] state that a maximum current of 5 mA for frequencies above 10 KHz. At lower frequencies this current may excite the sample and for human tissue cause contractions. In the designs covered in this thesis the amplitude of the voltage is restricted to 50 mV. This means that impedances down to 10 Ω can be measured conform the standard.

The used frequency range is another important factor. In EIS measurements the chosen frequency allows the user to evaluate a certain part of sample under test. Depending on the application it can be useful to only get a yes/no signal, or a complete analysis of the sample. Generally speaking, measurements of heart rate and cells are between 10 KHz and 100 KHz, imprinted polymers and DNA measurements at frequencies below 1 KHz depending on the polymer, setup or surface linkage [70-85]. To find the right measurement range it is key to do a thorough system analysis prior to the measurement and/or perform a full spectra sweep.

2.8 The selected design

A few considerations where kept in mind for the designs presented in this thesis:

For ease of use first designs are based on the sweep readout method. To speed up measurements the arbitrary wave method is applied for the NI USB 6245 platform.

- Since the contact resistance of the intended applications is low, compared to the solution resistance, the choice was made to use a two electrode setup. Other benefits of this setup are that no constant current source or second A/D convertor is needed.

- Most relevant bio-analytical measurements are conducted between 0.1 Hz and 1 GHz. At frequencies lower than 0.1 Hz the measurement time increases and the impedance magnitude gets too high. Above 1GHz the dipole moment, of the solution, starts to influence the measurement and is thus un-useful for measurements. The auto-balancing bridge setup, which has a wide frequency range, is highly accurate and can be connect to the ground is best suited for the intended applications.

The following chapter gives a detailed description of the adaptions made to the two point auto-bridge circuit to make it applicable for the presented setups.

Chapter 3

Sensor systems

Most commercial available impedance analyzers such as the HP 4294A have a large form factor, are high cost and need specialized personnel to operate. This makes them less suited for product development. If specialized low-cost readout devices would become available, for example a biosensor setup which is easy to operate, accurate, hand-held and supports a multichannel readout, the use in laboratory conditions would increase. The most basic impedimetric setup needs a current source and a voltage readout at a fixed frequency to measure the magnitude of the impedance. Advanced systems are able to measure the phase and magnitude at different frequencies by varying the frequency. Aside from adapting the excitation signal, the multiplexing possibilities and measurement range determine the usability of the system. Other additions which enhance the usability of such systems are extended data storage, integrated power supply and interfacing possibilities. The following paragraphs describe different EIS setups and measurement techniques.

3.1 Basic system overview

A measurement system designed for impedance measurements can be compared to a DSP setup (**Figure 3-1**). First, a software package generates a digital signal and sets all the measurement properties. Next, a direct digital synthesis (DDS) core transforms the digital signal to an analog wave. Then, a transmit stage, often consisting of amplifiers and buffers, feeds the signal to the sample under test. After some processing steps to amplify and filter the signal, the digital signal processor (DSP) converts it back to a digital signal. The last step processes the measured signal, compares it to generated signal, and calculates the impedance and phase values.

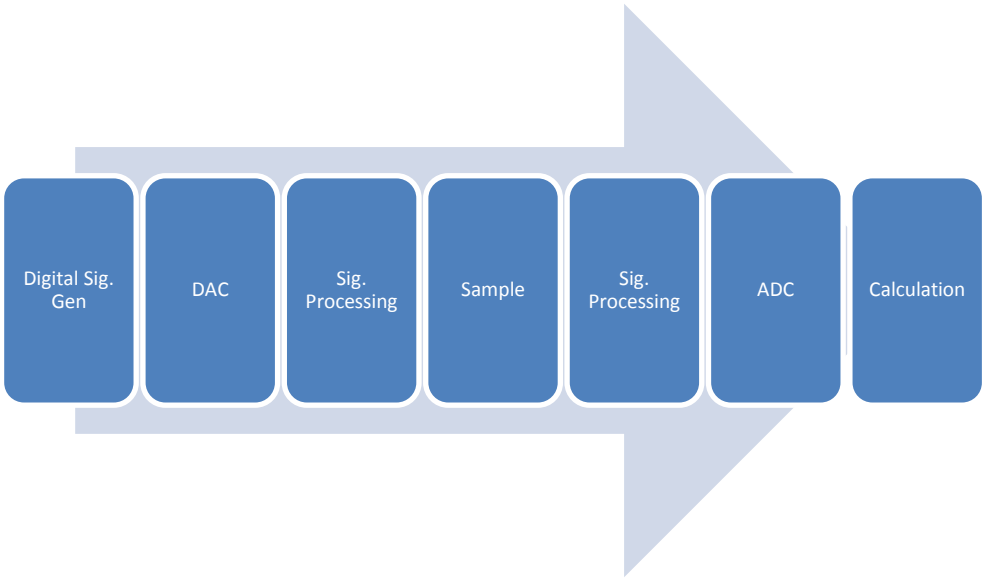

Figure 3-1 Overview DSP setup

3.2 Single channel impedance setup

Ideally, such a system would be easy to implement, experience no effect from internal or external noise, and integrate most of these components on a single-chip. The commercially available Analog Devices AD5933 integrates most of these features in a high precision impedance converter/network analyzer chip. **Figure 3-2** shows the block diagram of this convertor. Using the internal clock, the 27-bit DDS core generates frequencies between 1 K and 100 KHz with a 0.1 Hz frequency precision. The coupled DAC connects the converted signal to the output stage. The receiving stage consists of a programmable gain amplifier coupled to a low pass filter which in turn is connected to a 12 bit ADC. After conversion, a 1024 point DFT is performed resulting in a 2-complements number for both magnitude and phase of the signal. An inter-integrated circuit (I^2C) protocol bus transports the data to the registers. The AD5933 does not contain any memory to store the calculated data. Therefore external processing, PC or controller based, is needed to display the data.

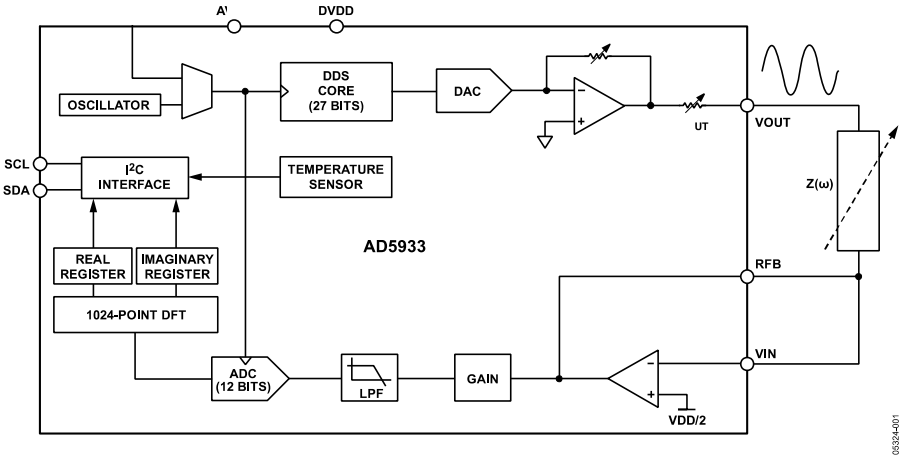

Figure 3-2 Block diagram AD5933 Impedance chip

The evaluation board (**Figure 3-3**) available for the AD5933 chip provides an excellent starting point for circuits based on this IC. This design adds a USB microcontroller to interface the I²C bus to an USB port. The supplied Visual Basic software programs and displays the result stored in a 64 kbyte electrically erasable read only memory (EEPROM). The board is also equipped with voltage convertors to enable USB power supply and subminiature coaxial connectors for connection with the sample holder.

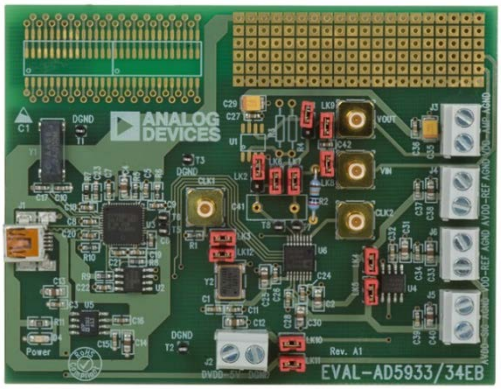

Figure 3-3 AD5933 Evaluation board

The initial designs for bio analytical sensor readout based on this evaluation board where developed in the ELPHYC group [86]. However, further adaptions where needed to enlarge the frequency range and expand the measurable impedance range from a few ohm to a couple of mega ohm. A PCB was added containing a multiplexer circuit, calibration resistors and feedback resistors together with a relay switching multiplexer for multi-channel readout (**Figure 3-4**). This system was tested on passive components and a liquid cell used for biological measurements [87].

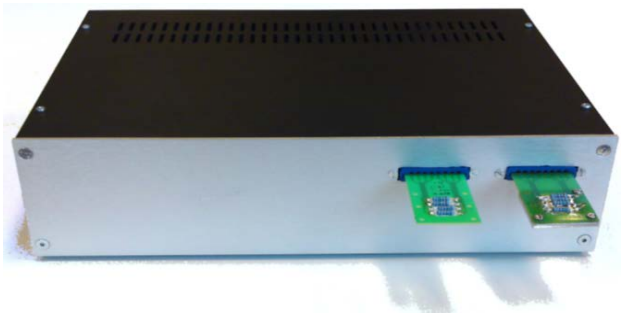

Figure 3-4 Adapted measurement setup based on the AD5933

3.3 Handheld multichannel impedance setup

The successful adaption of AD5933 circuit led to the development of the BioZ°(**Figure 3-5**). This device further increases the resolution, accuracy and the applicability while miniaturizing the setup to a handheld device.

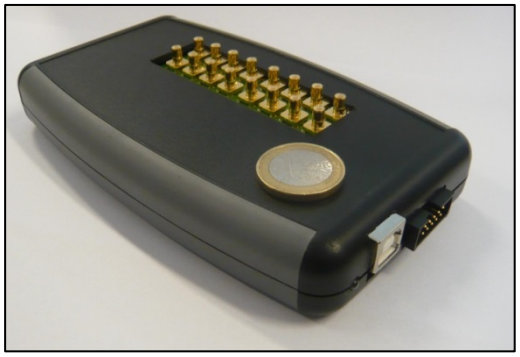

Figure 3-5 BioZ° device

3.3.1. Improvements

3.3.1.1 . Signal generation

In order to make a universal design applicable in bio analytical setups, a few design considerations need to be taken. One important aspect is the impedance range, since the measured magnitude depends strongly on the sensor layout, analyte, substrate and electrodes [88-91]. The measured |Z| and φ are directly related to the measured voltage which makes it important to have a good understanding of the working principles of the AD5933. Internally, the DDS core generates a sine wave at a programmable frequency and voltage. The frequency can be set depending on the master clock and the excitation voltage can be programmed into four ranges (**Table 3-1**).

Table 3-1 Excitation voltages and related DC bias

Range (register value)	Sine wave (Vp-p)	DC bias (V)
1	1,98	1,48
2	0,97	0,76
3	0,383	0,31
4	0,198	0,173

The chip can only handle positive voltages; therefore a DC bias voltage is always present in the output signal. In bio analytical measurements however, the amplitude and bias voltage can have a significant influence. For example, in cell measurements typical resting potentials of animal cells lay around 70 mV [92-94]. In such applications it is therefore important to keep externally applied excitation voltages well below 70 mV. The DC offset voltage can have an influence on charged particles when using an analyte [88, 95].

In the design of AD5933 a non-polar capacitor of 10 µF was placed in series with the output to remove the DC bias voltage. Since the chip only works with a positive voltage, this offset needs to be added again at the input stage. The excitation voltage is scaled using a voltage divider and a buffer amplifier. This OPAMP circuit creates a high pass filter circuit which has a roll off frequency of 4 Hz. For bio analytical measurements, the excitation voltage was limited to 60 mVpp. This output circuit is given in **Figure 3-6**.

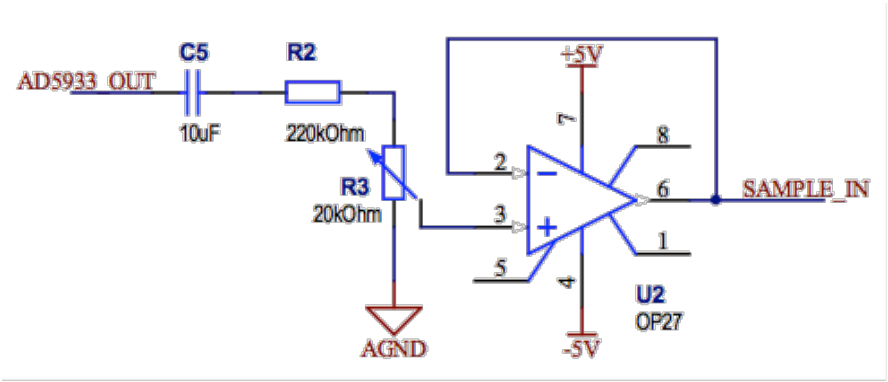

Figure 3-6 Output signal conditioning

3.3.1.2 . Signal capturing

After excitation the current resulting from the samples impedance is converted to a voltage by an OPAMP IV-convertor. This inverting circuit shown in **Figure 3-7** also amplifies the signal with a factor of R_{FB}/Z_{sample}. The following buffer circuit adds the DC bias to the signal using a regulator circuit fixed at -2,5 V. To ensure a low-noise conversion in the final conversion step the high-end Texas Instruments OPA627 precision high-speed OPAMP was chosen in the buffer amplifier circuit [96]. This low input bias current Difet-based component has a reliable, low-noise solution for audio-signal amplification, but its frequency response expands well beyond the audio spectrum [97].

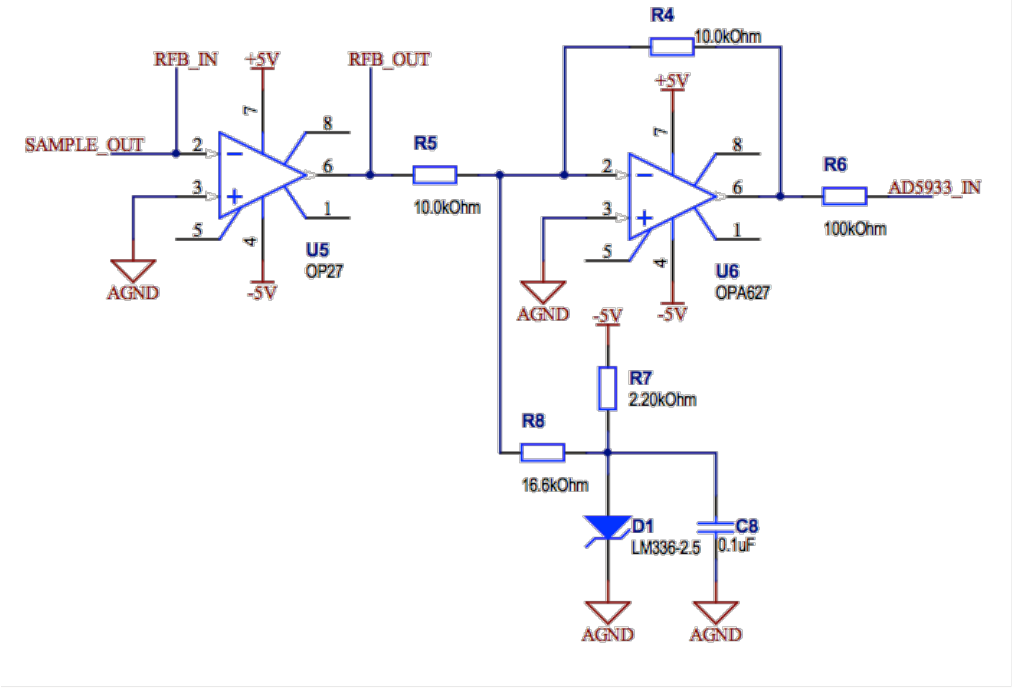

Figure 3-7 Input signal conditioning

3.3.1.3 . Resolution / accuracy

Since the impedance of target applications lies between 10 Ω and 10 MΩ, this basic circuit poses some problems. The AD5933 circuit has an input cutoff of 3 V and a 12-bit resolution this means that chip has a maximum resolution of 0.7 mV. The output voltage is fixed at 60 mV and the input voltage is determined by the sample impedance magnitude which can vary strongly during measurements. For a maximum analyzable impedance of 1 MΩ the lowest measurable impedance would be 244 Ω. Such an extended range means that 1-bit errors would have a large influence on low impedances (100 %) while at the maximum impedance such an error would only be 0.02 %. These variations and limited range would be inadequate for bio-analytical impedance measurements. To overcome this problem, a set of relay switchable resistors are used instead of the fixed resistor. By dividing the measurement range into several sub-ranges the resolution increases and the lowest measurable |Z| can be chosen. In our design the minimum amplification factor was set to 2. With the 0.7 mV resolution of the AD5933 and a 60 mV excitation voltage this would give a

maximum deviation of 0,58 %. To obtain this resolution, and taking a safety margin into account, five resistors are needed in order to measure the full impedance range.

To calculate the impedance, the CPU uses the ratio between the excitation and received voltage. This dimensionless value still needs to be multiplied with a known Gain Factor (GF) according to **formula (3-1)** to get the correct magnitude.

$$|Z|[\Omega] = \frac{1}{Gainfactor\ [\Omega^{-1}]\ * magnitude} \qquad (3\text{-}1)$$

The GF is a value stored on the controlling device after calibration over a known resistor. The phase value of the known resistors is also stored on the controller in order to calculate the sample's phase shift. Since this GF has a large influence on the |Z|, it is essential to record these values as accurately as possible. For this reason each impedance range was divided into two calibration subranges, giving a total of ten calibration resistors. **Table 3-2** illustrates the resulting ranges with Z_{min} and Z_{max} indicating the measurable impedance range for each calibration and feedback resistor. The feedback resistors were chosen from the E12 series to lower design costs. Each switching point was experimentally determined as described in [98].

To increase ease-of-use for the end-user, these fifteen resistors were incorporated in the device. Software controlled relay switching was applied to connect each feedback and calibration resistor when needed. Although these resistors could be switched by means of semiconducting components such as MOSFETS, parasitic capictance would hinder accurate impedance measurements. Relays are used to avoid these problems though putting some limits on the minimal size of the device.

Table 3-2 Impedance ranges

Z min (Ω)	Z max (Ω)	R feedback (Ω)	R calibration (Ω)
10	68	250	39
68	125	250	97
110	1,2 k	3,8 k	630
1,2 k	2,2 k	3,8 k	1,7 k
2,2 k	13 k	56 k	7,4 k
13 k	28 k	56 k	19 k
28 k	216 k	820 k	120 k
216 k	410 k	820 k	313 k
410 k	2 M	10 M	1,5 M
2 M	5 M	10 M	3,8 M

3.3.1.4 . Frequency range

A second important system parameter is the frequency range. As with the impedance, the frequency at which biosensors react depends on the type and layout of the sensor. For example, polymer-based immunosensors show the highest response around 80 Hz [99], DNA mutation [100, 101] sensors in the kilohertz range and cell proliferation measurements [102] around 100 kHz. In order to make the design universally applicable, the system needs to support a wide spectrum of excitation frequencies.

In case of the AD5933 impedance analyzer IC the excitation frequency range is directly proportional to the applied clocking signal. This clock, being either the internal 16 MHz oscillator or an externally applied signal, is used to both generate the excitation sine wave and analyze the resulting measured signal. The excitation signal is provided by a 27-bit phase accumulated DDS core. The input of this phase accumulator is taken from user-settable dedicated registers. As shown in **formula (3-2)**, since the absolute maximum applicable clock is equal to the internal clock of 16,6 MHz, users are given control over the excited signal up to a resolution of 0,119 Hz.

$$Frequency\ resolution = \frac{Clkmax}{\#bits} = \frac{16\ MHz}{2^{27}} = 0{,}119\ Hz \qquad (3\text{-}2)$$

After digitalization, the AD5933 performs a 1024 sample DFT on the measured signal. The algorithm performed by this DFT is represented in **formula (3-3)**, where x(n) is the output of the ADC, n is the sample number and X(f) is the signal amplitude at a specific frequency f.

$$X(f) = \sum_{n=0}^{1023} (x(n)(\cos(n) - jsin(n))) \qquad \textbf{(3-3)}$$

When the internal oscillator of the AD5933 is used, the lower limit of the analyzable frequency range lies at 1/1024 of the 16,6 MHz oscillator frequency, being 16,3 kHz. As the excitation voltage upper frequency limit of the IC is set at 100 kHz, only a very narrow spectrum of frequencies is available to perform impedance measurements. Applying a range of external clocks can broaden the range. The required clock frequency range was determined by performing impedance sweeps in the excitation range from 10 Hz to 100 KHz with varying clock frequencies applied by a Keithley 3390 function generator. Although it was possible to sweep the entire range with one clock frequency in the tenths of kilohertz range, it is not desirable to do so due to delays in measurement time as stated in [103]. This research showed that it would be ideal to have an distinct clock for each frequency to keep measurement deviation around 0.1 % and ensuring high speed measurements. Experimentally, a fixed ratio of 1500 between the clock an excitation signal was ideal. Out of the numerous options available, such as the division of a high-accuracy crystal oscillator, a programmable microcontroller or a dedicated IC's, the Maxim DS1077 clock IC was chosen. This small IC can deliver frequencies ranging from 8,1 KHz to 66,6 MHz.

As can be seen in **Figure 3-8** the fixed clock/excitation ration of 1500 can only be applied for excitation frequencies up to 44 KHz with the lowest measurement frequency limited to 5.4 Hz. It is however possible to perform impedance spectroscopy over four decades, i.e. from 10 Hz to 100 kHz, while keeping measurement deviation around 0.1 %. The measurement time of these sweeps, performed with 10 points per decade over four decades, was 11,2 s. This makes the DS1077 IC a viable clocking solution for the AD5933 and allows for fast, reliable, and broad-spectrum frequency sweeping.

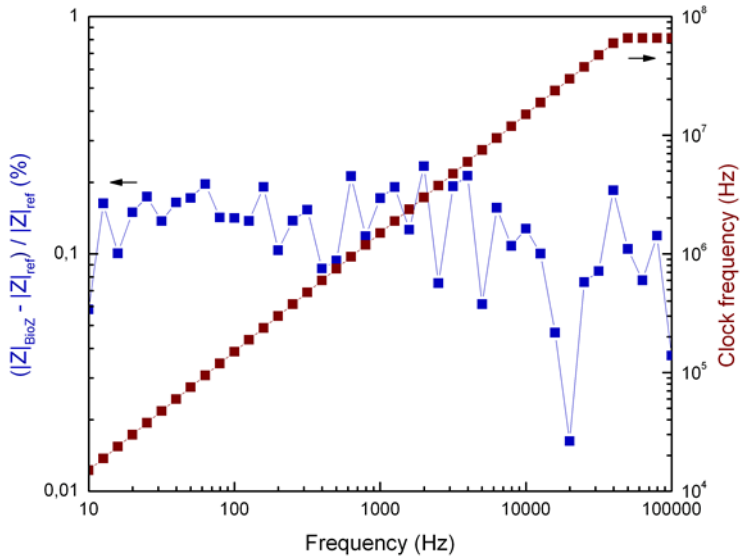

Figure 3-8 Relative impedance magnitude error and clock frequency versus measurement frequency

3.3.2. Software

The AD5933 board is not able to perform measurements by itself, nor can it store or display them. To perform a measurement, the system needs to be programed by a controller.

The interfacing between this controller and chip is done using an I²C bus, which is also compatible with the Maxim frequency chip and the Texas Instruments PCA9536 I²C I/O expander. The connection diagram of this interface is given in **Figure 3-9**. The Future Technology Devices International Ltd. (FTDI) FT232R USB to UART convertor [104] and Microchip Technology Inc. 16F627 PIC [105] convert the signal from the host to the different I²C controllers and makes the BioZ° detectable by the PC as a virtual COM-port.

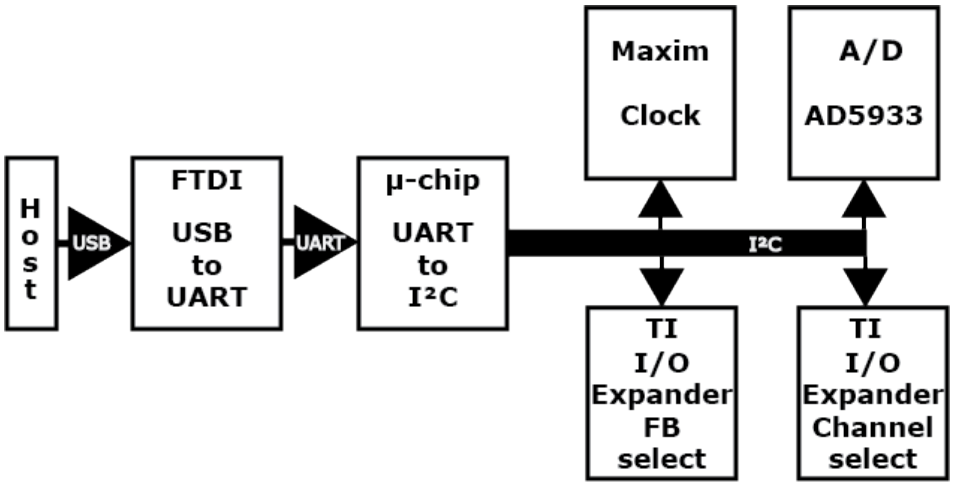

Figure 3-9 Controller interface

The chip of the evaluation board is programmed in Visual Basic (VB). Although this program is useful for basic measurements with the board, it is not suited for use with the expanded system. Since the BioZ° is controlled via PC, a program can be written to satisfy all user groups. LabVIEW, a graphical program language, was used to develop a measurement routine and a monitor system. **Figure 3-10** shows the flowchart of the measurement routine. The first step in any measurement is the calibration. In this process the GF is determined by measuring all calibration resistors with their compatible feedback resistor. The measured values are stored in a calibration file in the measurement map on the PC. This calibration procedure is identical to the measurement protocol. First an array with measurement frequencies is generated. Next the selected channel is connected to the sample. Then, the programmable clock is set to the master clock and the chip is programmed with the desired frequency and gain factor. At this point the real measurement takes place, the excitation signal is placed over the sample, the resulting voltage is measured and after completion of the DFT, the |Z| and φ are calculated using the gain factor. The magnitude value will then be checked if it lies within the measurement range. If not, the next feedback resistor is selected and this process is repeated until a valid value is measured. Then, the next frequency is placed at the output until the sweep is completed. At the end of the measurements the AD5933 is powered down and the impedance data is stored in a text file on the PC.

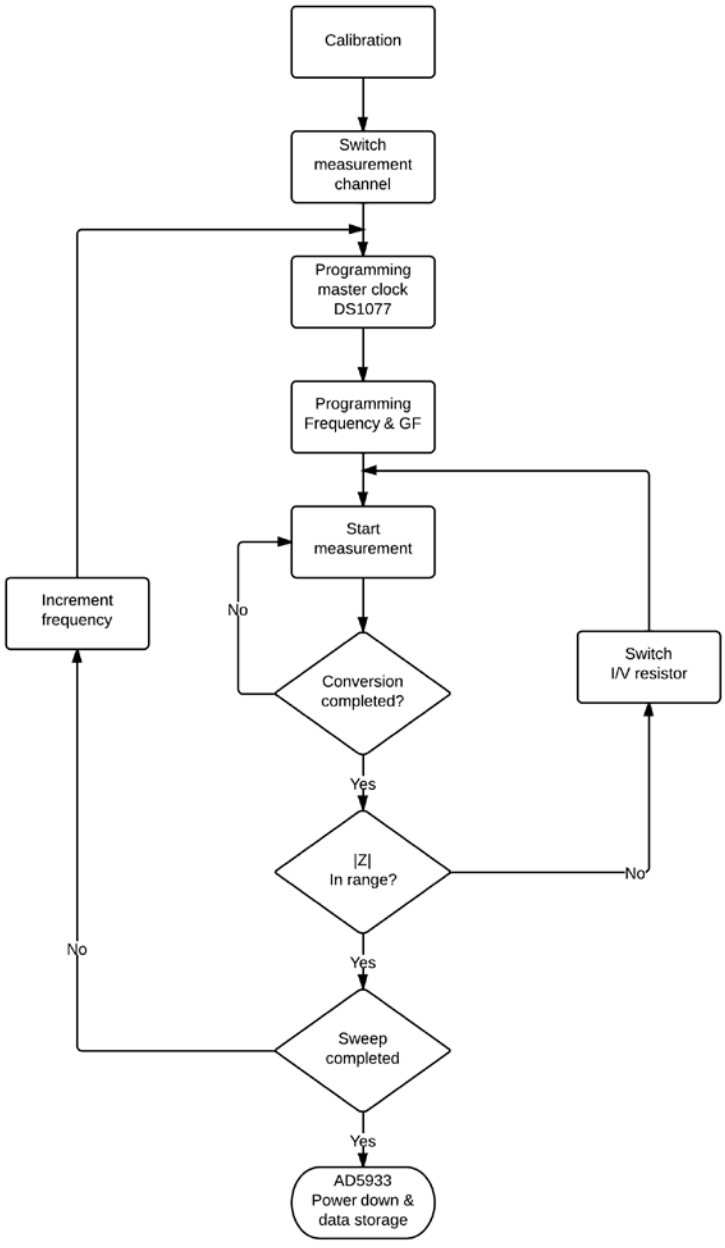

Figure 3-10 Measurement protocol BioZ°

3.3.3. System performance test

To evaluate the accuracy of the system, a set of E12 resistors within a range of 10 Ω and 1 MΩ was measured. Each decade was divided into 12 subdivisions according to the Renard standard series. 1% metal film resistors were used for an almost flat frequency response within the measured spectrum of 10 Hz to 100 kHz and tight temperature tolerance. The impedance magnitude should equal the resistance, while the phase should approach zero for the entire frequency range. **Figure 3-11** shows the deviation in impedance (%) and phase (°) with respect to the measured set of resistors for the BioZ° unit. These measurements were performed at a fixed frequency of 1 kHz, thus central within the logarithmic frequency spectrum of 10 Hz to 100 kHz.

The deviation in impedance lies well below 1 % for the largest part of the resistor range with one exception at 100 Hz where the mains frequency causes a large deviation. The average magnitude deviation lies at 0.44 %. Furthermore, the deviation in phase is always less than 1 °. A significantly lower deviation can be seen around resistor values approaching the on-board calibration resistors. Incorporation of a larger set of resistors would decrease deviation but would also require much more computational power, thus reducing measurement speed. It would however be possible in particular applications to build calibration resistors approaching the value of a specific sensor type.

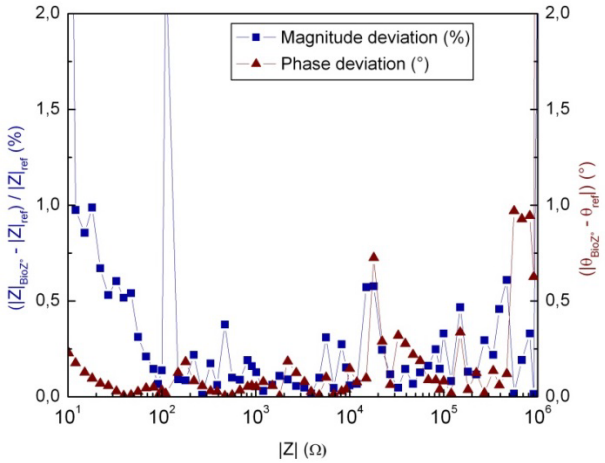

Figure 3-11 Relative impedance magnitude error and phase error versus impedance magnitude

Furthermore, although measurements on resistors give a good indication of device accuracy, these components cause no phase shift between voltage and current, nor do they inhibit charging behavior and resulting time constants. To analyze noise and drift parameters of the BioZ° units on more complex circuitry, an equivalent circuit of a measurement cell used for DNA-denaturation measurements was constructed. A resistor of 84 kΩ was placed in parallel with a 3 nF capacitor to emulate the interfacial double layer of a diamond substrate placed in a conducting PBS solution. A 306 Ω resistor was placed in series with this circuit to take into account liquid resistivity and losses due to connectors and cables [106].

The circuit was continuously measured for a duration of 24 hours with a measurement time set at 44 s per sweep, resulting in a total of almost 2000 sweeps. The difference between the measured and average magnitude value was calculated at the beginning, the center, and at the end of the frequency spectrum. **Figure 3-12** shows this relative magnitude for a frequency of 15 Hz, 1 kHz and 100 kHz. No distinct drift is present in the signal as the measured magnitude fluctuates around its average value for the complete 24 hours duration. In general the noise level lies below 0.4 %.

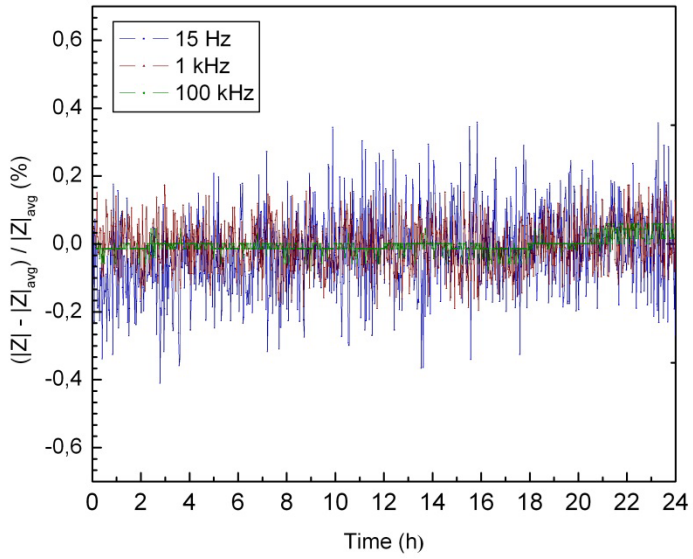

Figure 3-12 Relative impedance magnitude drift of an equivalent RRC circuit versus time

3.4 Ninety-six Channel impedance setup

The first successful measurements with the BioZ° board lead to the design of an expansion board to enable multi-cell proliferation measurements. The goal of the these measurements was to test the reaction of different living organisms on certain chemicals over time. The most important parameters for these experiments are to be non-invasive, preferably with the same form factor of current multi-well plates and have a small form factor.

A fast full biological screening of a sample of interest is the ultimate goal of many ongoing biosensor researches. Array-based sensors are a good step towards this common goal. The discussed setup has already been used in the quasi-simultaneous detection of different target molecules, such as histamine and nicotine [107, 108]. There are however several problems to overcome to further upscale this technique to be used in multi-cell proliferation measurements. For example chemical crosstalk [109], wiring, and form factor, all need to be carefully considered. After some market research the choice was made to use the Roche E-plate 96 well plates with interdigitated gold electrodes as basis for the design. Due to the standardized size of these well plates the system is compatible with existing lab equipment, thereby greatly increasing usability. Each well in the plate has a golden finger structure deposited at the bottom as shown in **Figure 3-13**. To reduce the amount of wiring, the wells are grouped per 8 by using a common counter electrode. The second part of **Figure 3-13** shows a cross section of an electrode, with (a) being the gold layer placed on a chrome interface (b) on top of the glass plate (c).

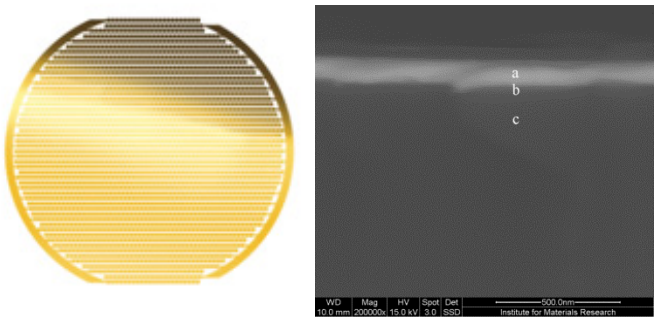

Figure 3-13 Gold interdigitated electrode layout (left) and cross section (right)

A new multiplexer system 'Impediplexer', show in **Figure 3-14** was developed to interface these plates with the BioZ°. The 96 wells of the plate are all wired to the connector and interfaced with the measurement unit through spring contacts. These contacts developed by Interconnect devices Inc. have a special tip to ensure good contact and extend life cycle as can be seen at the right side of **Figure 3-14**. To avoid inter well interferences a switching delay of 100 ms was implemented. The switching is done by Omron latching relays, controlled by Texas Instruments PCA9353 i²C I/O expanders [110]. This allows for complete control over the multiplexer by a single I²C bus compatible with the BioZ°. The measurement software previously discussed in this chapter has been adapted to incorporate these inter well switching times. During measurements a different base resistivity of 35 Ω, 55 Ω, 80 Ω or 105 Ω with ± 5 Ω accuracy, was measured between different wells and the input connector of the multiplexer. The value of this base resistance depends on the placement of the well on the plate. The highest resistivity corresponds to the largest distance between input connector and the well. The largest part of this resistance is caused by the electrodes of the well plate itself, as documented by the manufacturer.

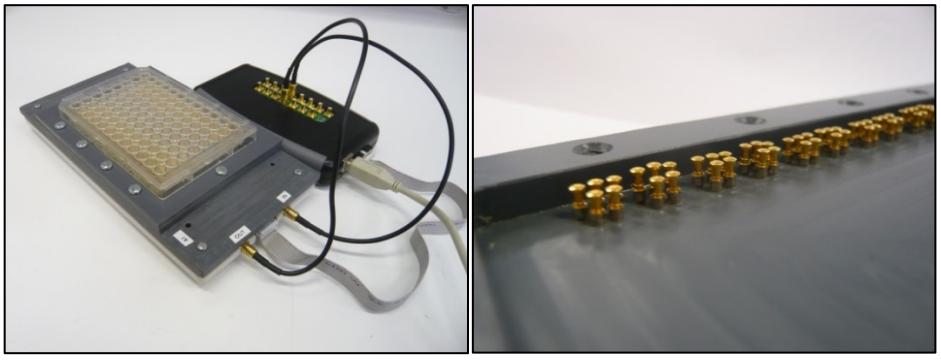

Figure 3-14 (Left) BioZ° connected with the Impediplexer (right) tip contacts

The Impediplexer system can be controlled using the software of the handheld multichannel system discussed in the previous section.

3.5 DAQ based impedance setup

The BioZ° measurement system however has some limitations. The measurement time for a frequency sweep starting at 100 Hz till 100 KHz takes about 7 to 10 seconds depending on the number of frequencies selected. For the impediplexer, the measurement time further increases due to switching delays. For the 96 channel measurement the measurement time can run up to 10 minutes. This is still acceptable for slow changing measurements such as the proliferation measurements. For faster systems, a different approach needs to developed. If instead of measuring one frequency at a time a whole range of different signals is combined to one arbitrary signal, measurement time can be reduced to less than one second. The AD5933 chip only allows for frequency sweeps or single frequency measurements. For the construction of the arbitrary wave other possibilities need to be examined. The first design was aimed to measure signals from 10 Hz up to 100 KHz and to have a impedance range from 1 Ohm to a few mega ohm using a DAQ for signal generation.

3.5.1. Measurement method

First thoughts need to go to the measurement setup. For such a system, it is important to have as little as possible frequency dependent components. This is because the combination of all frequencies to one signal makes it difficult to filter signal distortions. This is also one of the biggest restrictions of the technique, the signal needs to be as pure as possible a shift or even a small distortion at one frequency can shift or suppress the signal at another frequency. This stresses the importance of a well-balanced measurement system, able to measure the smallest signal difference and fast enough to register possible signal shifts.

The National Instruments USB-6251 DAQ card (**Figure 3-15**) [111], with two 16 bit analog outputs at 2,86 MS/s and 16 single ended 16 bit analog inputs at 1,25 MS/s, is an excellent platform to perform these experiments. It has a USB port, on board timing mechanisms, and can be controlled via LabVIEW. The board has a programmable output range which can be set from ±100 mV up to ±10 V with the full 16 bit resolution. This makes it possible to measure signals differences as low as 3 µV. The DAQ card has a screw terminal breakout board which, with some small adaptations can be interfaced with the sample.

Figure 3-15 NI USB 6251 DAQ measurement card

There are a few different ways to readout a sample. The circuitry needed should be frequency independent and if possible containing only a few components. The easiest way would be to directly connect the sample to the screw terminal; unfortunately it is not possible since no voltage drop would occur and the input value would equal the output value. If a known resistor is added to the circuit the input functions as a voltage divider. The formula for this voltage divider is given in **formula (3-4)** where the magnitude of the impedance is equal to the output voltage multiplied with the ratio between the known resistor and the input voltage minus the known resistance.

$$V_{in} = V_{out} * \frac{R_1}{|Z| + R_1}$$
$$|Z| = V_{out} * \frac{R_1}{V_{in}} - R_1 \qquad (3\text{-}4)$$

This circuit is the easiest way to measure impedance, is low-cost since only one external resistor is needed, and does not need an external power supply. But there are some issues, such as the excitation voltage which can vary strongly over the sample causing dangerous current through the sample. Another problem is that the resistor with a known value is connected with the sample. For example if this resistor has a small value compared to the sample, the measured voltage is very small and a high resolution is needed to measure small impedance differences and vice versa. For this setup to function properly the value of the resistor needs to be in close range of the samples |Z|, thus making it impractical for large measurement ranges.

To overcome this problem the circuit is adapted to an current to voltage convertor, as displayed in **Figure 3-16**. The addition of this OPAMP convertor

keeps the sample excitation voltage constant and has the added advantage of signal amplification. If a switching board was incorporated in the design as with the BioZ° device the maximum signal to noise ratio could be kept over the entire impedance measurement range. The most important design factor is the OPAMP, the bandwidth of this component can alter the signal response at certain frequencies changing the samples response to the arbitrary wave. The Texas Instruments OPA627 high-speed precision OPAMP [96] used in the BioZ° is perfectly suited for the purpose. For calculation of the impedance **formula (3-4)** needs a bit of tweaking. The measured voltage depends on the output voltage amplified with the ratio of the inverting amplifier. Since the second amplifier is a buffer circuit the value is unchanged and the impedance can be calculate by the formula given in **(3-5)**. The voltage at the input of the DAQ card is inverted compared to the original signal and needs to be restored before calculation.

$$V_{in} = -V_{out} * \frac{R_2}{|Z|} \qquad (3\text{-}5)$$

$$|Z| = -V_{out} * \frac{R_2}{V_{in}}$$

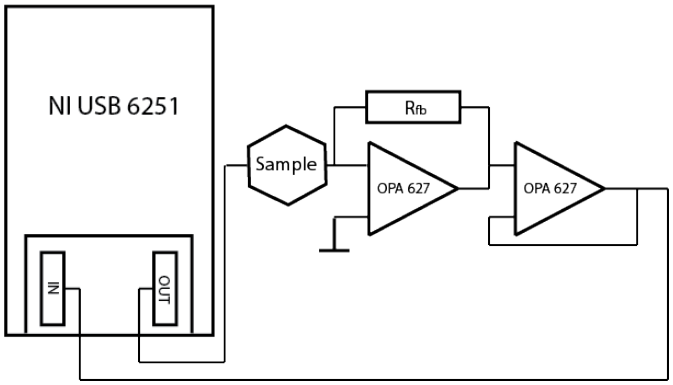

Figure 3-16 DAQ auto-balancing bridge circuit

3.5.2. Direct measurement method

3.5.2.1 . Software

First, the signal needs to be generated. The most straightforward way is to generate an array with all measurement frequencies. For ease of use, these frequencies are all equally spaced to fit a logarithmic scale. The arbitrary wave is then composed by adding all frequencies with equal amplitude of one. Next the wave is rescaled so it would not to exceed the maximum allowed excitation voltage. The signal is then placed at the output and after three waveform cycles processed by the PC.

A few steps need to be taken before the impedance can be calculated. The formulas previously discussed are only valid for a single waveform. To use the same formulas for an arbitrary wave, the signal needs to be divided in its individual frequency components. A complex algorithm based on the Fourier transform and a search a find function is first used on the out- and input signal. The function evaluates the whole spectrum, calculates the amplitude values on each measurement frequency, compares and places all values in an array format. The software then computes the impedance value and phase depending on the chosen circuit. Next, the values are displayed in a graph and stored on the hard disc. The flowchart of the measurement software is displayed in **Figure 3-17**.

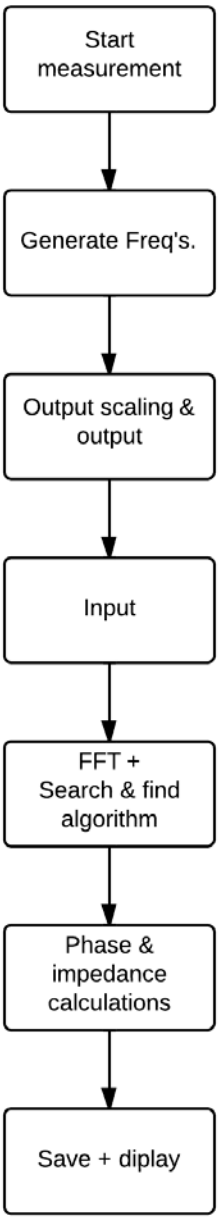

Figure 3-17 Flowchart direct measurement method

3.5.2.2 . System evaluation test

This measurement method yields good results for small frequency ranges. When measuring impedances over larger ranges, this method has some limitations. For example, a series circuit of a resistor with a resistor/capacitor in parallel reduces the measurement range significantly. This can be seen in **Figure 3-18**, where the average value for 250 measurements of a 330 Ω resistor in series with a 2 KΩ resistor and a 330 nF capacitor with the IV-convertor circuit is shown. For the first part of the measurement the impedance is in range with the feedback resistor, giving nice results. At higher frequencies the impedance of the sample drops giving a higher amplification which distorts the returned signal. This difference in amplification level can be explained by evaluating all frequency components as single signals. For lower frequencies the signal amplification level is around one while at higher frequencies, where the impedance drops with a factor of 10 and more, the signals amplification exceeds the allowed input voltage of the DAQ card. For the measured signal this unbalance leads to an incorrect result of the Fourier transformation. It can be concluded that for a limited measurement range of up to 2 decades with a well-balanced system, the maximum deviation of the measurement is around 1 %. This error goes up to 80 % making this technique unusable for extended ranges.

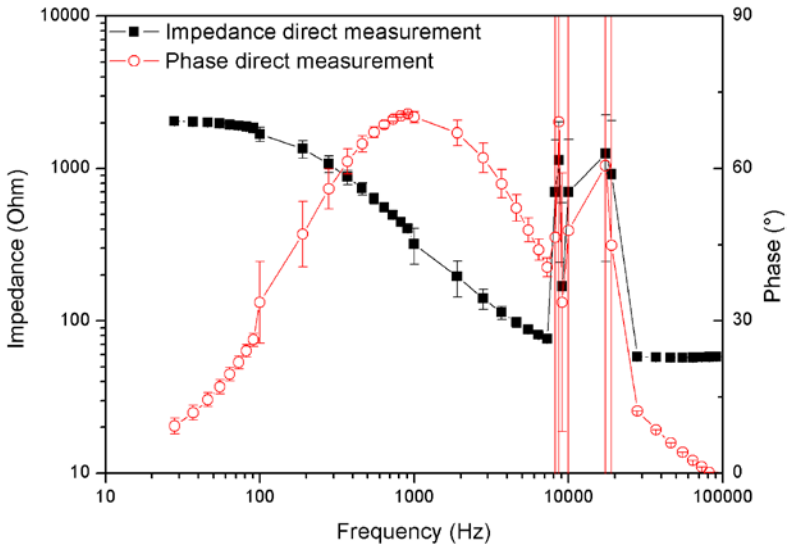

Figure 3-18 System evaluation test of a R-RC parallel circuit with the direct measurement method

3.5.3. Adapted waveform

A simple software solution can be used to overcome the above mentioned problem. By modeling the output signal, based on the sample under test, less signal power could be focused on lower impedances. To increase the signal to noise ratio the gained power can then be redistributed over frequencies where the impedance of the sample is too high, compared to the feedback resistor. This signal calibration has a second advantage, the power for frequencies with a large signal amplitude, and thus easily measurable, can be reduced leaving more power available for measuring extra frequencies.

3.5.3.1 . Software

The first step will generate the selected frequency and place them in the measurement array. Next, in contrast to the direct method, each frequency will be sequentially placed at the output with the maximum allowed excitation voltage amplitude. The impedance at each frequency is calculated from the signal returned from the sample, and placed in an array. This measurement is repeated, with a lower signal amplitude, for all frequencies where the input signal exceeds the maximum allowed input voltage.

When this scan is finished, the maximum peak to peak voltage together with these impedance values is used to calculate the optimal voltage at each frequency. First the signal amplification factor is determined using **formula (3-5)**. These values are then multiplied with the maximum allowed peak to peak voltage and summed together to calculate the total peak to peak value. This value is subsequently used to rescale the values to the desired excitation voltage. The summary of these steps can be found in **Formula (3-6)**

$$V_{fn} = \frac{V_{pp}}{\sum Amp_{fn} * V_{pp}} \qquad (3\text{-}6)$$

Next, these components are merged, to compose the adapted waveform and placed at the output. As with the direct waveform, three sequences of this resulting waveform are measured before being processed by the PC.

A complex algorithm based on the Fourier transform, an exact Blackman window and a search function is first used on the out- and input signal. The function evaluates the whole spectrum, calculates the amplitude values on each measurement frequency, compares and places all values in an array format. The Blackman window [112] is applied, during this conversion, to reduce the spectral

leakage caused by the windowing of the FFT. Next the software applies a filter to compensate for deviations caused by the transfer function of the OPAMP. The resulting signal is used to compute the impedance value and phase depending on the chosen circuit. Next, the values are displayed in a graph and stored on the hard disc. The flowchart of the software controlling the adapted waveform is given in **Figure 3-19**.

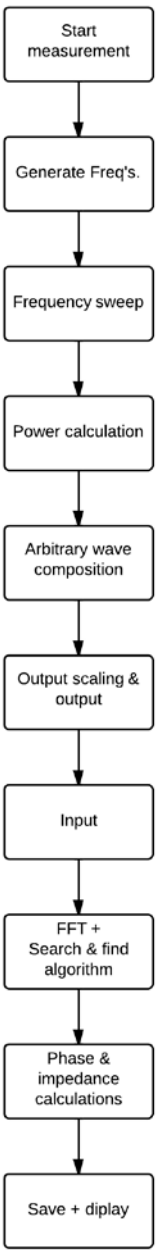

Figure 3-19 Flowchart adapted waveform method

3.5.3.2 . System evaluation test

The same circuit as in the previous measurement is used to compare a commercial HP 4294A impedance analyzer and the NI USB 6251. **Figure 3-20** shows similar results for the adapted waveform and the commercial device. Compared to the direct method the noise at higher frequencies, due to the bad signal to noise ratio, has disappeared. The maximum deviation between 250 measurements over 4 decades is 0.5 % and the magnitude of the adapted waveform is equal to the one measured with the commercial device. The biggest difference between the two setups is the speed. The Adapted wave form only needs 1 s to measure a frequency spectra from 10 Hz and 100 KHz while the HP 4294A needs about 30 s for a similar range. From the tested methods the adapted waveform shows the most promise to do a fast accurate frequency sweep.

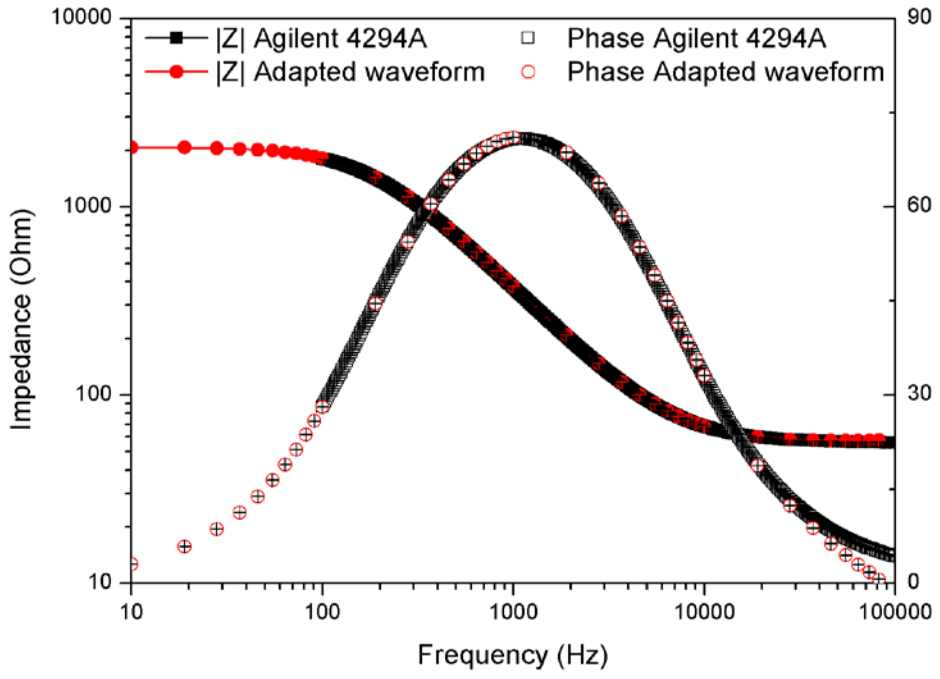

Figure 3-20 Comparasive impedance mesurement between the HP 4294A and the adapted wave form in a frequency window from 10 Hz to 100 KHz for an Randles circuit

3.6 µ-controller based impedance setup

3.6.1. Measurement system

Latest advances in electronics offer an increasing number of small form factor, high resolution analog in-output devices. Systems such as the raspberry PI, the beagle board, or other specific DSP [113, 114] systems are becoming widely available on the consumer market. Most of them have excellent processing capabilities but are still relatively high cost and sometimes lack a decent ADC convertor.

The Arduino community, is developing µ-controller solutions for a number of years, tries to make a compromise between these systems by combining less powerful processors with great I/O possibilities. To make these systems useful for impedance measurements a few basic conditions need to be met. First, the wanted frequency range needs to be determined. As with the other developed devices, the goal is to have a measurement range starting at 100 Hz up to 100 KHz. Following the Nyquist criteria the sample frequency should be at least twice the maximum frequency. Tests with the NI USB-6251, sampling at double the frequency gave unsatisfactory results. These experiments showed that a sampling rate of seven to ten times the maximum frequency keeps the error rate within 1%. For the ADC and DAC this would mean a minimum sample rate of 1 MSPS. Not only the sample frequency but also the resolution has a great influence on the measurement quality. Measurements with the previous systems showed that a 10-bit resolution should be sufficient for measurements with a peak to peak voltage of 1 V. The Arduino DUE (**Figure 3-21**) based on the ARM Cortex-M3 chip offers an on-board high precision 12 –bit ADC and DAC with a theoretical time resolution of 1 MSPS which is ideal for the proposed applications.

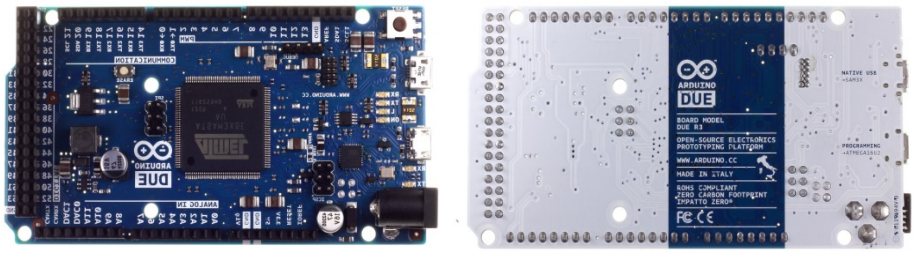

Figure 3-21 Arduino Due board

Before the sample can be connected with the device a few alterations need to be made. The DUE, just as the AD5933 chip can only handle positive voltages. The circuits previously discussed for the AD5933 chip can be reused for this design. Only the D.C. voltage added in the last stage of **Figure 3-7** is lowered to 1,5 V.

The use of the Arduino chip has other advantages. It is low-powered, has onboard memory and a processing unit which makes it possible to make a true standalone measurement device. As for most Arduino devices a lot of extension shields are available for the DUE. These shields can expand the number of usable measurement applications. In this design two shield layers are added to the Arduino DUE measurement board. The first layer contains an SD-shield with a WIFI module shown in **Figure 3-22**. The addition of the SD-card offers extended data storage to support the DUE's 512 KB flash memory for long term measurements. The WIFI controller can be used to remotely control the device and to retrieve the stored values. The 2nd layer is displayed in the right side picture of **Figure 3-22**. This empty breakout board is used for all I/O circuitry needed to connect the sample.

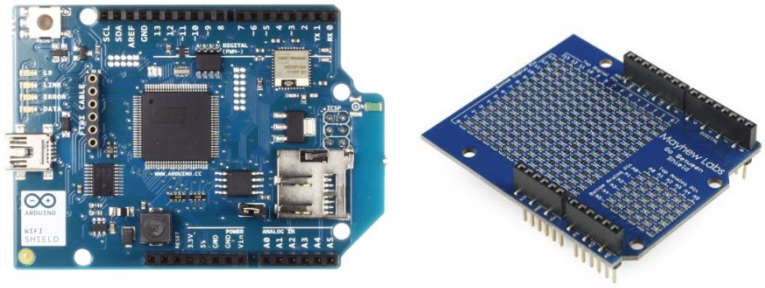

Figure 3-22 Arduino shields (left) WIFI module (right) breakoutboard

3.6.2. Software

Unlike the previously discussed systems, the Arduino has an onboard processor capable of controlling the impedances measurements. For test and power supply purposes the µ-controller was connected to the PC via USB. The chip was programmed in the Arduino development software. The flowchart shown in **Figure 3-23**, first declares the in- and output pins and then a txt file with header is generated. Subsequently, all values from a pre-stored file are placed at the output and are sequentially read and reconverted to a digital signal by the ADC. After a complete output cycle the RMS value is calculated and the zero crossings determined. The impedance is then calculated with the ratio of the RMS in- output signal multiplied with the value of the feedback resistor. The phase is determined by calculating the elapsed time between the zero crossings of the input and output signal compared to the total signal time. The calculated values are stored in the txt file on the SD-card. This file can be post evaluated with the discussed processing software.

The use of the Arduino software (**Figure 3-23**) has one disadvantage compared to the other user interfaces. If the measurement range, feedback resistor or the number of frequencies changes, the devices needs a complete reboot with the adapted software. These changes need to be programmed in the Arduino software directly. To increase the usability of the software a LabVIEW program able to program and control the Arduino is written. The software first creates an array with all measurement frequencies. Next, the needed amount of samples, corresponding with selected sample frequency, are calculated and stored in a text file. This file can then be uploaded to the Arduino and the measurement will start after the start button is pressed.

An average measurement starting at 10 Hz up till 100 KHz takes about 8 seconds and 132 mA/h. To turn the device into a standalone setup, a 9 V battery was connected to the second layer of the Arduino shield. The device is able to measure up to 48 hours with a one minute interval.

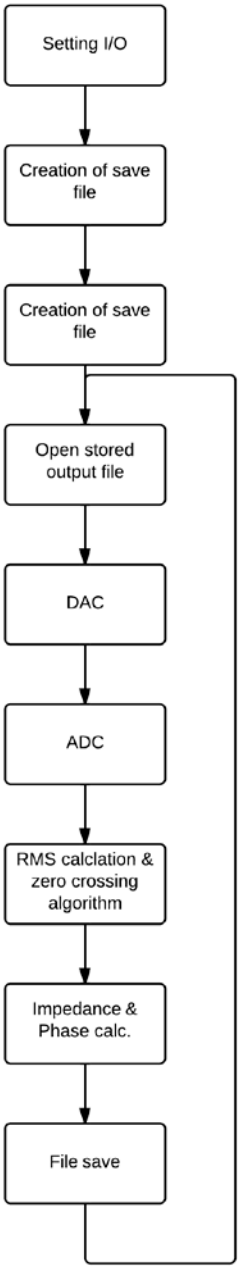

Figure 3-23 Flowchart Arduino software

3.6.3. System evaluation test

To evaluate the systems performance a series circuit of a 3,9 KΩ resistor and a parallel circuit of a 4,7 KΩ resistor with a 0,1 µF capacitor was compared to the calculated value, the arbitrary wave and the Arduino system. **Figure 3-24** shows the average impedance and phase of 250 measurements. The impedance values of the calculated and arbitrary wave correspond nicely with a standard deviation below 2%. The Arduino has a constant deviation of 150 Ω, this error can be corrected in the software and is caused by the dc offset voltage which is added at the input of the system. The Arduino has a voltage difference between the in- and output causing a small unbalance in the system which can be solved by a little tweaking. The phase of the calculated and arbitrary wave show perfect correlation, the DUE on the other hand has a large error above 3 kHz. This error originates from the zero crossing's algorithm random noise which interferes with the measurement signal causes false positive zero crossings. At higher frequencies the input signal is much smaller than at the low frequencies, making it more sensible for this random noise resulting in a higher error rate. If more feedback resistors would be added to the design this fault would drop significantly and the error would be in limit with the error rate at the lower frequencies.

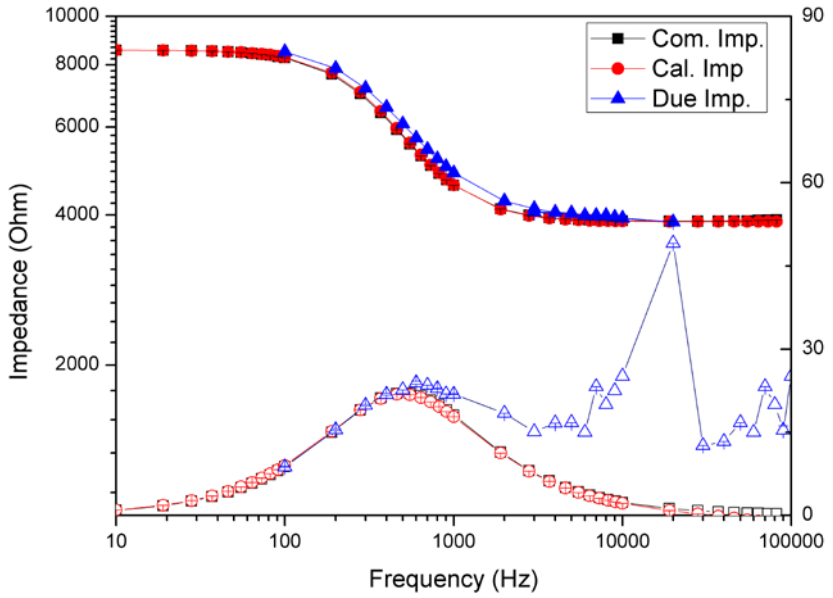

Figure 3-24 Compartive test between Arduino DUE, HP 4902A and the simulated value.

3.7 Dataprocessing

3.7.1. Analysis software 1.0

A separate program is written for post processing of the impedance data. The flowchart of this program is displayed in **Figure 3-25** First the data is loaded in the program, for now there is no automatic update of the data possible. Next, the user selects to either display the data in a Bode plot, a Nyquist plot or a time plot. For all display options it is important to select the channel of interest and, if needed, select a time stamp. Then the data will be displayed and the user can select data to save for export to data processing software.

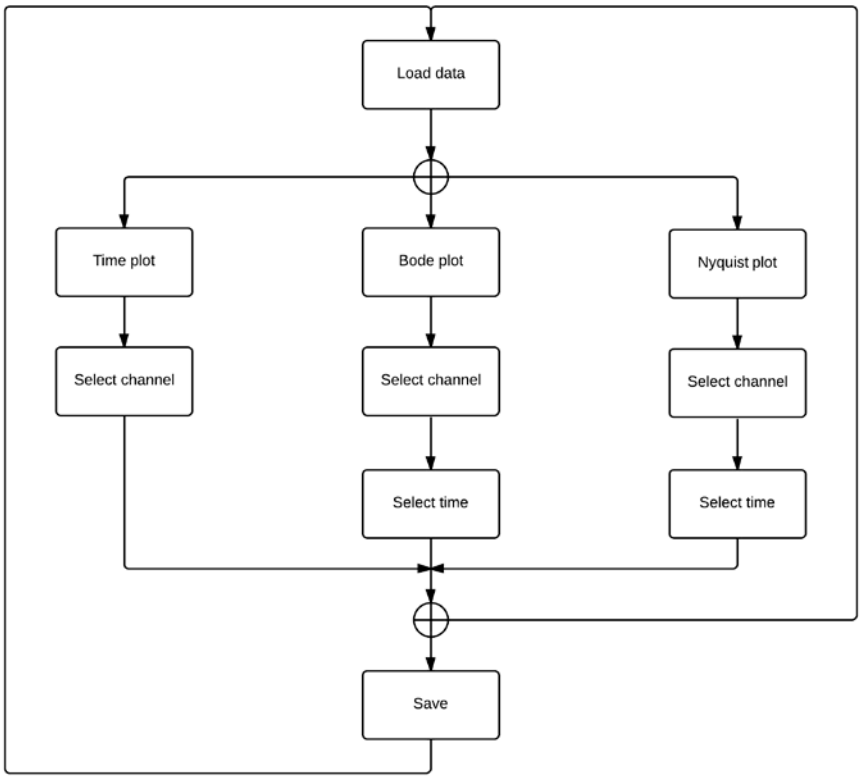

Figure 3-25 Flowchart analysis software v1.0

3.7.2. Analysis software 2.0

The first version of the software could only cope with a limited amount of measurement channels. To display the 96 channels, of the impediplexer, in one graph, a selection window is added to all subroutines of **Figure 3-25**.

For further evaluation of the measurement two additional subroutines are added to the software. The first routine recalculates all values depending on a selectable starting point following **formula (3-7)** and has 2 selection bars to display a chosen part of the measurement.

$$Z_{recal.\ n} = Z_n - Z_0 \qquad (3\text{-}7)$$

The second routine focuses on the fitting of measurement data, the proliferation measurements discussed in the following chapter follow a quadratic growth. For ease of interpretation a detection algorithm based on three well known fitting functions is incorporated in the software. The user can select to fit the data based on a least of squares, bisquare or least absolute residual function. The flowchart of the added functions is displayed in **Figure 3-26**.

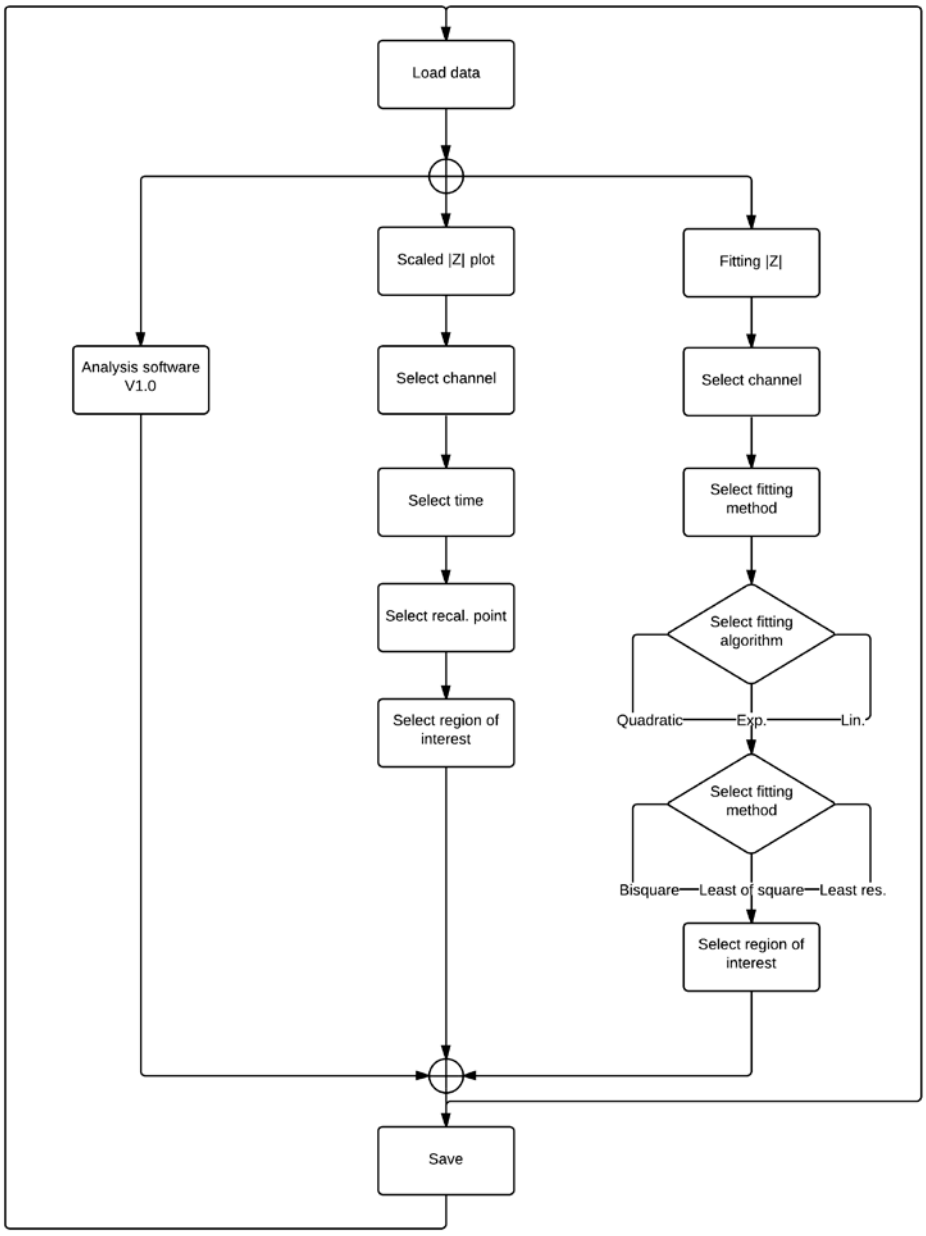

Figure 3-26 Flowchart analysis software v2.0

3.7.3. Analysis software 3.0

To further evaluate the impedance behaviour, an update version of the processing software was developed. Commercial software such as 'ZSimWin' [115] and mathematical software such as 'Matlab' [116] can be used to calculate an equivalent circuit of the measured sample. These packages can do a great estimation of the equivalent components at a certain point in time but they lack an easy display option for fitting over time. The third version of the evaluation software incorporates these functions in two subroutines. The first calculates the equivalent circuit of the sample at a chosen time. The function uses a Levenberg-Marquardt algorithm (LMA) [117], which is primarily used to solve least squares curve fitting problems. The LMA tries to fit a set of dependent and independent variables to the model curve, while minimalizing the sum of squares. **Formula (3-8)** shows this dependency.

$$S(\beta) = \sum_{i=1}^{m} [y_i - f(x_i, \beta)]^2 \qquad (3\text{-}8)$$

To theoretically calculate the magnitude and phase data of a known circuit at a known frequency, the real and imaginary components need to be determined first. **Formula (3-9)** for example can be used to calculate the impedance of a Randles circuit. The real value is a composition of the series resistor and the Re component of the parallel circuit. The Im part of the impedance only depends on the parallel circuit.

$$Re = R_s + \frac{R_p * \frac{1}{2\pi f C}^2}{R_p^2 + \frac{1}{2\pi f C}^2} \qquad (3\text{-}9)$$

$$Im = \frac{R_p^2 * \frac{1}{2\pi f C}}{R_p^2 + \frac{1}{2\pi f C}^2}$$

$$|Z| = \sqrt{Re^2 + Im^2} \; and \; \theta = \tan^{-1}\frac{Im}{Re}$$

To use the LMA algorithm to fit the data, these formulas need to be derived to make |Z| the dependent variable and Rs, Rp, Cp and f independent variables such as shown in **formula (3-10)**. Before the algorithm can calculate the components some initial guess values for the independent variables need to be given. Since the frequency dependency of such a circuit is known, this information can be used to calculate the best possible starting values.

$$|Z| = \sqrt{\left[R_s + \frac{R_p * \frac{1}{2\pi f C}^2}{R_p^2 + \frac{1}{2\pi f C}^2}\right]^2 + \left[\frac{R_p^2 * \frac{1}{2\pi f C}}{R_p^2 + \frac{1}{2\pi f C}^2}\right]^2} \qquad (3\text{-}10)$$

$$|Z| = \sqrt{\frac{4\pi^2 C^2 f^2 {R_p}^2 {R_s}^2 + {R_p}^2 + 2R_p R_s + {R_s}^2}{4\pi^2 C^2 f^2 {R_p}^2 + 1}}$$

The |Z| for example will start at it is maximum value and due to the changing reactance of the capacitor with a rising frequency, start to drop to it is minimal value as can be seen in **Figure 3-27**. The φ on the other hand will start at zero, rise till its maximum value, and then go back to zero. When the frequency is infinity the influence of the R/C parallel circuit can be compared to a short circuit making it an excellent starting value for the series resistance. At low enough frequencies, where the phase is zero, the capacitor has an impedance value close to infinity making the parallel and series resistance the only 2 impedance determining components. Here the parallel resistance is the impedance value minus the series resistance. The starting value of the capacitance is calculated at the maximum phase angle. The formulas used as initial guess values are summarized in **formula (3-12)**. However, in EIS experiments capacitors often do not behave ideally. Instead, they act like a constant phase element as defined in **formula (3-11)**. For a constant phase element, the exponent α is less than one. The "double layer capacitor" on real cells often behaves like a CPE, not a capacitor. While several theories (surface roughness, “leaky” capacitor, non-uniform current distribution, etc.) have been proposed to account for the non-ideal behavior of the double layer, it is probably best to treat α as an empirical constant with no real physical meaning. If the capacitor in the measurement circuit is replaced by a constant phase element the software uses the same formula as for the capacitor to determine the initial guess value a CPE constant of 1 is added for α.

$$Z_{CPE} = \frac{1}{(j\omega)^{\alpha} * Y_0} \qquad (3\text{-}11)$$

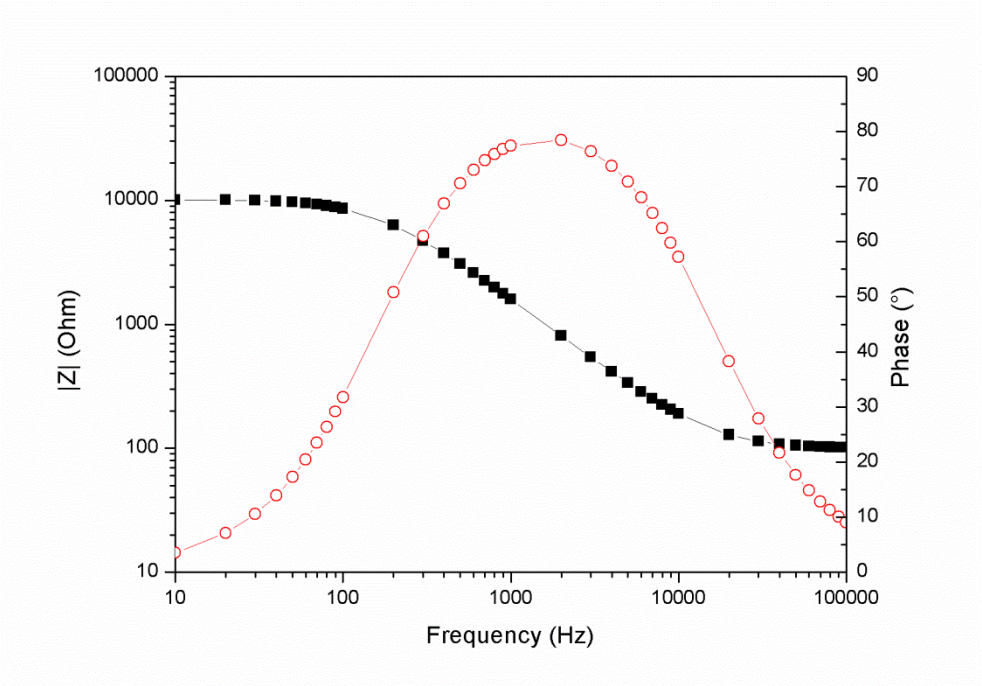

Figure 3-27 Impedance progress of the Randles circuit over time

$$f_{\infty} \qquad R_s = Re \qquad (3\text{-}12)$$

$$f_0 \qquad R_P = Re - R_s$$

$$\varphi_{90^\circ} \qquad C = \frac{1}{2 * \pi * f * Im}$$

These starting values gives good results but in experiments where only a limited amount of the frequency spectra is measured, however these starting values are not accurate enough to resolve certain measurements. In these cases the initial value for the series resistance stays the same but the formula for the parallel resistance and capacitor needs a little tweaking. This adaption is shown in **formula (3-13)** where the parallel resistance and capacitance depend on the Im and Re values at a frequency lower than the one used to determine the series resistance. After a number tests on of different impedance circuits, this combination of both the real and imaginary value as starting values yields the best fitting results and is thus incorporated in the software.

$$f_{\infty} \qquad R_s = Re \qquad (3\text{-}13)$$

$$f_{n<\infty} \qquad R_P = \frac{Im^2 + (Re - R_s)^2}{(Re - R_s)^2}$$

$$f_{n<\infty} \qquad C = \frac{1}{2 * \pi * f * \sqrt{\frac{{R_p}^2 * (Re - R_s)}{R_p - (Re - R_s)}}}$$

The 2nd subroutine focuses on measurements over an extended period of time. In many bio-analytical experiments the calculated equivalent circuit components change over time [118, 119]. To simplify analysis of these measurements the software performs an iterative fitting process using the algorithms presented in the first subroutine. The results are then displayed in separate time graphs for interpretation ease. The user is also able to save all relevant data in a format that can easily be integrated in data processing software such as Origin. **Figure 3-28** gives an overview of all the adaptions made to the previous processing software.

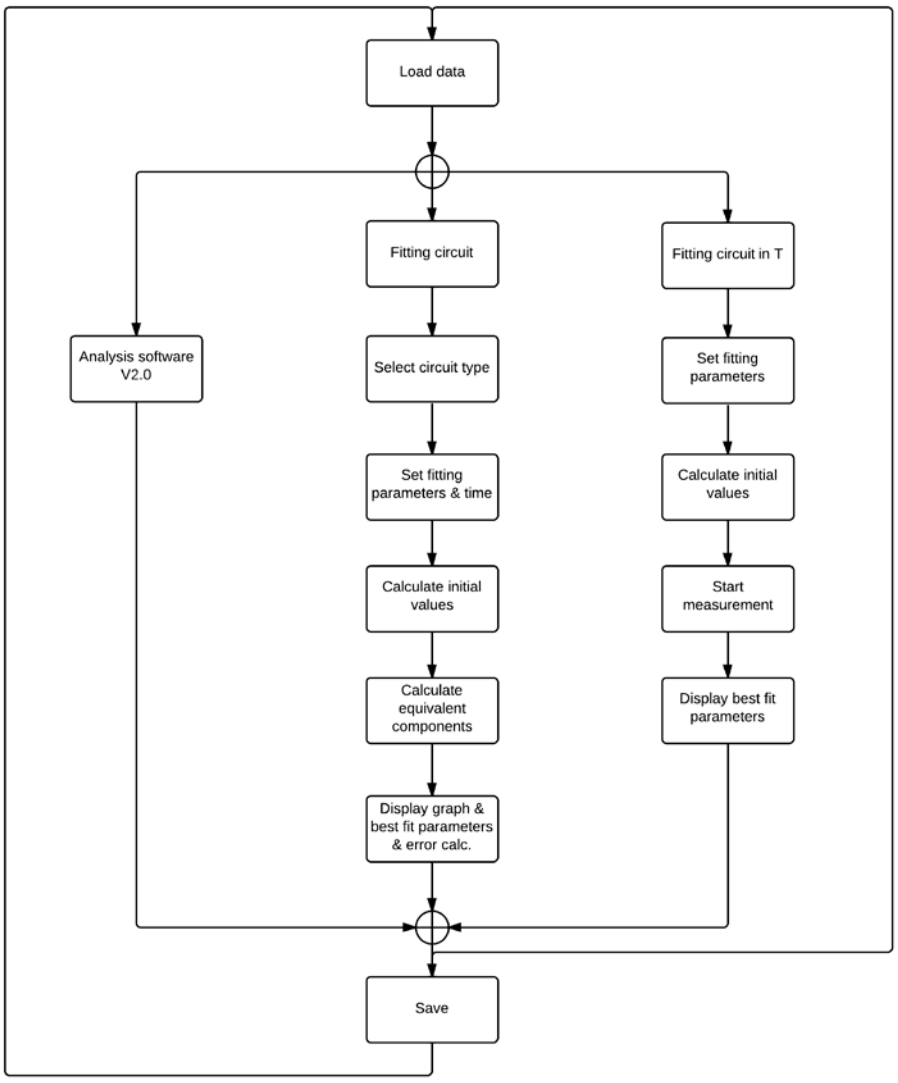

Figure 3-28 Flowchart analysis v3.0

3.8 Discussion impedance setups

Table 3-3 compares the four systems based on their measurement range, measurement time, voltage level, error rate and frequency range. The BioZ° gives excellent results in the range from 10 Ω up to 1 MΩ and a frequency range from 100 Hz to 100 KHz. But a measurement takes about 7 s and the system can only operate when controlled with a host PC. The arbitrary wave system on the other hand gives excellent results for the adapted waveform. A range from 5 Ω up to 4 MΩ in a measurement range from 0,1 Hz up to 100 KHz can be measured 3 decades at a time with a measurement time proportional to 10 times the lowest frequencies. The constant signal wave has a higher error rate and can only measure a smaller portion of the spectra. The system is still not truly standalone and the used hardware comes at a cost. On the other hand the Arduino system, which is a low-cost system based on commercial available components, has lower specs but the measurement system is standalone and only needs a few external components.

Table 3-3 Comparison between impedance, frequency, measurement time and error of the four presented setups

	BioZ°	**Direct waveform**	**Adapted waveform**	**Arduino DUE**
|Z| Range (Ω)	10 - 1 M	200 - 1 M	4 - 4 M	100 - 1 M
F Range (Hz)	100 - 100 K	10 - 100 K	0,1 - 100 K	100 - 100 K
Time	7 s	1 s	7 s	6 s
Error	0,1 %	3 %	0,05 %	2 %

Chapter 4
Applications

A number of different bio analytical applications are currently available for impedance based measurements [55, 57, 120-123]. To further evaluate the system performance in lab conditions a number of tests are adapted to interface with the different systems.

4.1 Measurement cells

There are numerous layouts possible for the interfacing between the measurement unit and sample under test. An important division can be made based on the electrode structure, number of channels, or method of target addition. The simplest setups use a conducting electrode at either side of the sample or the sample holder. This method is used for example in the liquid cell design, here the sensor layer is placed on top of one electrode while the other electrode is place inside the electrolyte [124]. Another electrode structure places the sensor layer on the electrode plane. This method is called the coplanar method. The addition of liquids to the sample can be as simple as adding droplets with a syringe to more complex microfluidic structures. The number of measurement channels can vary from a single cell to complete arrays.

4.1.1. Single channel addition cell

A single channel teflon addition cell was build using the two electrode setup. This sensor was designed for characterization measurements in lab setups and allows fast, stable temperature tests.

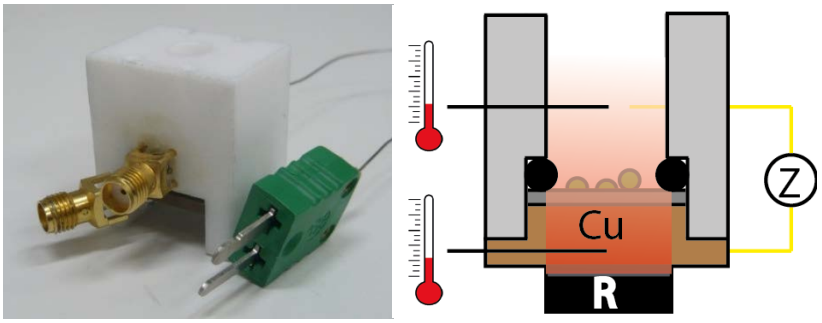

Figure 4-1 Single channel teflon addition cell

Figure 4-1 shows the liquid cell setup, the copper lid at the bottom functions as sample holder, measurement electrode, temperature conductor and, together with the O-ring, as sealing mechanism for the liquid container. The cylindrical measurement chamber can hold a maximum volume of 0.57 ml has a height of 20 mm and a diameter of 6 mm. An 22 Ω power resistor is connected to the copper lid for temperature control. The heat output of the system is directly proportional to the supplied power. The temperature is monitored with a K-type thermocouple connected in the liquid and copper.

The temperature of the system is closely monitored with a PID controller. A schematic overview of the unit is shown in **Figure 4-2**. The Pico Technology TC-08 data logger embedded in the system has an internal temperature reference [125]. The LabVIEW controlled system has 4 low voltage high power outputs available for connection with the power resistor. These channels use the LM675 high power voltage OPAMPs to buffer the voltage for each channel and a National Instruments 16-bit low-power DAC [126] to control the system.

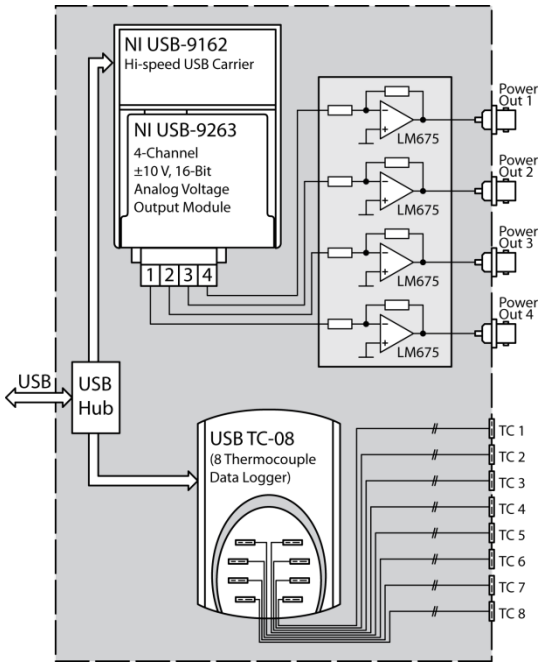

Figure 4-2 Temperature control unit

4.1.2. Four channel addition cell

Even though the temperature is closely monitored, artificial effects such as nonspecific binding or environmental changes can influence the results in biological measurements. If on the other hand a second sample with the same characteristics is introduced in the system, differential measurement between the sensor and a reference can help to rule out unwanted effects in the cell. A 4-channel measurement cell, based on the liquid cell design, was constructed for this purpose (**Figure 4-3**). The main difference is a 350 µl measurement chamber with four equally spaced mounting places more technical details can be found in [98].

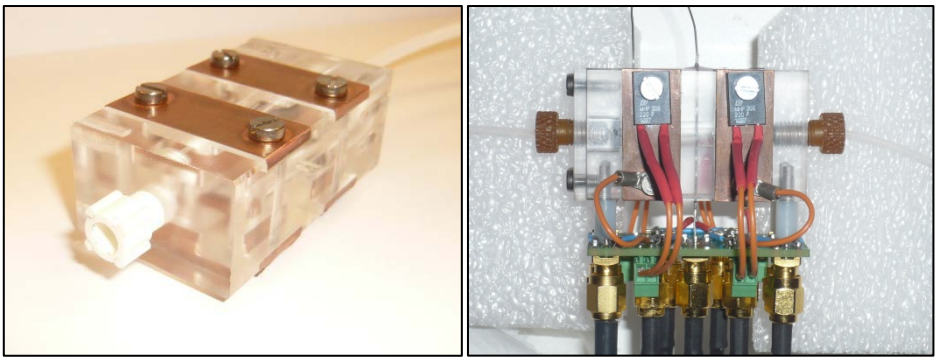

Figure 4-3 Four channel flowcell

4.2 Application 1: Electrolyte impedances and temperature dependency

4.2.1. Introduction

Since most biosensor measurements are performed in a liquid cell, the influence of different ionic solutions at different temperatures should be investigated to understand their influence on the measured impedance [127]. This section discusses measurements performed on a single well setup mimicking relevant DNA measurement concentrations measured with the single channel setup.

4.2.2. Methods and materials

4.2.2.1 . Chemicals

In the DNA measurement protocol of ref [128], PBS is used as buffer solution, NaOH to denature the DNA, and nuclease free water to dissolve DNA. For this test, a 1 l stock of 10x PBS was prepared by dissolving 80 g NaCl, 2 g KCl, 14.4 g Na_2HPO_4, and 2.4 g KH_2PO_4 in 0.8 l of distilled water. The solution was toped up to 1 l with 1 M NaOH solution purchased at VWR (Belgium) and Nuclease free water, containing diethylpyrocarbonate (DEPC) for DNA preservation obtained from Ambion Applied Biosystems (Japan).

4.2.2.2 . Setup

In **Figure 4-4(a)** the setup is represented which was used to measure the impedance of PBS at different concentrations. A nanocrystalline diamond sample (NCD), functioning as a working electrode, was mounted on a copper back contact using silver paste. Diamond has a high thermal conductivity, is transparent in a wide region of wavelengths, is chemically inert, has a wide electrochemical window, and can be made semiconducting by chemical doping [129]. Diamond is biocompatible allowing eventually for in vivo applications and, moreover, it is suited for covalent attachment of biochemical receptors [130-132]. A rubber O-ring with an inner diameter of 7 mm and a Teflon lid containing a circular opening of equal size was pressed onto the sample to create a reaction well. The well was filled with 140 µL of reaction fluid. A gold wire was placed in the fluid 1 mm above the NCD surface which is used as counter-electrode. Both were connected to the single channel impedance setup via 50 Ω coax-cables. All concentrations were measured in the same well to prevent crosstalk between different wells. The setup was put in an oven (Binder E28) at a temperature of 37 C° ±5 % and functioning as a Faraday cage. An identical setup, represented in **Figure 4-4(b),** was used to measure the impedance of all solution, at different temperatures. The same frequency range

and volume as in the previous test was used. The setup was put in the oven but now it was exposed to different temperatures, ranging from 37 to 50 °C.

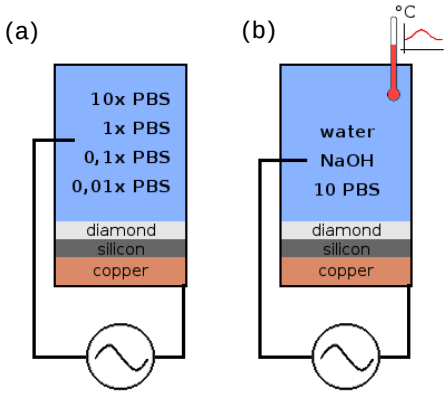

Figure 4-4 Experimental setup for impedimetrical differences at various concentrations of PBS (a), and various temperatures of nuclease-free water, NaOH and PBS (b)

4.2.3. Results and discussion

The impedance is measured for PBS at different concentrations (10x PBS, 1x PBS, 0.1x PBS and 0.01x PBS all with a volume of 140 µl) in a frequency range of 100 Hz to 100 kHz and an ambient temperature of 37 °C. All concentrations were measured in the same well to prevent inter-well confounding. In **Figure 4-5(a)**, the real and imaginary parts of the impedance are represented in a Nyquist plot. It can be observed that all concentrations show different plots and sequentially the lowest concentration shows the highest impedance and vice versa. Secondly, the temperature dependence of PBS, NaOH, and nuclease-free water was measured in a frequency range of 100 Hz to 100 kHz, with a volume of 140 µL; again the setup was put in an oven but now it was exposed to different temperatures ranging from 35 °C to 50 °C. In **Figure 4-5(b),(c) and (d**), the real and imaginary parts of sequentially NaOH, 10x PBS and nuclease-free water are represented in Nyquist plots for three different temperatures. It can be seen for all solutions that the greatest difference occurs in the lower frequency ranges. Furthermore, it can be seen in **Figure 4-5(b) and (c)** that for NaOH and 10x PBS the difference in impedance is the greatest in the temperature leap from 35 °C to 42 °C, both in real and imaginary part, unlike nuclease-free water where the greatest difference is found between 42 °C

and 49 °C, as shown in **Figure 4-5(d)**. To investigate the linearity of this process, the impedance of NaOH, 10x PBS, and nuclease-free water, when increasing the temperature, was linearly fitted for 100 Hz, 1 kHz, 10 kHz and 100 kHz providing a Coefficient of determination (R^2) as a measure for linearity. In table 1 it becomes apparent that the impedance decrease per increasing °C diminishes with rising frequency. However, a decrease in R^2 is observed above 11 kHz, probably caused by the parasitic capacitance described earlier.

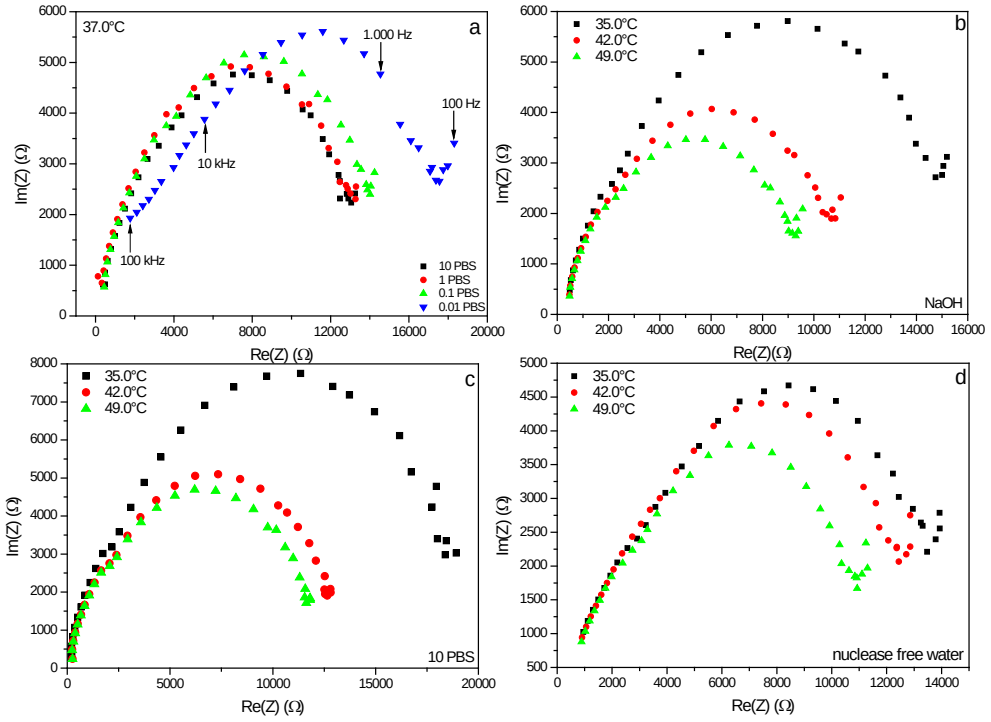

Figure 4-5 Nyquist plot showing the real and imaginary part of the impedance for 10x PBS, 1x PBS, 0.1x PBS and 0.01x PBS (a), for NaOH at 35.0 °C, 42.0 °C and 49.0 °C (b), for 10x PBS at 35.0 °C, 42.0 °C and 49.0 °C (c) and for nuclease-free water at 35.0 °C, 42

Table 4-1 Impedance decrease (%) per increasing °C for NaOH, 10 x PBS and nuclease-free water for 100 Hz, 1 kHz, 10 kHz, 100 kHz.

Fluid	Frequencies			
	100 Hz	**1 KHz**	**10 KHz**	**100 KHz**
NaOH	-3.1% (R^2=0.874)	-2.6% (R^2=0.879)	-0.7% (R^2=0.759)	-0.6% (R^2=0.830)
10x PBS	-3.1% (R^2=0.780)	-2.5% (R^2=0.789)	-0.8% (R^2=0.790)	-0.5% (R^2=0.691)
Nuclease free water	-1.7% (R^2=0.998)	-1.3% (R^2=0.905)	-1.0% (R^2=0.981)	-0.7% (R^2=0,951)

4.2.4. . Conclusion

These measurements demonstrate the accuracy and robustness of the system. The resolution is more than adequate for DNA measurements since hybridization gives a 20 % decrease in impedance as described in [128]. This was shown by the detection of different PBS concentrations and temperature effects in the liquid cell. At frequencies above 10 KHz the capacitive influence of the switching relay causes a measurement deviation. This capacitor was measured and compensated for in future measurements.

4.3 Application 2: Temperature dependency

4.3.1. introduction

Biological measurements are often performed under wet cell conditions at different temperatures. These temperatures for example include room temperature, 37 °C for in vivo applications and 70-80 °C for the monitoring of hybridization [128, 133]. Therefore, the unit should not only function properly when measuring solid state components, but also when measuring wet cell biosensors setups at different temperatures. This setup is tested on the multichannel, Arbitray wave and µ-controller based setup.

4.3.2. Methods and materials

4.3.2.1 . Chemicals

A 1 l stock of 10x PBS was prepared by dissolving 80 g NaCl, 2 g KCl, 14.4 g Na_2HPO_4, and 2.4 g KH_2PO_4 in 0,8 l of distilled water. The solution was toped up to 1 l with 1 M NaOH solution purchased at VWR (Belgium)

4.3.2.2 . Measurement protocol

A 10 x 10 mm boron-doped diamond substrate, a common immobilization platform for DNA sensors, was mounted into the single channel teflon cell, after which the cell was filled with 140 µl of PBS solution. Furthermore, a thermocouple was mounted into the copper and a second one was mounted in the fluid, to monitor the temperature. A heat profile ranging from room temperature to 85 °C for the BioZ° and from room temperature to 60 °C for the adapted waveform and Arduino Due was utilized to verify the functionality of the setup in the range of biologically relevant temperatures. These temperatures were applied in steps of 10 °C with a heating rate of 0.66 °C/min by a programmable hot plate. After each step the setup was allowed to stabilize for 15 min. After reaching the maximum temperature the setup was again allowed to stabilize for 15 min after which the setup was cooled down by means of convection, following the protocol as described above. This way a temperature range from 35 to 85 °C and 30 to 60 °C was obtained. During this process, the impedance was monitored with the BioZ°, the adapted waveform and Arduino Due by performing frequency sweeps from 100 Hz to 100 kHz with ten divisions per decade. The working and counter electrode of the cell were connected to the impedance unit with 50 Ω coaxial cables with SMB-connectors.

4.3.3. Results and discussion

Biological effects in wet cell conditions usually occur on the interface between an immobilization layer and an electrolyte [26, 128, 133]. This makes the interface region, and more specifically its distinct double-layer capacitance, the most interesting region for performing impedance spectroscopy. For this setup the double layer capacitance is mostly present around a frequency of 12.5 kHz.

4.3.3.1 . Handheld multichannel impedance setup

In **Figure 4-5** the impedance at 12.5 kHz is shown over time as well as the measured temperatures of both the copper and liquid. It can be observed that the measured impedance is inversely proportional to the cell temperature. The Nyquist plot, shown in **Figure 4-5** confirms that an increase in temperature causes a decrease in both real and imaginary impedance. Changes in the real impedance are related to resistive components, in this case most likely related to the purely resistive liquid. Higher temperature causes higher ion mobility in liquids, thus increasing conductivity and decreasing impedance. The imaginary impedance can relate to the diamond-PBS interfacial capacitance. Boron-doped diamond behaves like a semi-conductor, where an increase in temperature increases the number of free electrons and thus also increases conductivity.

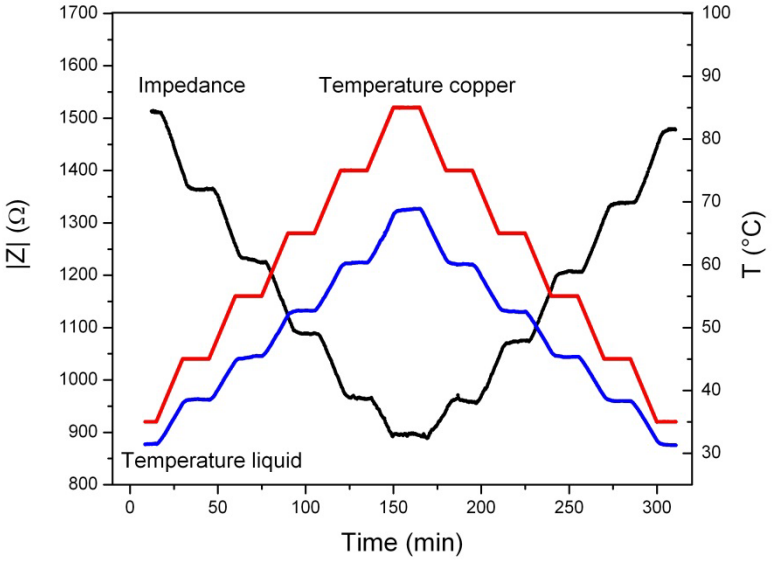

Figure 4-6 Impedance magnitude of a temperature profile 30 - 85 °C of a titanium substrate, in the teflon cell with a PBS buffer measured with the BioZ° at 12.5 KHz

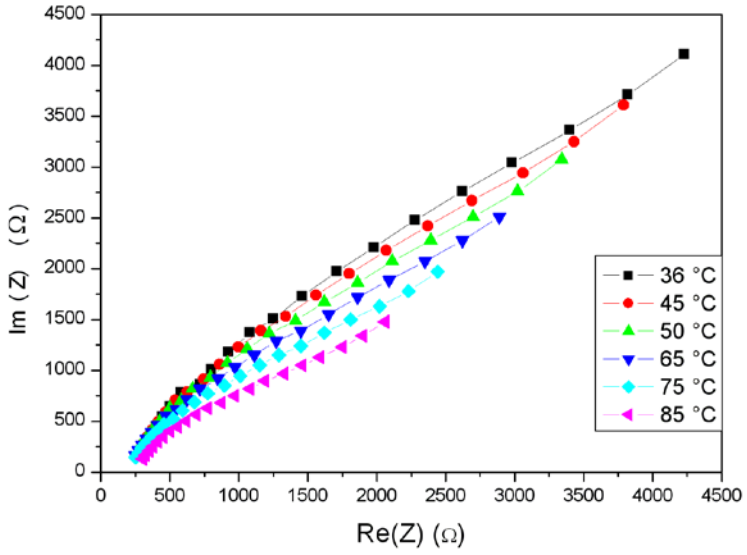

Figure 4-7 Nyquist plot of a temperature profile from 30 - 85 °C of a titanium substrate, in the teflon cell with a PBS buffer measured with the BioZ

4.3.3.2 . DAQ based impedance setup : Adapted waveform

In **Figure 4-8** the impedance at 12.5 kHz is shown over time together with the set and copper temperature for the heat profile ranging from room temperature to 60 °C. As with the BioZ°, the temperature is inversely proportional to the impedance and the signal stabilizes after each temperature step. However with a steady state error of less than 0.1 % and a measurement speed of 1 s, instead of 7 s, the arbitrary wave outperforms the previous setups in terms of speed and resolution.

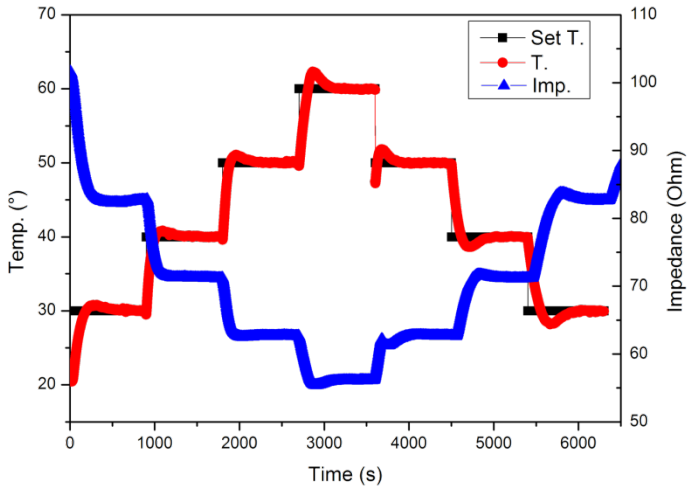

Figure 4-8 Impedance magnitude of a temperature profile 25 - 60 °C of a titanium substrate, in the teflon cell with a PBS buffer measured with the adapted waveform at 12.5 KHz

4.3.3.3 . µ-controller based impedance setup

Figure 4-9 shows the impedance at 12.5 kHz over time together with the set and copper temperature for the heat profile ranging from room temperature to 60 °C. Compared to the other systems the DUE has a lot of noise on the signal. The standard deviation of signal lies around 1 % but remains stable after each temperature stabilization step. The system is thus fitted for comparative measurements were a little standard offset is allowed

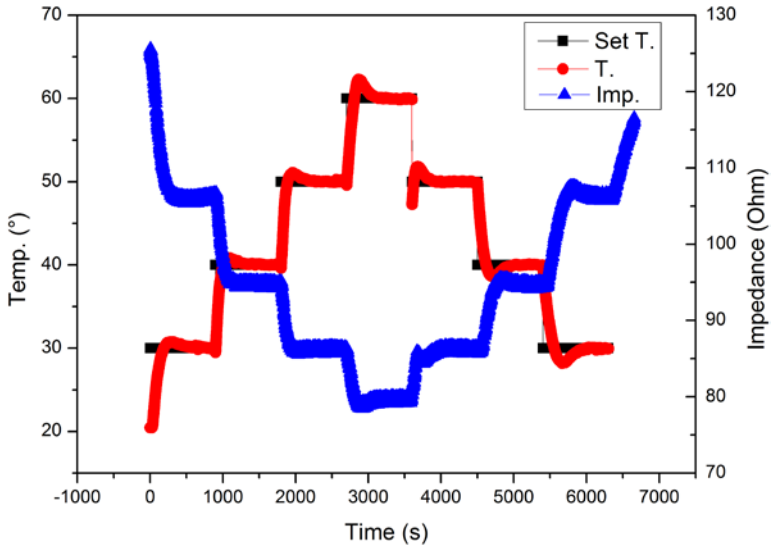

Figure 4-9 Impedance magnitude of a temperature profile 25 - 60 °C of a titanium substrate, in the teflon cell with a PBS buffer measured with the Arduino Due at 12.5 KHz

4.3.4. Conclusion:

A temperature profile of PBS, a common buffer in bioanalytical test, is measured with the BioZ°, the adapted waveform and the Arduino Due. The impedance for these setups is measured at 12.5 KHz where the double layer is most present. All devices are able to distinguish between the discrete temperature steps but the adapted waveform has the highest resolution and the fastest measurement time. The Arduino Due has a fixed deviation, as described in the previous chapter, and has a standard deviation of 1%. This setup is thus better suited for applications where a bit of noise is allowed and a standalone system is wanted.

4.4 Application 3: Biomimetic sensor

4.4.1. Introduction

Biomimetic sensors use a synthetic recognition layer to monitor biological events. These Molecularly Imprinted Polymers (MIPs) are produced with an imprinting technique which leaves cavities in a polymer matrix with an affinity to a certain template molecule. In this work, L-nicotine and histamine were chosen as template molecules and measured with the BioZ°.

4.4.2. Methods and materials

4.4.2.1 . Chemicals

L-nicotine, with chemical formula $C_{10}H_{14}N_2$, is a low cost readily available molecule. It can be detected in urine sample in concentrations ranging from 300 nM (non-smokers) to 6,3 µM (smokers). Previous research has shown the possibilities for nicotine MIP manufacturing, making it an ideal target molecule for device and sensor verifications [88, 134-136].

Histamine ($C_5H_9N_3$) is most commonly generated by mast cells and basophils and plays an important role in allergies [137] and the irritable bowel syndrome [138]. Bacteria in spoiled food are also known to release histamine making this an interesting target molecule in food industry applications [135, 139]. For example a sensor sensitive to histamine can detect the transformation of the amino acid histidine into histamine when fish starts to spoil. Similarly to L-nicotine this molecule was previously used as a target in impedimetric MIP sensors [95].

The chemical structure of these low-molecular weight molecules can be seen in **Figure 4-10** [140].

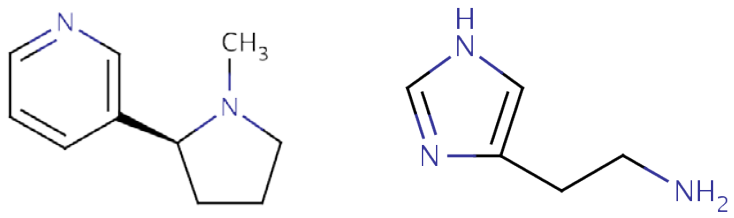

Figure 4-10 L-nicotine (left) and histamine (right) molecules

A 1 l stock of 10x PBS was prepared by dissolving 80 g NaCl, 2 g KCl, 14.4 g Na_2HPO_4, and 2.4 g KH_2PO_4 in 0,8 l of distilled water. The solution was toped up to 1 l with 1 M NaOH solution purchased at VWR (Belgium)

4.4.2.2 . Measurement protocol

Thin titanium plates of 10 mm by 10 mm were chosen as sensor substrates for the MIP immobilization. The main advantage of titanium, aside from being a material of choice for in-vivo applications like implants, is the natural occurrence of oxide layers on the surface. This allows silanization of the surfaces to enable anchoring of the sensor layer. Thorough cleaning of the substrates is required as a first step in this sensor immobilization process. The samples were first placed in an ultrasonic bath filled with isopropanol for 2 min. The cleaned surfaces were then subjected to a solution of 10 % y-MPS in toluene under nitrogen atmosphere for 3 hrs, after which they were rinsed with toluene and ethanol to remove unbound silane moieties. The MIP and NIP mixtures were subsequently introduced to the surface and heated to 65 °C for 10 min to activate polymerization. A top view scanning electron microscope (SEM) picture of the resulting MIP sample, consisting of a solid layer of MIP particles on the Ti substrate, can be seen in **Figure 4-11(left)**. **Figure 4-11(right)** shows a side view of the sample with the substrate and a layer of MIP flakes visible.

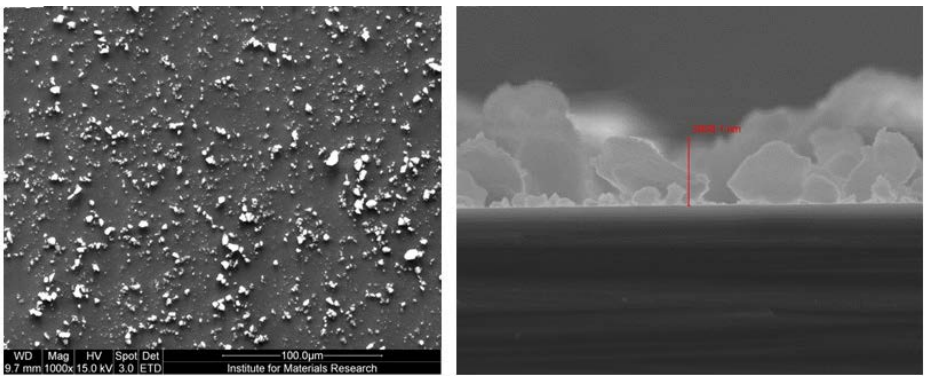

Figure 4-11 SEM pictures of the MIP layer immobilized on Ti substrate, top (left) and side (right) view of the sample

In biomedical readout applications the MIP sensors would be exposed to clinically relevant liquids containing an unknown concentration of target molecules. Here a PBS buffer was used to mimic biological conditions. This water-based salt solution functions both as a buffer as well as mimicking the osmotic concentrations and ion concentrations of fluids present in the human body. Analytes were prepared by dissolving varying concentrations of target molecule in this buffer solution.

Two aluminum working electrodes are covered with a conductive polymer loaded with either MIP or NIP particles. The four channel setup, discussed in **section 4.1.2** was used to mount the functionalized samples. In order to prevent impedance changes, due to temperature effects, the copper temperature was set to 37 °C for all measurements.

4.4.3. Results and discussion

Concentration curves are commonly used to demonstrate the applicability of biosensors in clinical settings. The impedimetric response of the sensor is measured when exposed to a range of (clinically relevant) concentrations. The samples were allowed to stabilize for about 1 hour after which increasing concentrations of nicotine were added, resulting in a total concentration range of 0.1 µM to 2 µM. The MIP layer was measured differentially against a NIP to rule out external influences on the signal. The concentration curve in **Figure 4-12** shows the impedance magnitude response of the differential MIP-NIP signal in respect to the values measured just before addition of the first concentration. These measurements were performed at a frequency of 150 Hz and fitted logarithmically with a least of squares fitting algorithm. The error bar in the graph display the standard deviation after signal stabilization. A differential response of 0.1 % is measured at the lowest detectable concentration of 200 nM, while the sensor seems to saturate at concentrations slightly above 1 µM. The sensor layer is thus sensitive enough to detect the nicotine level of a single cigarette (6.16 µM) but still needs some adjustments to reach the detection level of a urine test which is 1.23 nM [141].

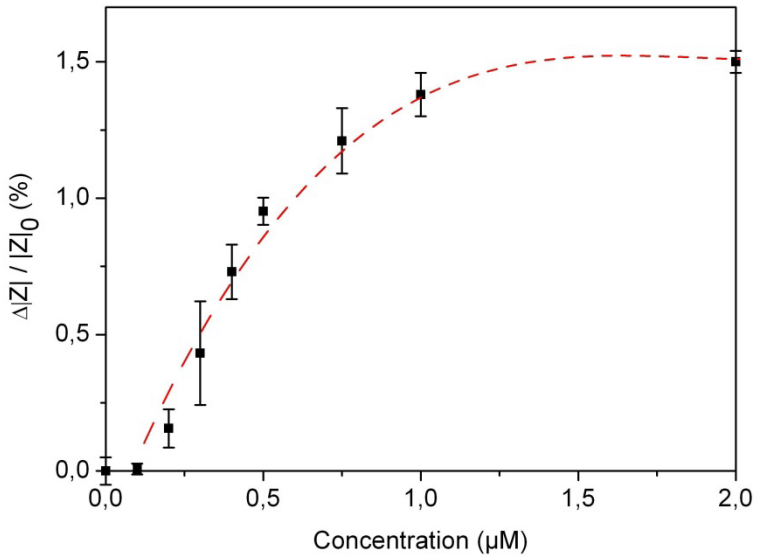

Figure 4-12 Impedance magnitude response of the differential MIP-NIP of Nicotine at 150 Hz

These measurements were repeated on a MIP-based histamine sensor. The impedance changes caused by the binding of histamine to the MIP layer was analyzed. **Figure 4-13** shows the response of the differential MIP-NIP impedance magnitude upon addition of 2 nM of histamine. Upon addition of the target molecule a slight decrease in magnitude can be seen. This change is most likely due to temperature differences between the added liquid and the buffer solution. After addition the impedance magnitude of the MIP increases significantly in respect to the impedance of the NIP. The response of the histamine is much higher in respect to the nicotine response. This could be related to differences in the sensor layer due to the different target molecule or the fact that sample are manually prepared and mounted into the measurement cells.

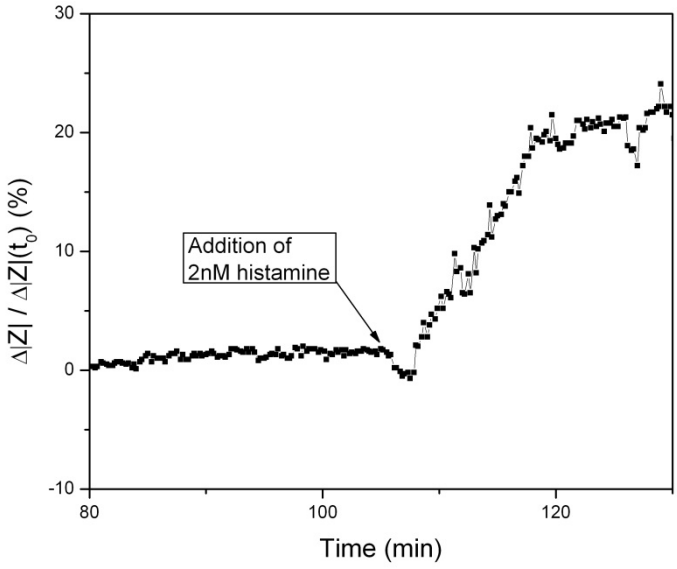

Figure 4-13 impedance magnitude response of the differential MIP-NIP for 2 nM histamine at 150 Hz

To better understand the mechanics of the impedimetric MIP read-out, the real and imaginary parts of the impedance were plotted. **Figure 4-14** shows the real part of the MIP impedance at the selected frequency of 150 Hz versus time, while the imaginary part can be seen in **Figure 4-15**. Upon addition of histamine the real part of both the MIP and NIP impedance increases towards a stable level which is most likely due to changes in the medium upon histamine addition. The difference in slope is possibly a consequence of the stabilization period of the MIP. Addition of histamine causes a decrease in imaginary MIP impedance of about 20 % while the NIP decreases only 2 %.

The signal response of the MIP particles are manifested most clearly in the imaginary part of the impedance. This is possibly due to the attachment of negatively charged histamine molecules to the MIP layer instead of the neutrally charged, highly conducting PBS. Their capacitive components cause an increase in capacitance, resulting in a decrease in capacitive reactance and thus also a decrease in imaginary impedance.

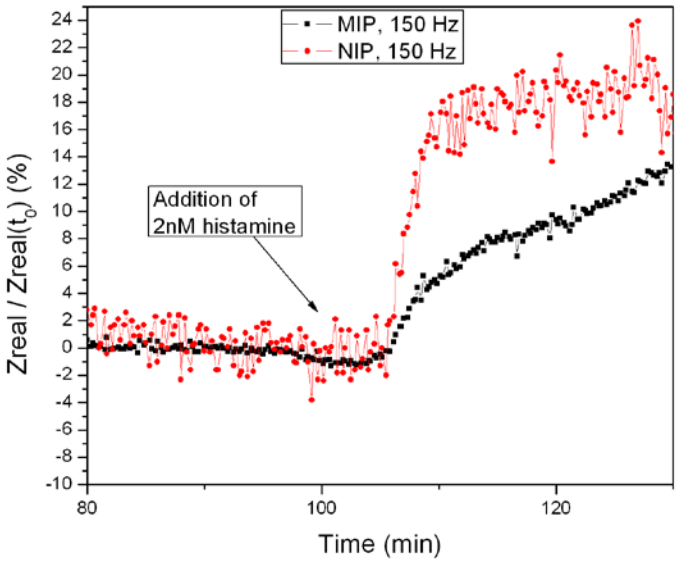

Figure 4-14 Real part of the MIP impedance at 150 Hz upon addition of 2 nM histamine

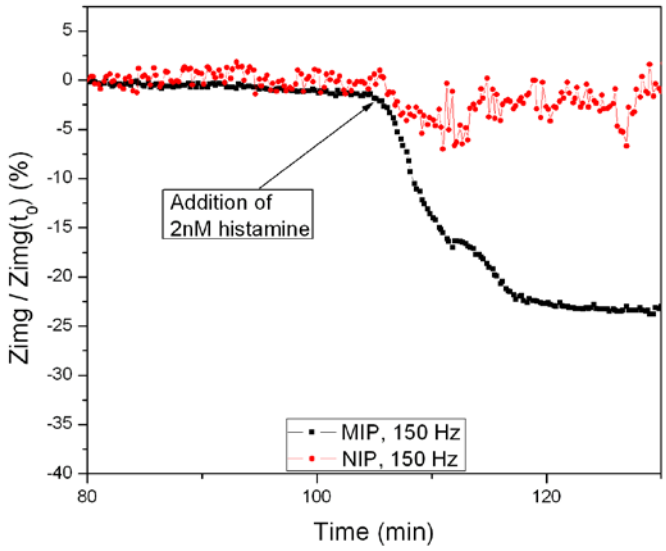

Figure 4-15 Real part of the MIP impedance at 150 Hz upon addition of 2 nM histamine

4.4.4. Conclusion

The impedimetric response of clinically relevant concentrations of histamine and nicotine were measured with the BioZ°. The setup was sensitive enough to detect the nicotine level of a single cigarette but the sensor layer still needs some adaptions to have the same sensitivity as the commercially available urine test. For the histamine sensor a level of 2 nM could be detected which is much lower than the concentrations relevant for food poisoning. The measurements indicate the possibilities of the impedance technique biomimetic sensor readout.

4.5 Application 4: Proliferation measurements

4.5.1. Introduction

Common day proliferation tests are mostly optical single end-point techniques [142, 143]. The use of absorbance, fluorescence or luminescence compounds necessary for these methods can severely interfere with the cell growth, which can affect the monitoring [144, 145]. Electrochemical impedance spectroscopy can provide an outcome for this problem. It is label-free and non-invasive monitoring can help to distinct behavior associated with the cell cycle. Previous examples include proliferation measurements on lymphocytes and leukemia cells [123] and ex vivo monitoring of cancer cell behavior [146]. Furthermore, this technique can be used in the readout of living cell based biosensors and has possible applications in the detection of cancer cells [147].

4.5.2. Methods and materials

4.5.2.1 Cells

Three different cell lines were used in this experiment Murine derived BV-2 cells **Figure 4-16 (left)**, Chinese hamster overy cells (CHO) **Figure 4-16 (middle)** and human embryonic kidney 293 cells (HEK293T) Figure 4-16 (right). Cells were cultured in flasks (NUNC, Roskilde, Denmark) with Dulbecco's Modified Eagle's Medium (DMEM), L-glutamine and high glucose (4500 mg/ml) without pyruvate (Invitrogen, Merelbeke, Belgium) supplemented with 10% fetal calf serum (FCS) and 100 µg/ml penicillin and 100 µg/ml streptomycin (1% P/S). The cells were incubated in a humidified incubator (5% CO_2) at 37 °C. After loosening the cells mechanically, the resulting cell suspension was centrifuged for 10 minutes at 800 rpm with a Jouan B3.11 (Thermo electron corporation, Waltham, MA, USA) and the cell pellet was re-suspended in fresh cell growth medium (DMEM).

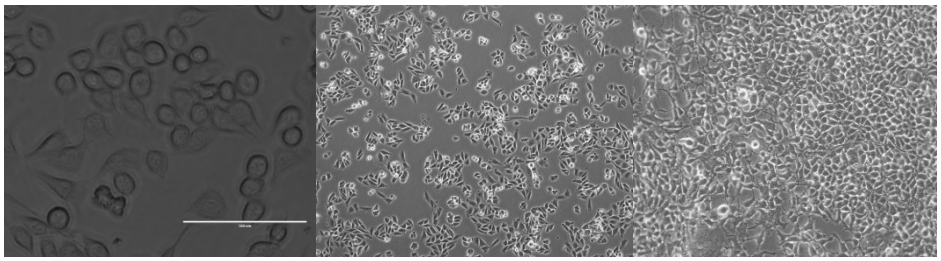

Figure 4-16 BV2 cells (left), CHO cells (middle) and HEK cells (right)

In proliferation measurements a biological cell undergoes four different phases. First, a lag phase where the bacteria adapts to the growth conditions. In this period the bacteria is not yet able to divide and the synthesis of RNA, enzymes and other molecules occurs. During the log phase the bacteria starts to multiply. The number of new cells depends on the present population and the available growth medium. The doubling of cells stops when the medium is depleted, in this stationary phase the number of new cells created equals the cell death rate. In the last phase, also known as the death phase, the bacteria die from starvation, too low or too high temperature, or the wrong growth conditions. **Figure 4-17** shows the kinetic curve of cell growth which can be modeled with a modified Gompertz model [149].

4.5.2.2 Measurement setup

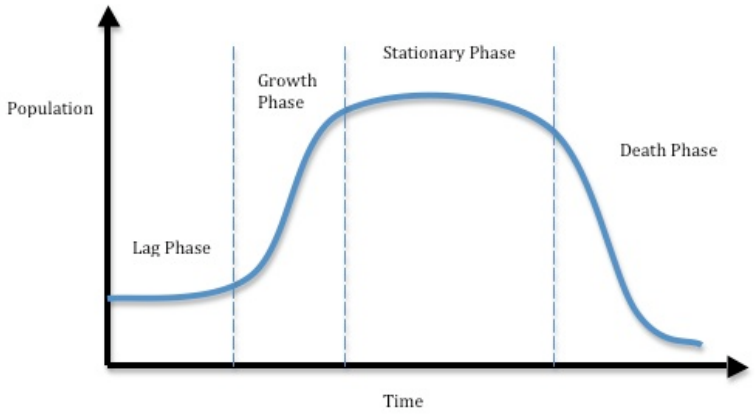

Figure 4-17 Modified Gompertz model for cell growth [148]

Cells were seeded on a Roche E-Plate 96 for quantification of cell proliferation. Each well with a dimension of 6.94 mm² has 16 interdigitated gold electrodes at the bottom with 80 µm finger electrodes. The impediplexer was used to connect the multichannel setup with the well plate and to switch between wells.

4.5.2.3 Spectral modeling

A Schematic view of a single well with cells seeded at the bottom together with its equivalent electrical circuit is given in **Figure 4-18** In this circuit the electrodes and the liquid commonly behave like pure resistors, as do present connectors and wires leading to the electrochemical cell. These are all summed together in the serial resistor R_S. The parallel circuit consisting of the double-layer capacitance Q_{dl} and resistance R_{dl} can be seen at the interface between a solid material and conducting liquid. The living cell on top of the gold electrode can also be reduced to a parallel Qc-Rc circuit.

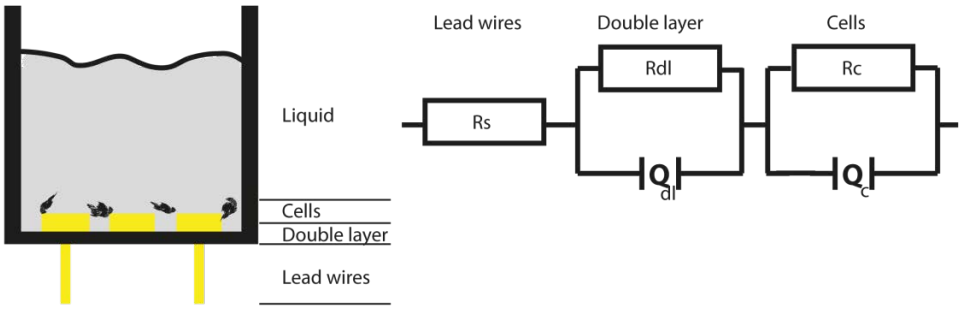

Figure 4-18 Equivalent circuit of the proliferation experiment

4.5.3. Result and discussion

4.5.3.1 Spectrum analysis

To gain insight in the behavior of each of the three analyzed cell types, an amount of 30000 cells/well of respectively BV2, HEK and CHO cells was seeded with 100 µl of DMEM medium into the wells. To rule out resistivity difference between measurements, the DMEM medium was identical for all measurements discussed. **Figure 4-19** shows the initial Bode plots after a stabilization period of 20 minutes. In the low frequency range, 100 Hz to 10 KHz, the impedance drops for the three cell types under study. This corresponds to the typical phase shift of capacitive components. At higher frequencies the phase goes towards zero which makes it possible to distinguish individual components with the

developed software. In the high frequency region of the Bode plot a differentiation in the impedance magnitude between the 3 cell types can be made due to differences in the surface coverage. When measuring an equal amount of CHO (15 µm), HEK (13 µm), and BV2 cells (8 µm) the CHO cells will, because of a larger double layer interaction caused by a higher surface coverage, show a higher impedance.

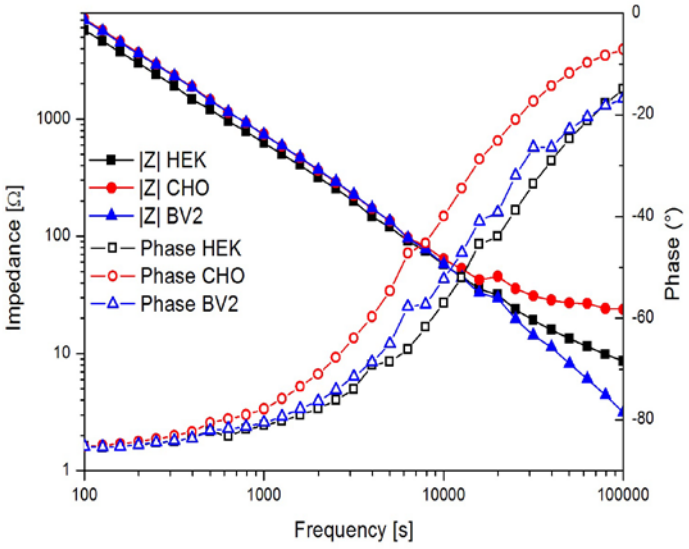

Figure 4-19 Spectral analysis from 100 Hz to 100 KHz of the BV2, CHO and HEK cells

Due to the limited frequency window, the influence of the cell resistance R_C and the cell capacitance Q_C cannot be discerned, and can thus be neglected in the equivalent circuit model. The remaining parallel R-RQ circuit is usually referred to as a Randles circuits [150]. Due to the compact size of the multiplexer on which the well plates are placed, the effect of lead and connector resistance can also be ignored. It can thus be concluded that the changes in magnitude of the impedance measured is primarily related to double layer (R_{dl}) and liquid resistivity (R_L).

4.5.3.2 Ideal excitation frequency

Although it is possible to monitor the electrode coverage by exciting the wells with the whole frequency range, a single ideal excitation frequency can be

determined to achieve the most distinct results and the most accurate monitoring of proliferation. To determine this ideal working frequency, the maximal impedimetric response was recorded for each measured frequency for the three cell types. An amount of 30000 cells/well of respectively BV2, HEK and CHO cells was measured twice in quadruplets for 100 hours. **Figure 4-20** shows the maximal response between 1 kHz and 100 kHz during the measurement time. The BV2 and HEK cells will reach a maximum at 20 kHz, while the highest response for the CHO cells is at 15 kHz. This is likely due to the denser surface coverage of the CHO cells. Most commercially available equipment will only evaluate a few frequencies between 10 and 100 KHz and take the average impedance change over this range and will thus have a reduced sensitivity for cell changes. This shows the advantage of performing a frequency sweep where the ideal frequency can be found and the detection limit can be optimized.

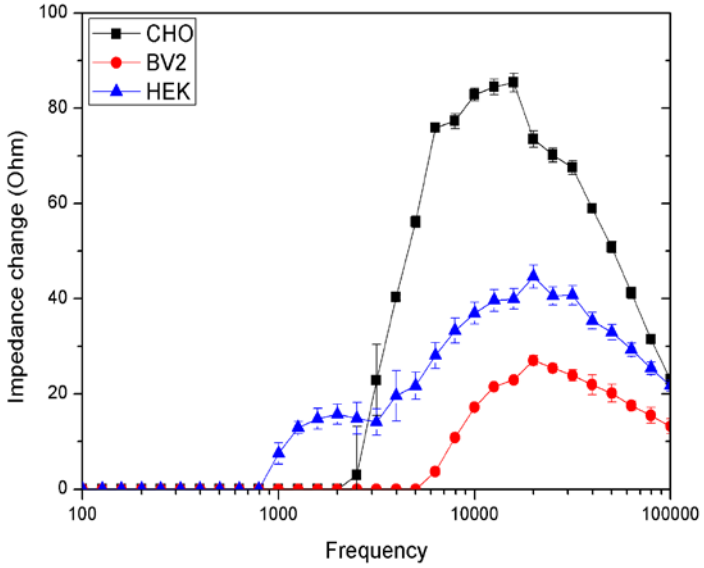

Figure 4-20 Maximum impedance response during cell growth of CHO, BV2 and HEK cells

4.5.3.3 Proliferation monitoring

To illustrate the practical usability of the setup, different amounts of BV2, HEK and CHO cells were continuously monitored over a time interval of 100 hours. Amounts of 1000, 3000, 6000, 10000 and 30000 BV2, HEK and CHO cells/well were seeded, together with reference channels only containing culture medium. These reference channels are used to rule out external effects, e.g. temperature fluctuations, which would affect the absolute impedance values [151]. The average impedance of the wells versus the measurement time is given in **Figure 4-21**. The measured impedance of the reference channel is subtracted from all channels. Measurements were performed at an excitation frequency of 20 kHz for BV2 and HEK cells and 15 kHz for CHO cells, as was determined in the previous paragraph. Since the measured impedance is related to electrode-cell interaction, one can see the evolution of population size for each concentration of seeded cells. The impedance change over time progresses differently for each cell type. The evolution and magnitude of this change depends on two factors, the size of the cells and their doubling time. BV2 doubles in approximately 15 h while HEK (24 h) and CHO (14-17 h) need more time to grow [152]. The monitoring of this dynamic evolution of growth can be advantageous for drug tests. For drug testing purposes classical end point methods, for example an absorption test [153] or an enzyme-linked immunosorbent assay (ELISA) only yields static data [154]. This cannot give a clear indication of the number of cells present in the setup. In such tests, EIS can be used to get an indication of the number of available cells, the cell type and the growth stage.

Since the starting impedance of the interdigitated structures at the wells can be determined, it is possible to have an indication of the number of cells present. When knowing the cell line, the magnitude of the impedance change and the measurement duration the graphs can be used to get an indication of the number of cells at the start of the measurement. If the doubling time of the cells in the specific medium is known and the start value would be multiplied with this factor, a rough estimate for the number of cells present in the well can be made. If on the other hand only the measurement time and the starting amount of cells are known, the evolution of the graphs can also be used to determine the studied cell type. For this purpose it is evident that a gross number of cells needs to be quantified with this technique in order to find the right growth curve.

The three discussed types all have different growth curves, which are reconfirmed over multiple measurements at different times and at different locations on the well plate. For example in **Figure 4-22 (top)**, a drop in impedance is noticed on all wells containing a population of BV2 cells. This drop during the stabilization phase is most likely due to nesting of the cells on the

electrodes. After this stabilization, an increase in impedance is observed on the wells containing the relatively high amount of 30000 cells. The wells containing lower amounts need more time to start their growth phase. The impedance reaches a distinct maximum after a certain time interval, when the maximum measurable population size is reached. After this maximum, impedance decreases almost exponentially and the medium changes from the normal pink to a darker yellow color. This is most likely caused by cell death which can be initiated by, among others, necrosis, apoptosis, or autophagy. Further research is needed to make a decisive conclusion. **Figure 4-21** shows pictures taken with the Zeiss Axiovert 100 to verify these findings. **Figure 4-21 (left)** shows the 30000 BV2 cells directly after seeding. The cells are spread all across the surface of the well and there is a large distance between individual cells. 30 h later, in **Figure 4-21 (middle)** the cells have already more than doubled their numbers and the cells are still growing. **Figure 4-21 (right)** shows the start of the cell death stage. In the center of the cells little black dots start to occur which indicate cell death. The HEK cells in **Figure 4-22 (middle)** exhibit a similar behavior as the BV2 cells, though these cells reach a maximum measurable population earlier, which results in a steeper rise time. The maximum CHO population (**Figure 4-22 (down)**) is reached after a similar time as the BV2 population, this population size is maintained much longer.

For future drug experiments these growth curve where used to determine the ideal starting concentrations. This concentration should be high enough to see the drug effects but low enough to be able to study their effects. For ease of preparation and monitoring this concentration was chosen so the cells would be in their growth phase after twenty four hours. For the BV2 cell line this was a concentration of thirty thousand cells while for the HEK and CHO cells a concentration of ten thousand cells seemed better suited.

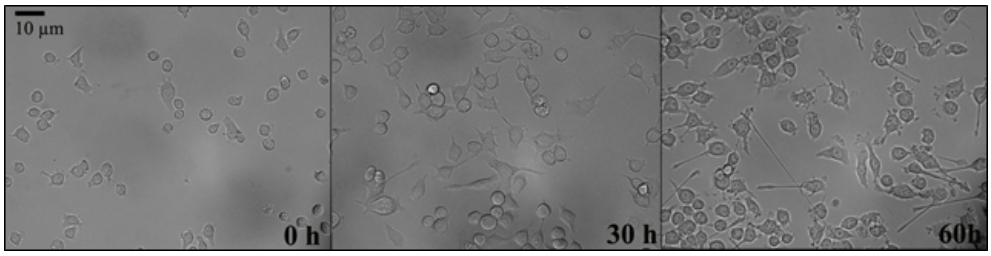

Figure 4-21 Growth of 30000 BV2 cells at the start (left) after 30 h (middle) and 60 h (right)

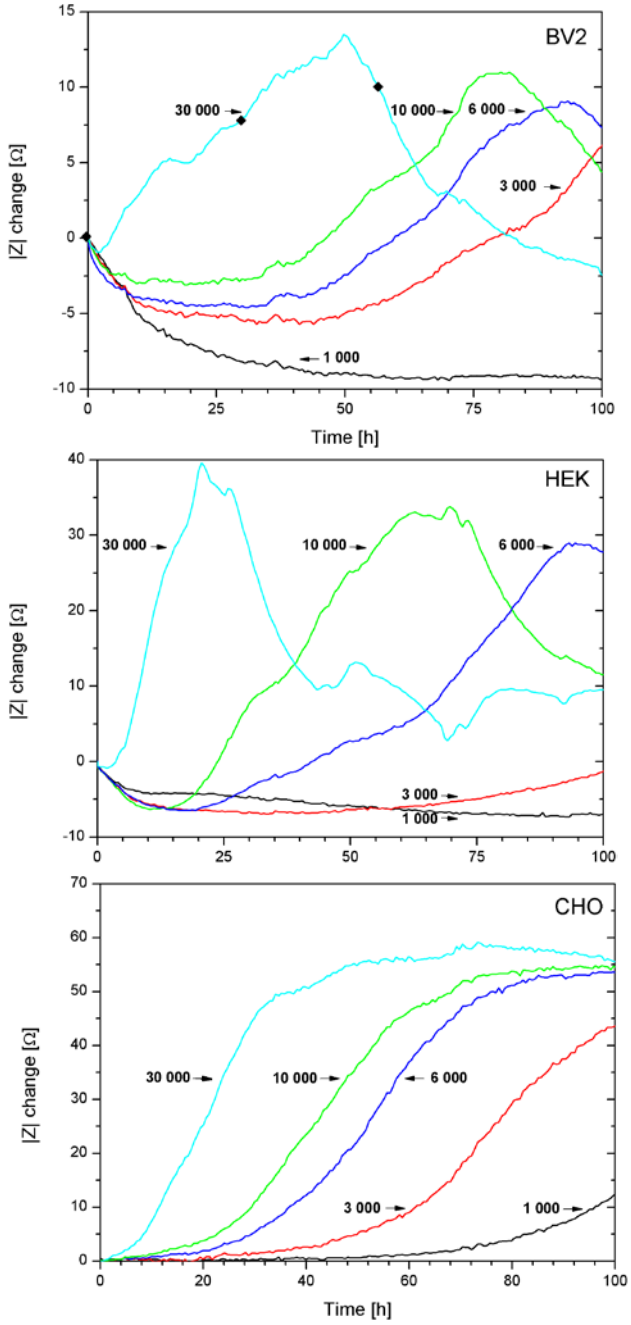

Figure 4-22 Growth curve of different concentrations of BV2 (top), HEK (middle) and CHO (down) cells

Converting the measured impedance and phase to the equivalent circuit could, since the measured difference is caused by an increase or decrease in electrode coverage, yield some more insights in the cell evolution. **Table 4-2**. Presents the values for this conversion using **equation (3-10)** at the start, maximum value and end of the measurement for an amount of 30.000 cells. A relatively small change, 17 to 43 Ω could be seen in the series resistor of the three types of investigated cells. The double layer components, on the other hand, have a larger change. The constant phase element value drops, for all cells, to approximately 0.5 µF. However, the parallel resistance of the different cells changes more diverse.

Table 4-2 Equivalent circuit values of cell growth

		Rs (Ohm)	Rdl (Ohm)	Qdl (µF)	n	R²
CHO	**T0**	103	53911	13,12	0,42	1
	Tmax	165	362899	0,67	0,64	0,99
	T100	165	286791	0,56	0,68	0,99
HEK	**T0**	43	51726,4	15,3	0,45	0,97
	Tmax	79	71834	18,8	0,44	0,99
	T100	66	115398	0,68	0,73	1
BV2	**T0**	63	66427	10,8	0,43	0,99
	Tmax	76	79500	22,9	0,31	0,98
	T100	70	108049	0,65	0,74	1

When the types of cells, their amount and measurement time are known than the state of the cells can be deduced from the graphs. This can be of interested for drug research, since some drugs might have a bigger impact at a different stage of cell growth.

4.5.4. Conclusion:

Experiments were conducted to test the compatibility of the impediplexer in proliferation measurements. The test showed that the impedance scanning did not interfere with the cell growth and has the advantage of continuous proliferation information. Next different amounts of cells were seeded to find the optimal starting concentrations for future drug tests. 30000 BV2 and 10000 HEK and CHO cells give a high enough response while leaving enough time to administer the drugs. The impedance setup thus seems perfectly suited for use in proliferation experiments.

4.6 Application 5: Drug test

4.6.1. Introduction

Neurodegenerative diseases such as Alzheimer's are the result of a progressive loss of function or structure of neurons. Although inflammation mostly does not take part in the initiation of these diseases, it can contribute to disease progression. The key players in these inflammatory responses are astrocytes and microglia [155]. BV2, used in the test experiments is a type of glial cells that are the resident macrophages of the brain and spinal cord.

4.6.2. Methods and materials

4.6.2.1 Cells

Murine derived BV-2 cells were cultured in flasks (NUNC, Roskilde, Denmark) with Dulbecco's Modified Eagle's Medium (DMEM), L-glutamine and high glucose (4500 mg/ml) without pyruvate (Invitrogen, Merelbeke, Belgium) supplemented with 10% fetal calf serum (FCS), 100 µg/ml penicillin and 100 µg/ml streptomycin (1% P/S). The cells were incubated in a humidified incubator (5% CO_2) at 37 °C. After loosening the cells mechanically, the resulting cell suspension was centrifuged for 10 minutes at 800 rpm with a Jouan B3.11 (Thermo electron corporation, Waltham, MA, USA) and the cell pellet was re-suspended in fresh cell growth medium (DMEM).

4.6.2.2 Drugs

First test studied the effects of direct and delayed addition of two growth promoters. Lipopolysaccharide (LPS), a bacterial-derived endotoxin considered to be an inducer of microglial activation and phorbol 12-myristate 13-acetate (PMA), a potent tumor promoter which activates protein kinase C in vivo and in vitro. Next two growth inhibitors, minocycline (MINO), able to block the secretion of inflammatory cytokines (IL-1β and IL-6) in microglial cells and apocynin (APO), an inhibitor of NADPH oxidase activity and thus effective in preventing the production of the superoxide in human white blood cells or neutrophilic granulocytes, are tested. Lastly a promoter/inhibitor mixture was measured to study the effects caused by combining the two.

4.6.2.3 Measurement setup

cells were seeded on a Roche E-Plate 96 for quantification of cell proliferation. Each well with a dimension of 6.94 mm^2 has 16 interdigitated gold electrodes at

the bottom with 80 µm finger electrodes. The impediplexer was used to connect the multichannel setup with the well plate and to switch between wells.

4.6.3. Results and discussion

4.6.3.1 Direct vs delayed addition

At the start of the measurement 30000 cells were seeded in the well plate. A concentration of 100 ng/ml LPS, 100ng/ml PMA, 2 mM APO and 400 µg/ml MINO. Together with a mixture of LPS (100 ng/ml) and MINO (400 µg/ml), LPS (100 ng/ml) and APO (2 mM), PMA (100 ng/ml) and MINO (400 µg/ml), PMA (100 ng/m) and APO(2 mM) was added to the wells. These mixtures together with a control line were tested in quadruplets. **Figure 4-23** shows the effect of direct addition of the compounds. Compared to the control signal the promoters show no significant change in growth speed. This is probably due to lag phase where the cells are still adapting to the growth conditions. The toxic effects of the inhibitors on the other hand show direct effect on the cells. In the mixed compounds the inhibitors seem to take the upper hand and the cells start to die.

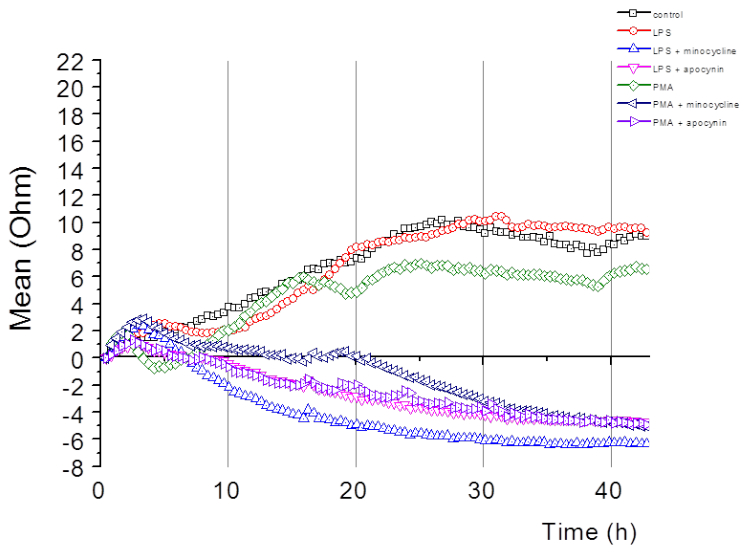

Figure 4-23 Impedance response over time at 20 KHz of the direct addition of promotors, inhibitors and a mixture of both to the BV2 cells

In the second experiment (**Figure 4-24**) the compounds are added after 12 h which should match the growth period of the cells. In contrast to the first test, PMA exhibits a positive effect on the cell growth even in combination with APO which shows the strong promoter effects of PMA. LPS on the other hand shows no effect on the cell growth. As with the direct addition, the toxic effects of the inhibitors cause cell death.

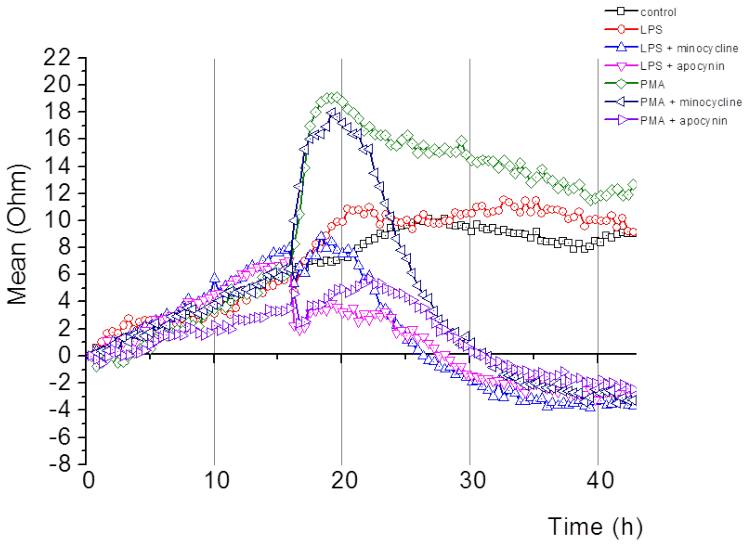

Figure 4-24 Impedance response over time at 20 KHz of the delayed addition of promotors, inhibitors and a mixture of both to the BV2 cells

An absorbance test was conducted during both measurements. This endpoint method was used after 16 hours and again after 24 hours to verify the results of the impedance measurement. In **Figure 4-25** A1 and A2 show the direct addition of the chemical compounds. As with the impediplexer, both promoters show no effect on the cell line while both inhibitors induce cell death. The measurements of the delayed addition also confirm the impedance measurements.

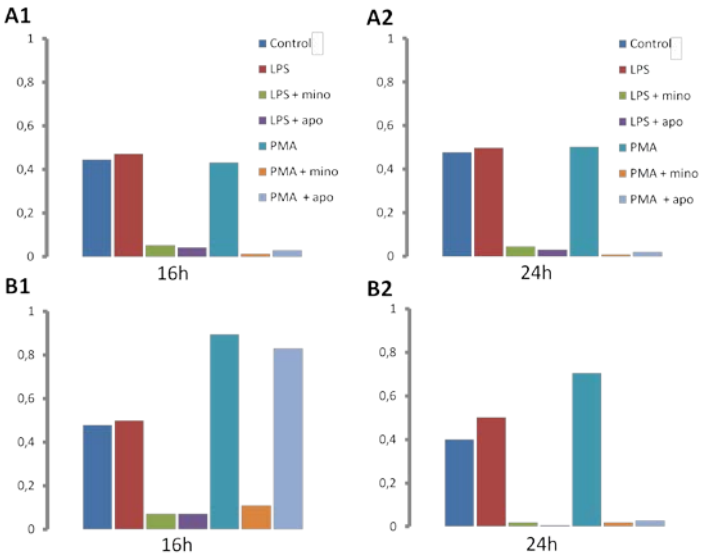

Figure 4-25 Absorbance verification test of the direct and delayed addition of different compounds on the BV2 cells

These measurements show that the growth phase is the best moment to evaluate the effects of a certain compound on cell growth. To truly test the effect of a compound on a cell, not only the addition time but also the compound concentration should be investigated.

4.6.3.2 Dose response test

In the final experiment for this setup the dose response of the pure compounds was measured. **Figure 4-26** shows the impedance change, for the different compounds over 24 h. In contrast to the first measurements, LPS shows an effect on the cell growth. It shows that the dose of the first experiments was too low to trigger the promoter effect. PMA shows to be a strong promoter for all concentrations. However, this fast cell growth causes faster depletion of the measurement medium causing early cell death compared to the control line. For APO and MINO a minimum concentration of the inhibitor is needed before the toxic reaction has an effect on the cells.

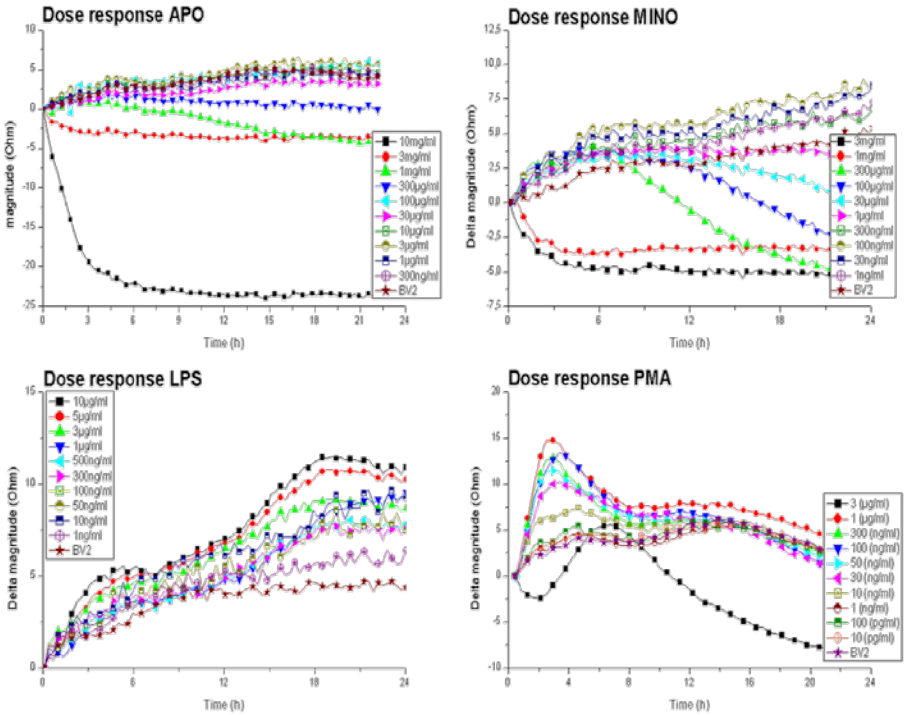

Figure 4-26 Dose response curves of different promotors and inhibitors at 20 KHz over 24 h

4.6.4. Conclusion

The effects of the different growth promoters and inhibitors of BV2 cell line have been tested with the impediplexer together with the BioZ°. If these drugs are added at the start of the measurement no change in impedance is observed for the promoters while the toxicity of the inhibitors does influence the growth. If the compounds are added during the growth phase the promoters do exhibit an growth enhancement. The promoter PMA even suppresses the effect of growth inhibitor Apocynin. These findings where verified with an absorbance test. Next the dose response of the different promoters has been established. Proving PMA as the strongest promoter and MINO the strongest inhibitor. The application of impedance scanning in drug research shows a lot of promise and can, in future applications, better identify the effects of compounds on different types of cancer cells and tumors.

4.7 Application 6: Aptamer sensor

4.7.1. Introduction

Peanut allergy is a lifelong disorder which can cause serious food related allergic reactions and in some cases even be life threatening. Detection of the allergen is commonly performed by immunoassay techniques relying on the use of expensive and relatively unstable antibodies. [156] Presents a novel aptamer sensor for the label free detection of Ara h 1, the most important peanut allergen. These Aptamers are peptides that can specifically bind to a target molecule. In this section the protocol and setup are reused to verify the systems response.

4.7.2. Methods and materials

4.7.2.1 Chemicals

The allergen, Ara h 1, was purchased from INDOOR biotechnologies (Cardiff, Wales) and used as received. The aptamer was obtained from IDT technologies (Leuven, Belgium) and had the following 80 base pairs sequence as described in [78].

5'TCGCACATTCCGCTTCTACCGGGGGGGTCGAGCTGAGTGGATGCGAATCTGTGGGT GGGCCGTAAGTCCGTGTGTGCGAA 3'

The 5'end was modified with an amino group and a C_6 carbon spacer. 1-ethyl-3-(3-dimethylaminopropyl) (EDC) was purchased from Thermo Scientific (Aalst, Belgium), 11-mercapto-undecanoic acid (95%), horse radish peroxidase (Mr ~ 40 kDa, HRP) and bovine serum albumin (Mr ~66.5 kDa, BSA) from Sigma Aldrich (Steinheim, Germany). All compounds used for the preparation of the buffers, 2-(N-morpholino) ethanesulfonic acid (MES) buffer, tris(hydroxyamino) methane-glycine-potassium (TGK) buffer and PBS buffer, were obtained from commercial resources (Sigma Aldrich and Fisher Scientific) and were of highest purity. Ethanol (anhydrous, 99.9%) was of analytical grade. Buffers were adjusted to the right pH by addition of hydrochloric acid (HCl) and sodium hydroxide (NaOH) solutions in MilliQ water.

4.7.2.2 functionalization method

The two-step functionalization method consists of forming a self-assembled monolayer (SAM) of thiols followed by the covalent binding of the amine modified aptamer via directed EDC coupling [131]. To reduce non-specific binding, the remaining part of the surface is blocked by immersing it into a bovine serum albumin (BSA) solution. After this step, the aptasensor is ready for use.

4.7.2.3 Measurement setup

The adapted waveform setup was connected to the Perspex flow cell with an internal volume of 110 µl onto which samples were mounted horizontally. A gold wire (diameter 500 mm) at a distance of 1.7 mm of the sensor surface was used as a counter electrode. The working electrode was pressed onto a copper lid, serving as a back electrode as well as heat sink. Miniaturized thermocouples were integrated in the heat sink and in the liquid (**Figure 4-27**). In previous research, this flow-through measurement sensor cell has been used for the electronic detection of serotonin in human blood plasma and of histamine in bowel fluid by MIP-type receptors [89].

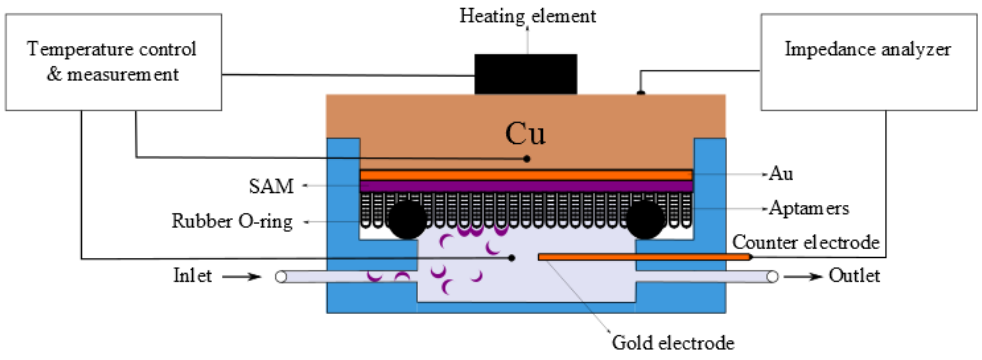

Figure 4-27 Measurement cell with temperature control unit

4.7.3. Results and discussion

The formation SAM layer could not be monitored in real-time due to use of the non-ionic solvent ethanol. The Nyquist plot of the sample were recorded directly after the formation of the SAM on the gold substrate and subsequently after the coupling of the aptamer to the surface. **Figure 4-28** shows the impedance data from 100 Hz to 100 kHz at 37.0 °C. In order to more precisely determine the effect of the different functionalization steps, the data was fitted with the developed software as a series circuit of a resistor with a resistor/CPE in parallel. After each functionalization step, significant changes in the Nyquist plots **(a)** and the impedance data **(b)** are observed. In the first step, the capacitance is affected by forming the SAM layer while aptamer attachment resulted mainly in an increase of the charge transfer resistance. The effect on the parameters of the three element circuit is given in **Table 4-3**.

Table 4-3 Equivalent circuit of Gold, Gold+SAM and Gold+SAM+Aptamer

	Gold	**Gold + SAM**	**Gold + SAM +aptamer**
Rs (Ω)	1191	1234	1678
Cbio (µF)	1.2	0.41	0.4
Rbio (Ω)	3687	1390	1220

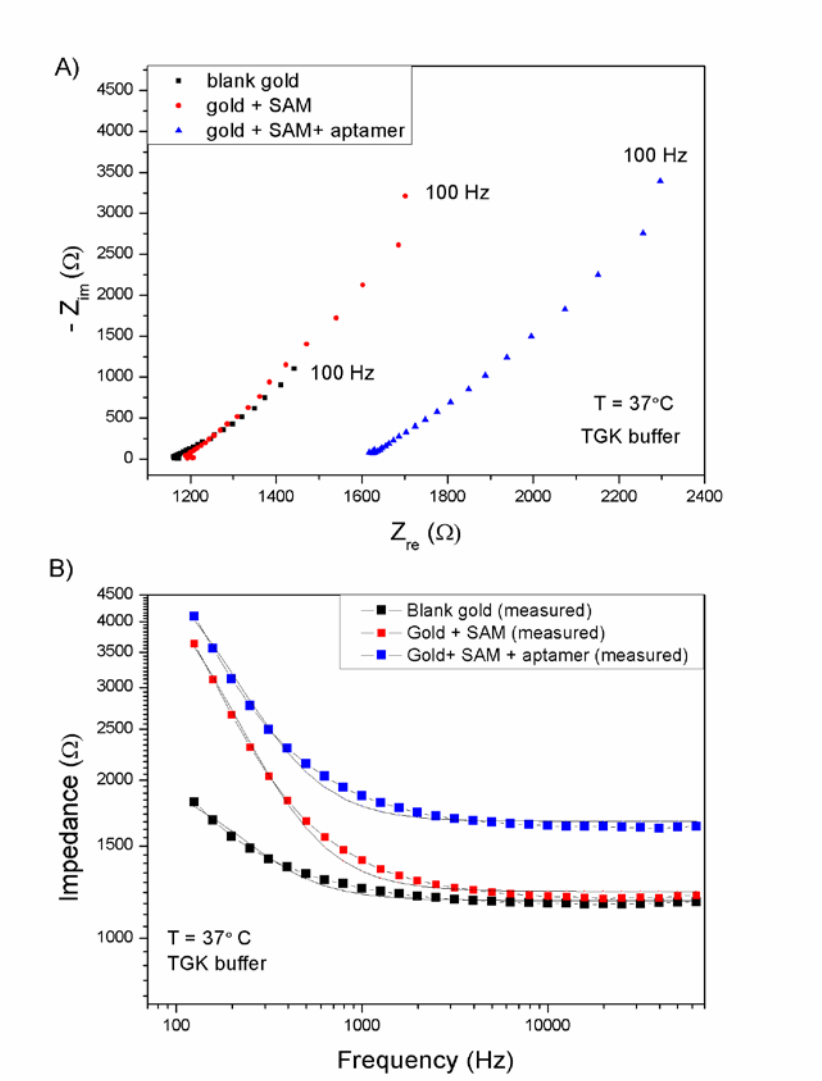

Figure 4-28 a) Nyquist plots obtained after measuring blank gold (black solid squares), the same sample modified with SAM (red solid circles) and followed by aptamer attachment (blue solid circles). b) This data was fitted with a three parameters equivalent circuit and the results of the measured (filled squares) and fitted (solid lines) impedance data are shown. The frequency and impedance are both plotted logarithmically. All measurements were performed in TGK buffer at 37°C

4.7.4. Conclusion

The different stages of the formation of the SAM layer could not be monitored in real-time due to use of the non-ionic solvent ethanol. However it was possible to use the impedance measurement technique to measure the final layers in a conducting buffer. The technique shows a lot of promise but still needs some adaption to be useful in the continuous monitoring of the layer formation.

4.8 Application 7: Electrical impedance tomography

4.8.1. Introduction

Electrical impedance tomography (EIT) is a non-invasive imaging technique which uses impedance spectroscopy to examine tissue and fluid conductivity. The conductivity of a biological sample depends on the free ion content and differs considerably between various tissues and different functional states. This property could be used to reconstruct static images of fat, bone or long tissue [146, 157, 158] or even image an acute stroke or epileptic seizure [159-161]. This section test the usability of the standalone impedance unit in these measurements.

4.8.2. Methods

4.8.2.1 Measurement setup

Two disposable Ag-AgCl electrodes (**Figure 4-29**) covered with a thin coating of a 0.5 percent saline base conductive gel were connect to the standalone impedance unit. The patches were attached 10 cm apart at the lower part of right arm.

Figure 4-29 Ag-AgCl electrode [162]

4.8.3. Results and discussion

Figure 4-30 shows the result of a full spectra frequency scan with the arm of the patient fixated in a right angle. The sweep shows a more resistive behavior at frequencies above 10 KHz with the phase angle going towards zero. In most EIT measurements [121, 163] a frequency window from 10 KHz to 1 MHz is monitored since most relevant changes happen at these frequencies. For following experiments the excitation was set at 82 KHz which is the highest measureable frequency of the standalone impedance setup.

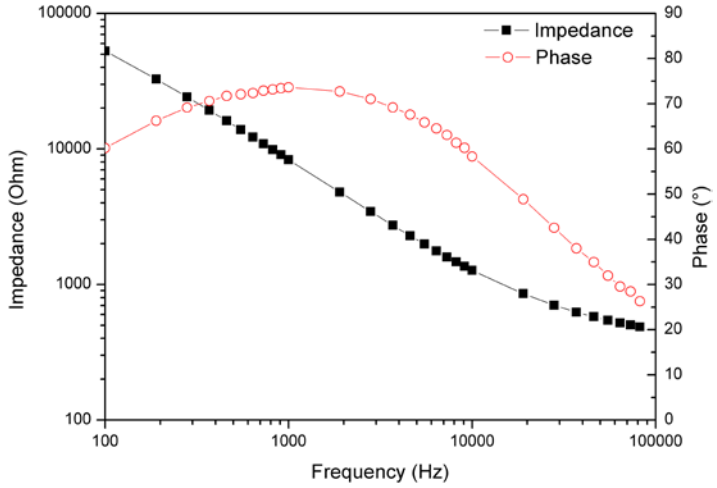

Figure 4-30 Impedance scan from 100 Hz to 100 KHz of the right arm of the patient

The second experiment monitors the impedance change of the right arm in two different positions at 82 KHz. The patient starts with the arm fixated in an right angle. After five minutes the arm is stretched and held upright for 5 minutes after which the experiment is repeated. The results in **Figure 4-31** show a fast stabilization after each fixation step of the arm. The noise of the measurement stays within a few ohm which is much smaller as the change caused by the different positions of the arm. This experiment shows that EIT is excellently suited for the characterization of biological tissues.

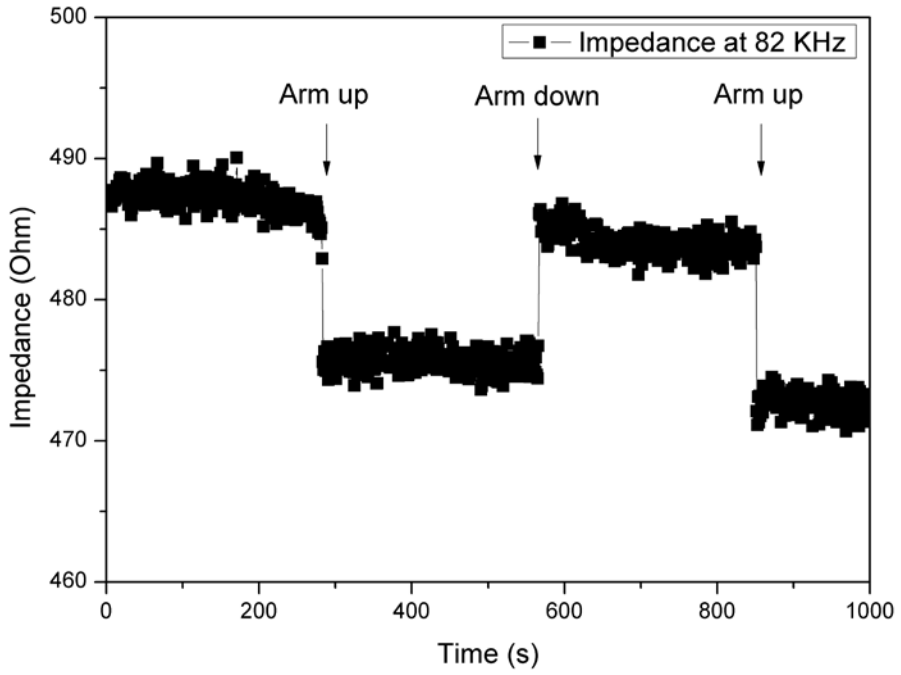

Figure 4-31 Impedance monitoring of different arm positions at 82 KHz

4.8.4. Conclusion

These experiments show that the standalone impedance analyzer, in combination with two Ag-AgCl electrodes is perfectly suited for the monitoring of biological tissue. The accuracy is high enough to distinguish between different arm positions and can be used, in future applications, to monitor the recovery of skin burns.

Chapter 5
General conclusions and future outlook

The constant evolution of biological sensors has given a boost to the development of new E-health applications. Glucose sensors, blood and pregnancy tests all use a biological recognition element to detect a physiological change. However the readout of these biomimetic layers still needs some research. One of the methods suited for this readout is Electrochemical Impedance Spectroscopy. This powerful, non-invasive measurement technique is a well- established method in the field of biological research. Although impedance analyzers are readily available, a combination of high cost, large form factor and lack of a user-friendly operating method makes them unsuited for home use or smart device integration.

5.1 Conclusion

This work tries to give a complete overview of the steps necessary to develop an impedance based system usable in bio-analytical measurements.

First, a commercially available development board, based on the AD5933 impedance chip, was adapted to perform basic measurements. The DC voltage of the output signal was removed before sample excitation, re-added at the input stage and an multiplexer board was added to broaden the impedance range.

The experiences and problems encountered during this design where used to build the BioZ°. An extra frequency chip was added, compared to the development board to enlarge the frequency range. To enhance the measurement resolution low noise amplifiers where utilized and a PCB, containing the setup was designed. This system showed a good resolution on static components and could measure an impedance range starting at 10 Ω up to 1 MΩ with an error below 0.1 %. The average measurement time for an

impedance sweep was around 7 s. This is fast enough for a basic measurement, however for fast changing systems or for large arrays this might not suffice.

An alternative measurement method using an arbitrary wave was proposed to speed up measurements. A commercially available high speed DAQ measurement card was adapted for this purpose. First a direct waveform was generated with equally powered sine waves. System evaluation showed that this method had to cope with large deviations and a limited frequency window. A second method adapted this waveform by calibrating the signal to the sample under test. This system showed an exceptionally fast response of one second, for a full frequency sweep, with an steady state resolution of less than 0.1 %.

Although these systems had a small form factor and where very accurate they still needed an external controller to process the measurement. For this purpose a system based on the commercially available Arduino DUE was designed to do standalone impedance measurements. Although the system has a lesser resolution it is able to perform standalone measurements.

The fourth chapter discusses possible applications applicable on each of the developed setups. These test showed that the impedance technique is perfectly suited for wet cell, DNA-, biomimetic and proliferation measurements [87, 106, 120, 122, 135, 164]. It offered a versatile scanning technique able to characterize a sample in the order of seconds while being noninvasive and adaptable to the different measurement needs. For example in proliferation experiments the use of an impedance readout can be used to continuously monitor the cells. Where in single end-point techniques the use of absorbance, fluorescence or luminescence compounds can greatly interfere with the cell growth and can affect the monitoring. **Table 5-1** gives an overview of the developed setups, their measurement range, measurement channels, standard deviation and control method.

Table 5-1 Overview of the different developt impedance setups

	AD5933	**BioZ° / impediplexer**	**Adapted arbitrary wave**	**Arduino DUE**
F. Spectrum	100Hz-100KHz	15 Hz - 100 kHz	0,1 Hz - 100 KHz	100 Hz-100 KHz
|Z| range	100 Ω – 1 MΩ	10 Ω – 1 MΩ	4 Ω – 4 MΩ	10 Ω – 1 MΩ
# channels	1	8 / 8 x 96	2	2
std	1 %	0.1 %	<0.1 %	1 %
standalone	x	x	x	v

This work showed that electrochemical impedance spectroscopy is a technique which, with some small modifications, is excellently suitable for bio-sensing applications. The proposed devices are all intended for lab use and enable the user to scan a large frequency spectrum with the ability to control the output voltage. A post processing program has been presented to evaluate the measurement data and to calculate the equivalent electrical components over time. Measurements on a wet cell showed that the setups were able to accurately measure temperature and solution changes relevant for the hybridization detection of DNA. The BioZ° and adapted waveform even showed that it was possible to detect small molecules such as histamine, nicotine and Ara h 1 with an synthetic recognition layer. The impediplexer, in combination with a measurement platform, proved to be a valuable real-time non-invading measurement system useful for cell cycle characterization and drug tests. These compact systems all needed a controller to initiate, store and display the measurement. The proposed DUE system was therefore focused on mobility. It uses an onboard controller to store the measurements on a SD-card. The addition of a WIFI controller makes it even possible to view and process data remotely.

5.2 Future outlook

Although this work is completely based on impedance spectroscopy as readout technique, the design strategies used can be converted towards other readout mechanisms. Recent advances include using the thermal resistivity of the biosensor layer for monitoring response. Similar to impedance spectroscopy this technique combines electronic readout with a non-invasive character and has been used with success for DNA SNP detection [165] and MIP's for detection of whole cells and for small organic molecules[166].

Future work could include porting the presented devices for this recently discovered measurement technique. A basic principles for smartphone-based thermal biosensor readout was already presented in [167]. Also the combination between impedance spectroscopy and other readout techniques could prove useful in biosensor characterization setups. Last but not least, the presented device could be used in applications other than biosensor readout. Impedance spectroscopy is used in numerous non-healthcare related industrial settings, including battery characterization [168], solar cell analysis [169] and oil quality testing [170]. The compact, user-friendly systems presented in this work can be a major improvement in respect to the commercial devices currently used in these settings.

References

1. Thomasnet. *Teardown: Google Glass More Than Sum of its Parts*. Available from: http://news.thomasnet.com/IMT/2014/08/07/teardown-google-glass-more-than-sum-of-its-parts/.
2. LG. *LG-Lifeband-SmartHealth-Review*. Available from: http://www.smarthealth.nl/review/wp-content/uploads/2014/05/LG-Lifeband-SmartHealth-Review.png.
3. Fitbit. *Wearables*. Available from: http://www.fitbit.com/.
4. Azoury, S.C. and J.R. Lange, *Epidemiology, Risk Factors, Prevention, and Early Detection of Melanoma.* Surg Clin North Am, 2014. **94**(5): p. 945-962.
5. Billington, C., J.A. Hudson, and E. D'Sa, *Prevention of bacterial foodborne disease using nanobiotechnology.* Nanotechnol Sci Appl, 2014. **7**: p. 73-83.
6. Chakravorty, S. and T.N. Williams, *Sickle cell disease: a neglected chronic disease of increasing global health importance.* Arch Dis Child, 2014.
7. Fan, Y., et al., *Estimating the Effectiveness of Early Control Measures through School Absenteeism Surveillance in Observed Outbreaks at Rural Schools in Hubei, China.* PLoS One, 2014. **9**(9): p. e106856.
8. Schora, D.M., et al., *Impact of Detection, Education, Research and Decolonization without Isolation in Long-term care (DERAIL) on methicillin-resistant Staphylococcus aureus colonization and transmission at 3 long-term care facilities.* Am J Infect Control, 2014. **42**(10 Suppl): p. S269-73.
9. Foxman, B. and L. Riley, *Molecular epidemiology: focus on infection.* Am J Epidemiol, 2001. **153**(12): p. 1135-41.
10. Google. *Google glass start*. 2014; Available from: https://www.google.com/glass/start/.
11. guardian, T. *Google smartwatches review: LG G Watch, Samsung Gear Live and Android Wear*. 2014; Available from: http://www.theguardian.com/technology/2014/jul/11/google-smartwatches-review-lg-g-watch-samsung-gear-live-android-wear.
12. Smarthealth. *Smarthealth review*. 2014; Available from: http://www.smarthealth.nl/review/category/reviews/activity-trackers-stappentellers/.
13. S. Black, I.K.a.D.S., *C-reactive protein.* J Biol Chem 2004. **279**: p. 48487-48490.
14. Cox Christophe, W.B., Machangu Robert, Billet Mic, and Ron Verhagen, *Rats for demining: an overview of the APOPO program*. 2003.

15. Ron Verhagen, C.C., Robert Machangu, Bart Weetjens and a.M. Billet, *Preliminary results on the use of Cricetomys rats as indicators of buried explosives in field conditions.*
16. Gardner, J.W. and P.N. Bartlett, *Electronic noses : principles and applications*. Oxford science publications. 1999, Oxford [etc.]: Oxford University Press.
17. Gardner, J.W. and P.N. Bartlett, *A brief history of electronic noses.* Sensors and Actuators B: Chemical, 1994. **18**(1–3): p. 210-211.
18. Turner, A.P.F. and N. Magan, *Electronic noses and disease diagnostics.* Nat Rev Micro, 2004. **2**(2): p. 161-166.
19. Medtronic. *Het MiniMed paradigm Veo-systeem- Een nieuw tijdperk in diabetesmanagement*. Available from: http://www.medtronic-diabetes.nl/productinformatie/paradigm-veo/index.html.
20. Mashable. *How the Samsung Galaxy S5 measures your heart rate*. Available from: http://mashable.com/2014/02/25/samsung-gs5-heart-rate/.
21. Dexcom. *Dexcom G4 platinum-system*. Available from: http://dexcom.com/.
22. Polar. *Heart rate sensor*. Available from: http://www.polar.com/us-en/products/accessories/H7_heart_rate_sensor.
23. Walmart. *Blood pressure monitors*. 2014; Available from: http://www.walmart.com/browse/home-health-care/blood-pressure-monitors/976760_1005860_1077045.
24. Parents. *10 Home pregnancy tests*. Available from: http://www.parents.com/pregnancy/signs/test/home-pregnancy-tests/#page=3.
25. Ybarra, C.M.a.G. *Fundamentals and Applications of Immunosensors* Available from: http://cdn.intechopen.com/pdfs/33741/InTech-Fundamentals_and_applications_of_immunosensors.pdf.
26. P. Cooreman, R.T., J. Manca, M. vandeVen, V. Vermeeren, L. Michiels, A. Ameloot and P. Wagner, *Impedimetric immunosensors based on the conjugated polymer PPV.* Biosens Bioelectron, 2005. **20**: p. 2151-2156.
27. Zou, Z., et al., *Functionalized nano interdigitated electrodes arrays on polymer with integrated microfluidics for direct bio-affinity sensing using impedimetric measurement.* Sensors and Actuators A: Physical, 2007. **136**(2): p. 518-526.
28. Hang, L., et al., *A high-performance DNA biosensor using polyhydroxylated fullerenol as 3D matrix for probe immobilization.* Electrochemistry Communications, 2014. **47**(0): p. 84-87.
29. Mashhadizadeh, M.H. and R.P. Talemi, *Application of diazo-thiourea and gold nano-particles in the design of a highly sensitive and selective DNA biosensor.* Chinese Chemical Letters, (0).
30. Shi, A., et al., *A sensitive electrochemical DNA biosensor based on gold nanomaterial and graphene amplified signal.* Sensors and Actuators B: Chemical, 2014. **200**(0): p. 206-212.
31. Blagus, T., et al., *A cell-based biosensor system HepG2CDKN1A–DsRed for rapid and simple detection of genotoxic agents.* Biosensors and Bioelectronics, 2014. **61**(0): p. 102-111.

32. Canbay, E., et al., *A microbial biosensor based on Lactobacillus delbruecki sp. bacterial cells for simultaneous determination of lactic and pyruvic acid.* Food Chemistry, 2015. **169**(0): p. 197-202.
33. Wen, G., et al., *Whole-cell biosensor for determination of methanol.* Sensors and Actuators B: Chemical, 2014. **201**(0): p. 586-591.
34. Buhl, A., et al., *Optical biosensor-based characterization of anti-double-stranded DNA monoclonal antibodies as possible new standards for laboratory tests.* Biosensors and Bioelectronics, 2009. **25**(1): p. 198-203.
35. Mu, Y., et al., *Selection of phage antibodies with GPX activity by combination of phage displayed antibody library with chemical modification and their characterization using a surface plasmon resonance biosensor.* Talanta, 2005. **66**(1): p. 181-187.
36. Rossi, G., et al., *Biosensor analysis of anti-citrullinated protein/peptide antibody affinity.* Analytical Biochemistry, 2014. **465**(0): p. 96-101.
37. Ann., J., *L. C. Clark.* NY Acad. Sci., 1962. **102**: p. 29-45.
38. Hick, S.J.U.a.J.P., J.P. Nature, 1967. **214**: p. 986-988.
39. Wang, J., *biosensors: 40 years of advances and challenges.* Electroanalysis, 2000(13): p. 983-988.
40. B. Liedberg, C.N.a.I.L., Actuat a-Phys, 1983. **4**: p. 299-304.
41. Zhao, Z. and H. Jiang, *Enzyme-based Electrochemical Biosensors*. Biosensors. 2010.
42. England, P.h.; Available from: http://www.phe-culturecollections.org.uk/.
43. U. Harborn, B.X., R. Venkatesh and B. Danielsson, *Evaluation of a miniaturized thermal biosensor for the determination of glucose in whole blood.* Clinica chimica acta, 1997. **267**: p. 225-237.
44. Y.-H. Zhenga, T.-C.H., D.-W. Sunb, J.-J. Xiaoa, F. Xua and F.-F. Wanga, *Detection of dichlorvos residue by flow injection calorimetricbiosensor based on immobilized chicken liver esterase.* Journal of food engineering, 2006. **74**: p. 24-29.
45. R. Rajkumara, M.K., A. Warsinkea, H. Möhwaldc and F. W. Scheller, *Thermometric MIP sensor for fructosyl valine.* Biosens Bioelectron, 2008. **23**: p. 1195-1199.
46. Homola, H.S.a.J., *Surface plamon resonance sensing of nucleic acids: a review.* Analytica Chimica Acta, 2013.
47. Sauerbrey, G., *Verwendung von Schwingquarzen zur Wägung dünner Schichten und zur Mikrowägung.* Z.Phys., 1959. **155**: p. 206-222.
48. Incontrol. *Continuous Glucose Sensors*. Available from: http://winthrop.files.wordpress.com/2008/10/glucosesensors.jpg.
49. Withings. *Bodyscales*. Available from: http://www.withings.com/.
50. depot, T.E. *Impedance Analyzers and LCR Meters*. Available from: http://www.testequipmentdepot.com/usedequipment/hewlettpackard/impedanceanalyzers/.
51. Packard, H. *HP4194A Impedance Gain/Phase Analyzer Operation Manual*. 1996; Available from: http://cp.literature.agilent.com/litweb/pdf/04194-90011.pdf.
52. Technologies, K. *Impedance analyzers*. Available from: http://www.keysight.com/en/pc-

1000000382%3Aepsg%3Apgr/impedance-analyzers?nid=-33831.0.00&cc=BE&lc=dut.
53. Niedermayer, A.O., E.K. Reichel, and B. Jackoby, *Yet another precision impedance analyzer (YAPIA)-Readout electronics for resonating sensors.* Sensors and Actuators a-Physical, 2009. **156**: p. 245-250.
54. Ferreira, J., et al., *AD5933-based spectrometer for electrical bioimpedance applications.* Journal of Physics: conference series, 2010. **224**(1).
55. Vandenryt, T., et al., *Combining Electrochemical Impedance Spectroscopy and Surface Plasmon Resonance into one Simultaneous Read-Out System for the Detection of Surface Interactions.* Sensors, 2013. **13**(11): p. 14650-14661.
56. Geerets, B., et al., *Optimizing the Thermal Read-Out Technique for MIP-Based Biomimetic Sensors: Towards Nanomolar Detection Limits.* Sensors, 2013. **13**(7): p. 9148-9159.
57. Murib, M.S., et al., *Electronic monitoring of chemical DNA denaturation on nanocrystalline diamond electrodes with different molarities and flow rates.* physica status solidi (a), 2013. **210**(5): p. 911-917.
58. van Grinsven, B., et al., *Heat-Transfer Resistance at Solid–Liquid Interfaces: A Tool for the Detection of Single-Nucleotide Polymorphisms in DNA.* ACS Nano, 2012. **6**(3): p. 2712-2721.
59. David Loveday, P.P., and Bob Rodgers, *Evaluation of Organic Coatings with Electrochemical Impedance Spectroscopy. Part 1: Fundamentals of Electrochemical Impedance Spectroscopy.* JCT CoatingsTech: p. 46-52.
60. David Loveday, P.P., and Bob Rodgers, *Evaluation of Organic Coatings with Electrochemical Impedance Spectroscopy. Part 2: Application of EIS to Coatings.* JCT CoatingsTech, 2001: p. 88-93.
61. David Loveday, P.P., and Bob Rodgers, *Evaluation of Organic Coatings with Electrochemical Impedance Spectroscopy. Part 3: Protocols for Testing Coatings with EIS. .* JCT CoatingsTech, 2005: p. 22-27.
62. Geenen, F., *Characterization of Organic Coatings with Impedance Measurements; A study of Coating Structure, Adhesion and Underfilm Corrosion*. 1990, TU-Delft.
63. Luo Bing, A.X., Yanshu Liang, Zhen Huang, Zhixia Qiao, Dahai Xia, Shengsheng Zhang, Zhancai Li, Fan Zhang, Peng Chen, *Evaluation on Protective Performance of Organic Coatings by Analyzing the Change Rate of Phase Angle at High Frequency.* International Journal of Medical Informatics ELECTROCHEMICAL SCIENCE, 2012. **7**: p. 8859 - 8868.
64. Dobbelaar, J.A.L., *The Use of Impedance Measurements in Corrosion Research; The Corrosion Behaviour of Chromium and Iron Chromium Alloys*. 1990, TU-Delft
65. Kennely, A.E., *Impedance.* Transactions of the american institute of electrical engineers, 1893: p. 172-232.
66. Britanica, E. *Lenz law*. Available from: http://www.britannica.com/EBchecked/topic/336163/Lenzs-law.
67. Agilent. *Impedance measurment handbook*. Available from: http://cp.literature.agilent.com/litweb/pdf/5950-3000.pdf.
68. Webster, J.G., *Medical Instrumentation Application and design*, ed. Wiley. 2010.

69. EIC, *891-04-62*.
70. Ungefroren H, S.S., Groth S, Gieseler F, Faendrich F., *Differential roles of Src in transforming growth factor-ß regulation of growth arrest, epithelial-to-mesenchymal transition and cell migration in pancreatic ductal adenocarcinoma cells.* Oncology, 2011. **38**(3): p. 797-805.
71. Quereda JJ, M.-A.L., Mendoça L, Majado MJ, Herrero-Medrano JM, Pallarés FJ, Ríos A, Ramírez P, Muñoz A, Ramis G., *Validation of xCELLigence real-time cell analyzer to assess compatibility in xenotransplantation with pig-to-baboon model.* Transplant Proc., 2010. **42**(8): p. 3239-3243.
72. Kute TE, S.L., Stehle JR Jr, Kim-Shapiro JW, Blanks MJ, Wood J, Vaughn JP., *Breast tumor cells isolated from in vitro resistance to trastuzumab remain sensitive to trastuzumab anti-tumor effects in vivo and to ADCC killing.* Cancer Immunol Immunother., 2009.
73. Hristov G, K.M., Li J, El-Andaloussi N, Mora R, Daeffler L, Zentgraf H, Rommelaere J, Marchini A., *Through its nonstructural protein NS1, parvovirus H-1 induces apoptosis via accumulation of reactive oxygen species.* Virol. , 2010. **84**(12): p. 5099-5022.
74. Greiner M, K.B., Jung V, Grobholz R, Hasenfus A, Stöhr RF, Tornillo L, Dudek J, Stöckle M, Unteregger G, Kamradt J, Wullich B, Zimmermann R., *Silencing of the SEC62 gene inhibits migratory and invasive potential of various tumor cells.* Int J Cancer., 2010. **28**.
75. Fecker LF, R.S., Kurbanov BM, Schmude M, Stockfleth E, Fechner H, Eberle J. , *Efficient melanoma cell killing and reduced melanoma growth in mice by a selective replicating adenovirus armed with tumor necrosis factor-related apoptosis-inducing ligand.* Hum Gene Ther., 2011.
76. E. Bongaers, J.A., F. Horemans, A. Weustenraed, L. Lutsen, D. Vanderzande, T. J. Cleij, F. J. Troost, R. J. Brummer and P. Wagner, *A MIP-based biomimetic sensor for the impedimetric detection of histamine in different pH environments.* Physica Status Solidi a-Applications and Materials Science, 2010. **207**: p. 837-843.
77. Boitano S, F.A., Schulz SM, Hoffman J, Price TJ, Vagner J., *Potent Agonists of the Protease Activated Receptor 2 (PAR(2)).* Med Chem, 2011.
78. Tran, D.T., et al., *Nanocrystalline diamond impedimetric aptasensor for the label-free detection of human IgE.* Biosensors and Bioelectronics, 2011. **26**(6): p. 2987-2993.
79. N. Bijnens, V.V., M. Daenen, L. Grieten, K. Haenen, S. Wenmackers, O. A. Williams, M. Ameloot, M. vandeVen, L. Michiels and P. Wagner, *Synthetic diamond films as a platform material for label-free protein sensors.* Physica Status Solidi a-Applications and Materials Science, 2009. **206**: p. 520-526.
80. Vermeeren, V., et al., *Impedimetric, diamond-based immmunosensor for the detection of C-reactive protein.* Sensors and Actuators B: Chemical, 2011. **157**(1): p. 130-138.
81. Petrák, V., et al., *Monitoring of peptide induced disruption of artificial lipid membrane constructed on boron-doped nanocrystalline diamond by electrochemical impedance spectroscopy.* physica status solidi (a), 2011. **208**(9): p. 2099-2103.

82. L. Grieten, S.D.J., A. Ethirajan, N. V. Bon, M. Ameloot, L. Michiels, K. Haenen and P. Wagner, *Real-time study of protein adsorption on thin nanocrystalline diamond.* Physica Status Solidi (A), 2011. **208**: p. 2093-2098.
83. Nakajima, K., T. Tamura, and H. Miike, *Monitoring of heart and respiratory rates by photoplethysmography using a digital filtering technique.* Medical Engineering & Physics, 1996. **18**(5): p. 365-372.
84. Miller, R.R., et al., *Sustained Reduction of Cardiac Impedance and Preload in Congestive Heart Failure with the Antihypertensive Vasodilator Prazosin.* New England Journal of Medicine, 1977. **297**(6): p. 303-307.
85. Westerband, A., et al., *Cardiovascular changes during laparoscopic cholecystectomy.* Surgery, gynecology & obstetrics, 1992. **175**(6): p. 535-538.
86. Oyen, T., *Master thesis*. 2009, Xios Hogeschool Limburg.
87. B. van Grinsven, T.V., S. Duchateau, A. Gaulke, L. Grieten, R. Thoelen, S. Ingebrandt, W. De Ceuninck and P. Wagner, *Customized impedance spectroscopy device as possible sensor platform for biosensor applications.* Physica Status Solidi a-Applications and Materials Science, 2010. **207**: p. 919-923.
88. Thoelen, R. 2008, Hasselt University.
89. M. Peeters, F.J.T., B. v. Grinsven, F. Horemans, J. Alenus, M. S. Murib, D. Keszthelyi, A. Ethirajan, R. Thoelen, T. J. Cleij and P. Wagner, *MIP-based biomimetic sensor for the electronic detection of serotonin in human blood plasma.* Sensors and Actuators B-Chemical, 2012.
90. J. Kafka, O.P., B. Abendroth and F. Lisdat, *A label-free DNA sensor based on impedance spectroscopy.* Electrochimica Acta, 2008. **53**: p. 7467-7474.
91. S. Y. Zheng, M.S.N., C. Y. Shih, W. Li and Y. C. Tai, *Resonance impedance sensing of human blood cells.* Sensor Actuat a-Phys, 2008. **145**: p. 29-36.
92. Fry, C.H. and R.I. Jabr, *The action potential and nervous conduction.* Surgery, 2010. **28**(2): p. 49-54.
93. Sunagawa, M., Pathophysiology 2010. **17**: p. 101-108.
94. Eder, C., American Journal of Physiology and cell physiology, 1998. **275**: p. 327-342.
95. Bongaers, E., et al., *A MIP-based biomimetic sensor for the impedimetric detection of histamine in different pH environments.* Physica Status Solidi a-Applications and Materials Science, 2010. **207**(4): p. 837-843.
96. Inc., T.I. *OPA627 datasheet*. 1998; Available from: http://www.ti.com/lit/ds/symlink/opa627.pdf.
97. Self, D., *Small signal audio design*. 2010: Focal Press.
98. Broeders, J., *Development and implementation of mniature impedimetric systems for biosensor readout*, in *Faculteit Industriële Ingenieurswetenschappen*. 2013, UHasselt.
99. Cooreman, P., et al., *Impedimetric immunosensors based on the conjugated polymer PPV.* Biosensors & Bioelectronics, 2005. **20**(10): p. 2151-2156.

100. Berdat, D., et al., *Biosensor for the detection of specific DNA sequences by impedance spectroscopy.* Transducers '07 & Eurosensors XXI, Digest of Technical Papers, Vols 1 and 2, 2007.
101. van Grinsven, B., et al., *Rapid assessment of the stability of DNA duplexes by impedimetric real-time monitoring of chemically induced denaturation* Lab on a Chip, 2011. **11**: p. 1656 - 1663.
102. Upadhyay, P. and S. Bhaskar, *Real time monitoting of lymphocyte proliferation by an impedance method* Journal of Immunological Methods, 2000. **244**(1-2): p. 133-137.
103. J. Broeders, S.D., B. Van Grinsven, W. Vanaken, M. Peeters, T. Cleij, R. Thoelen, P. Wagner and W. De Ceuninck, *Miniaturised eight-channel impedance spectroscopy unit as sensor platform for biosensor applications.* Physica Status Solidi a-Applications and Materials Science. **208**: p. 1357-1363.
104. International, F.T.D. *FT232R datasheet*. Available from: http://www.ftdichip.com/Support/Documents/DataSheets/ICs/DS_FT232R.pdf.
105. Inc., M.T. *PIC16F62X datasheet*. 2003; Available from: http://ww1.microchip.com/downloads/en/DeviceDoc/40300C.pdf.
106. Broeders, J., et al., *Miniaturised eight-channel impedance spectroscopy unit as sensor platform for biosensor applications.* Physica Status Solidi a-Applications and Materials Science, 2011. **208**(6): p. 1357-1363.
107. Doong, H.T.a.R., *Simultaneous determination of pH, urea, acetylcholine and heavy metals using array-based enzymatic optical biosensor.* Biosens Bioelectron, 2005. **20**: p. 1796-1804.
108. K. E. Sapsford, Y.S.S., J. B. Delehanty, J. P. Golden, C. R. Taitt, L. C. Shriver-Lake and F. S. Ligler, *Fluorescence-based array biosensor for detection of biohazards.* J. Appl. Microbiol., 2004. **96**: p. 47-58.
109. M. Suzuki and H. Akaguma, C.c.-t.i.f.-t.i.e.s., sensors and Actuators b-Chemical, 2000. **64**.
110. Inc., T.I. *PCA9535*. 2008; Available from: http://www.ti.com/lit/ds/symlink/pca9535.pdf.
111. Instruments, N. *NI USB-6251*. Available from: http://sine.ni.com/images/products/us/usb-6251_screw_mass_m.jpg.
112. Nuttall, A.H., *Some windows with very good sidelobe behavior.* Acoustics, Speech and Signal Processing, IEEE Transactions on, 1981. **29**(1): p. 84-91.
113. Beagleboard. *Beagleboard*. Available from: http://beagleboard.org/.
114. PI, R. *Raspberry PI*. Available from: http://www.raspberrypi.org/.
115. research, P.a. *ZSimWin*. Available from: http://www.princetonappliedresearch.com/Our-Products/Electrochemical-Software/ZSimpWin.aspx.
116. Mathworks. *Matlab 'The language of technical computing'*. Available from: http://www.mathworks.nl/products/matlab/.
117. Moré, J., *The Levenberg-Marquardt algorithm: Implementation and theory*, in *Numerical Analysis*, G.A. Watson, Editor. 1978, Springer Berlin Heidelberg. p. 105-116.

118. Ehret, R., et al., *On-line control of cellular adhesion with impedance measurements using interdigitated electrode structures.* Medical and Biological Engineering and Computing, 1998. **36**(3): p. 365-370.
119. Iskander, M.F. and S.S. Stuchly, *A Time-Domain Technique for Measurement of the Dielectric Properties of Biological Substances.* Instrumentation and Measurement, IEEE Transactions on, 1972. **21**(4): p. 425-429.
120. Peeters M, Jiménez-Monroy K.L , Libert C, Eurlings Y , Cuypers W, Wackers G, Duchateau S, Robaeys P, Nesládek M, van Grinsven B, Pérez-Ruiz E, Lammertyn J, Losada-Pérez P and Wagner P., *Real-Time Monitoring of Aptamer Functionalization and Detection of Ara*

H1 by Electrochemical Impedance Spectroscopy and Dissipation-Mode

Quartz Crystal Microbalance. Biosensors & Bioelectronics, 2014. **5**(3).
121. Hun, W., et al., *Multi-Frequency Electrical Impedance Tomography System With Automatic Self-Calibration for Long-Term Monitoring.* Biomedical Circuits and Systems, IEEE Transactions on, 2014. **8**(1): p. 119-128.
122. S. Duchateau, J.B., D. Croux, D. Janssens, J.-M. Rigo, P. Wagner, R. Thoelen and W. De Ceuninck, *Cell proliferation monitoring by multiplexed electrochemical impedance spectroscopy on microwell assays.* Physica Status Solidi (C) 2013. **10**: p. 882-888.
123. Chen, H., et al., *Evaluation of the cytotoxicity of cigarette smoke condensate by a cellular impedance biosensor.* Food and Chemical Toxicology, 2012. **50**(3–4): p. 612-618.
124. T. K. Karakach, R.M.F., S. E. Douglas and P. D. Wentzell, *An introduction to DNA microarrays for gene expression analysis.* Chemometrics and intelligent laboratory systems, 2010. **104**: p. 18-52.
125. Technology, p. *TC-08 Thermocouple Logger*. 2007; Available from: http://www.picotech.com/document/pdf/tc08-3.pdf.
126. Instruments, N. *NI USB-9263*. 2009; Available from: http://www.ni.com/pdf/manuals/372406b.pdf.
127. Lee, S.T., Z. Lin, and X. Jiang, *CVD diamond films: nucleation and growth.* Materials Science and Engineering: R: Reports, 1999. **25**(4): p. 123-154.
128. V. Vermeeren, N.B., S. Wenmackers, M. Daenen, K. Haenen, O. A. Williams, M. Ameloot, A. Vandeven, P. Wagner and L. Michiels, *Towards a real-time, label-free, diamond-based DNA sensor.* Langmuir, 2007. **23**: p. 13193-13202.
129. Gheeraert, E., et al., *Electronic states of phosphorus in diamond.* Diamond and Related Materials, 2000. **9**(3–6): p. 948-951.
130. Yang, W., et al., *DNA-modified nanocrystalline diamond thin-films as stable, biologically active substrates.* Nat Mater, 2002. **1**(4): p. 253-257.
131. Christiaens, P., et al., Biosens. Bioelectron., 2006. **22**: p. 170.
132. Tao, C., et al., *Surface modification of diamond-like carbon films with protein via polydopamine inspired coatings.* Applied Surface Science, 2009. **256**(1): p. 294-297.

133. Vansweevelt, R., et al., *Biological modification of carbon nanowalls with DNA strands and hybridization experiments with complementary and mismatched DNA.* Chemical Physics Letters, 2010. **485**(1–3): p. 196-201.
134. Thoelen, R., et al., *A MIP-based impedimetric sensor for the detection of low-MW molecules.* Biosensors & Bioelectronics, 2008. **23**(6): p. 913-918.
135. Horemans, F., et al., *MIP-based sensor platforms for the detection of histamine in the nano- and micromolar range in aqueous media.* Sensors and Actuators B-Chemical, 2010. **148**(2): p. 392-398.
136. Horemans, F., *Molecular imprinting as a tool for future proof sensor applications*. 2011, Hasselt University.
137. lin, R.Y., et al., *Histamine and tryptase levels in patients with acute allergic reactions: An emergency department–based study.* Journal of Allergy and Clinal Immunology, 2000. **106**: p. 65-71.
138. Barbara, G., et al., *Activated mast cells in proximity to colonic nerves correlate with abdominal pain in irritable bowel syndrome.* Gastroenterology, 2004. **126**(3): p. 693-702.
139. Macan, J., et al., *Long-term follow-up of histamine levels in a store fish meal sample.* Animal Feed Science and Technology, 2006. **127**(1-2): p. 169-174.
140. Database, H.M. *Histamine*. 2010; Available from: http://www.hmdb.ca/metabolites/HMDB00870.
141. Ihealth. *How long does Nicotine stay in your System, Blood, Urine, Hair and Tests*. Available from: http://www.ihealthblogger.com/2013/05/how-long-does-nicotine-stay-in-your-system.html.
142. Zhang, X. and S.-T. Yang, *An online, non-invasive fluorescence probe for immobilized cell culture process development.* Process Biochemistry, 2011. **46**(10): p. 2030-2035.
143. Quah, B.J.C., H.S. Warren, and C.R. Parish, *Monitoring lymphocyte proliferation in vitro and in vivo with the intracellular fluorescent dye carboxyfluorescein diacetate succinimidyl ester.* Nat. Protocols, 2007. **2**(9): p. 2049-2056.
144. Upadhyay, P. and S. Bhaskar, *Real time monitoring of lymphocyte proliferation by an impedance method.* Journal of Immunological Methods, 2000. **244**(1–2): p. 133-137.
145. Ding, L., et al., *A disposable impedance sensor for electrochemical study and monitoring of adhesion and proliferation of K562 leukaemia cells.* Electrochemistry Communications, 2007. **9**(5): p. 953-958.
146. Zou, Y. and Z. Guo, *A review of electrical impedance techniques for breast cancer detection.* Medical Engineering & Physics, 2003. **25**(2): p. 79-90.
147. Bollin, F., V. Dechavanne, and L. Chevalet, *Design of Experiment in CHO and HEK transient transfection condition optimization.* Protein Expression and Purification, 2011. **78**(1): p. 61-68.
148. Buck, W.D. *Modeled like bacterial growth*. Available from: http://www.improvementguru.com/2009/05/social-news-modeled-like-bacterial.html.

149. M.H. Zweitering, e.a., *Applied Environmental Microbiology.* Modeling of the Bacterial Growth Curve, 1990.
150. Lisdat, F. and D. Schafer, *The use of electrochemical impedance spectroscopy for biosensing.* Analytical and Bioanalytical Chemistry, 2008. **391**(5): p. 1555-1567.
151. van Grinsven, B., et al., *Customized impedance spectroscopy device as possible sensor platform for biosensor applications.* Physica Status Solidi a-Applications and Materials Science, 2010. **207**(4): p. 919-923.
152. standards, L. *http://www.lgcstandards-atcc.org*. 2013.
153. Mignen, O., et al., *Carboxyamidotriazole-induced inhibition of mitochondrial calcium import blocks capacitative calcium entry and cell proliferation in HEK-293 cells.* Journal of Cell Science, 2005. **118**(Pt 23): p. 5615-23.
154. Bi, J.X., J. Shuttleworth, and M. Al-Rubeai, *Uncoupling of cell growth and proliferation results in enhancement of productivity in p21CIP1-arrested CHO cells.* Biotechnology and Bioengineering, 2004. **85**(7): p. 741-9.
155. Kreutzberg, G.W., *Microglia: a sensor for pathological events in the CNS.* Trends Neurosci, 1996. **18**(8): p. 312-318.
156. Sicherer, S.H. and H.A. Sampson, *Peanut allergy: emerging concepts and approaches for an apparent epidemic.* J Allergy Clin Immunol, 2007. **120**(3): p. 491-503; quiz 504-5.
157. Cheney, M., D. Isaacson, and J. Newell, *Electrical Impedance Tomography.* SIAM Review, 1999. **41**(1): p. 85-101.
158. Brown, B.H., *Electrical impedance tomography (EIT): a review.* J Med Eng Technol, 2003. **27**(3): p. 97-108.
159. Yan, T., C.W.Y. Hui-Chan, and L.S.W. Li, *Functional Electrical Stimulation Improves Motor Recovery of the Lower Extremity and Walking Ability of Subjects With First Acute Stroke: A Randomized Placebo-Controlled Trial.* Stroke, 2005. **36**(1): p. 80-85.
160. Machado, C., et al., *Assessing acute middle cerebral artery ischemic stroke by quantitative electric tomography.* Clinical EEG and neuroscience, 2004. **35**(3): p. 116-124.
161. Seeck, M., et al., *Non-invasive epileptic focus localization using EEG-triggered functional MRI and electromagnetic tomography.* Electroencephalography and Clinical Neurophysiology, 1998. **106**(6): p. 508-512.
162. Bio-medical. *GS27 Pre-gelled Disposable sEMG* Available from: http://bio-medical.com/products/gs27-pre-gelled-disposable-semg-electrodes-150-pack.html.
163. Woo, E.J., et al., *Skin impedance measurements using simple and compound electrodes.* Medical and Biological Engineering and Computing, 1992. **30**(1): p. 97-102.
164. F. Horemans, J.A., E. Bongaers, A. Weustenraed, R. Thoelen, J. Duchateau, L. Lutsen, D. Vanderzande, P. Wagner and T. J. Cleij, *MIP-based sensor platforms for the detection of histamine in the nano- and micromolar range in aqueous media.* Sensors and Actuators B-Chemical, 2010. **148**: p. 392-398

165. van Grinsven, B., et al., *Heat-Transfer Resistance at Solid-Liquid Interfaces: A Tool for the Detection of Single-Nucleotide Polymorphisms in DNA.* Acs Nano, 2012. **6**(3): p. 2712-2721.
166. Peeters, M., et al., *Heat-transfer-based detection of l-nicotine, histamine, and serotonin using molecularly imprinted polymers as biomimetic receptors.* Analytical and bioanalytical chemistry, 2013.
167. Beyens, T., *De ontwikkeling van smartphone applicaties voor biosensor uitlezing*. 2013, Xios University College.
168. Xu, J., et al., *A new method to estimate the state of charge of lithium-ion batteries based on the battery impedance model.* Journal of Power Sources, 2013. **233**: p. 277-284.
169. Hoshikawa, T., R. Kikuchi, and K. Koichi, *Impedance analysis for dye-sensitized solar cells with a reference electrode.* Journal of Electroanalytical Chemistry, 2006. **588**(59-67).
170. Ulrich, C., et al., *Simultaneous estimation of soot and diesel contamination in engine oil using electrochemical impedance spectroscopy.* sensors and Actuators b-Chemical, 2007. **127**: p. 613-618.

Publications and Conference contributions

Publications:

- M. Peeters, K. I. Jiménez-Monroy, C. Libert, Y. Eurlings, W. Cuypers, G. Wackers, **S.Duchateau**, P. Robaeys, M. Nesládek, B. van Grinsven, E. Pérez-Ruiz, J. Lammertyn, P. Losada-Pérez, P. Wagner, 'Real-Time Monitoring of Aptamer Functionalization and Detection of AraH1 by Electrochemical Impedance Spectroscopy and Dissipation-Mode Quartz Crystal Microbalance', Biosensors & bioelectronics (2014)

- J. Broeders, D. Croux, M. Peeters, T. Beyens, **S. Duchateau**, T.J. Cleij, P. Wagner, R. Thoelen, W. De Ceuninck, Mobile application for impedance based biomimetic sensor readout, IEEE Sensors 13, 2659-2665 (2013)

- D. Croux, T. Vangerven, J. Broeders, M. Peeters, **S. Duchateau**, J. Boutsen, W. Deferme, P. Wagner, R.Thoelen, W. De Ceuninck, Disposable wireless MIP-based biosensor tags, Physica Status Solidi (a) 210, 934-944 (2013)

- **S. Duchateau**, J. Broeders, D. Croux, D. Janssen, J.-M. Rigo, P. Wagner, R. Thoelen and W. De Ceuninck, Cell proliferation monitoring by multiplexed electrochemical impedance spectroscopy on microwell assays, Physica Status Solidi (c) 10, 882-888 (2013)

- J. Broeders, D. Croux, A. Weustenraed, W. Vanaken, **S. Duchateau**, T.J. Cleij, P. Wagner, R. Thoelen and W. De Ceuninck, 'Embedded unit for point-of-care impedimetic biosensor readout', Proceedings of the IEEE 14th International Conference on High Performance Computing and Communications, 1571-1577 (2012)

- J. Broeders, **S. Duchateau**, B. Van Grinsven, W. Vanaken, M. Peeters, T. Cleij, R. Thoelen, P. Wagner, W. De Ceuninck 'Miniaturised eight-channel impedance spectroscopy unit as sensor platform for biosensor applications', Phys. Status Solidi A, 2011, 5, 1357 – 1363

- B. Van Grinsven, T. Vandenryt, **S. Duchateau**, A. Gaulke, L. Grieten, R. Thoelen, S. Ingebrandt, W. De Ceuninck, P. Wagner, 'Customized impedance spectroscopy device as possible sensor platform for biosensor applications', Phys. Status Solidi A, 2010, 9, 2110 – 2113

Oral presentations

- Engineering of Functional Interfaces 2014, Jülich (Germany) 14-15/07/2014, Arduino based impedance measurement platform, **S. Duchateau**, P. Wagner, W. De Ceuninck and R. Thoelen

- Engineering of Functional Interfaces 2013, Hasselt (Belgium) 8-9/07/2013, Arbitrary wave electrochemical impedance spectroscopy, a fast and reliable measurement technique, **S. Duchateau**, J. Broeders, D. Croux, P. Wagner, R. Thoelen and W. De Ceuninck.

- Engineering of Functional Interfaces 2012, Zweibruchen (Germany) 16-17/07/2012, Using impedance spectroscopy for in-situ cell growth monitoring, **S. Duchateau**, J. Broeders, D. Croux, M. Daenen, P. Wagner, J.M. Rigo, W. De Ceuninck and R. Thoelen.

- IEEE 9th International Conference on Embedded Software and Systems, Liverpool (UK) 25-27/06/2012, Embedded unit for point-of-care impedance based biosensor readout, J. Broeders, D. Croux, A. Weustenraed, W. Vanaken, **S. Duchateau**, T.J. Cleij, P. Wagner, R. Thoelen and W. De Ceuninck.

- Engineering of Functional Interfaces 2011, Linz (Austria) 19-20/07/2011, Using impedance spectroscopy for in-situ cell growth monitoring, **S. Duchateau**, D. Janssen, J. Broeders, M. Daenen, P. Wagner, J.M. Rigo, W. De Ceuninck and R. Thoelen.

- Engineering of Functional Interfaces 2010, Marburg (Germany) 15-16/7/2010, Impedance based DNA Spectroscopy, **S. Duchateau**, J. Broeders, P. Wagner, R. Thoelen and W. De Ceuninck.

- Engineering of Functional Interfaces 2009, Hasselt (Belgium) 18-19/6/2009, A fully automated impedance spectroscopy unit, **S. Duchateau**, T. Vandenryt, P. Wagner, R. Thoelen and W. De Ceuninck.

- Open innovation forum, Hasselt (Belgium) 04/03/2009, Automated impedance spectroscopy unit for biosensors, **S. Duchateau**, T. Vandenryt, P. Wagner, R. Thoelen and W. De Ceuninck

Poster contributions

- Biosensors 2012, Cancun (Mexico) 15-18/05/2012, Impedance spectroscopy for in situ cell growth monitoring, **S. Duchateau**, J. Broeders, D. Janssen, M. Peeters, D. Croux, M. Daenen, P. Wagner, JM. Rigo, R. Thoelen and W. De Ceuninck.

- Biosensors 2012, Cancun (Mexico) 15-18/05/2012, Increasing MIP-sensor usability in field application, J. Broeders, D. Croux, A. Weustenraed, M. Peeters, W. Vanaken, **S. Duchateau**, T.J. Cleij, P. Wagner, R. Thoelen and W. De Ceuninck.

- UHasselt NanoSensEU Symposium, Diepenbeek (Belgium) 25/04/2012, Advances in label-free biosensor readout techniques, D. Croux, J. Broeders, **S. Duchateau**, A. Wuestenraed, W. Vanaken, T.J. Cleij, P. Wagner, R. Thoelen and W. De Ceuninck.

- 8th IBRO Congress of neuroscience, Firenze (Italië) 14-18/07/2011, Using impedance spectroscopy for monitoring the proliferative activity of microglial cells, D. Janssen, **S. Duchateau**, K. Verboven, J. Broeders, W. De Ceuninck, R. Thoelen and J.M. Rigo.

- BPS Meeting 2011, Namur (Belgium) 25/05/2011, Using impedance spectroscopy for in situ cell growth monitoring, **S. Duchateau**, J. Broeders, K. Verboven, D. Janssen, P. Wagner, W. De Ceuninck and R. Thoelen.

- BNV-NNV Fysica 2010 Symposium, Utrecht (Netherlands) 23/04/2010, Electrochemical Impedance Spectroscopy, J. Broeders, **S. Duchateau**, P. Wagner, W. De Ceuninck and R. Thoelen.

- Diamond days, Hasselt (Belgium) 22-24/02/2010 Electrochemical Impedance Spectroscopy, **S. Duchateau**, J. Broeders, P. Wagner, W. De Ceuninck and R. Thoelen.

- BPS Meeting 2009, Hasselt (Belgium) 01/04/2009, The Quest for a fully automated impedance spectroscopy unit, **S. Duchateau**, T. Vandenryt, P. Wagner, R. Thoelen and W. De Ceuninck

- BPS Meeting 2009, Hasselt (Belgium) 01/04/2009, Nanospotting: an impedance based biosensor for the detection of DNA, T. Vandenryt, **S. Duchateau**, P. Wagner, R. Thoelen and W. De Ceuninck

Nomenclature

Ab	Antibody
AC	Alternating current
ADC	Analog-to-digital converter
Ag	Antigen
AM	Amplitude modulation
API	Application programming interface
APO	Apocynin
C	Capacitor
C_{dl}	Double layer capacitance
CHO	Chinese hamster ovary cell
CPE	Constant phase element
CRP	C-reactive protein
DAC	Digital-to-analog converter
DC	Direct current
DDS	Direct digital synthesis
DEPC	Diethylpyrocarbonate
DFT	Discrete Fourier transform
DMA	Direct memory access
DMEM	Dulbecco's Modified Eagle's Medium
DNA	Deoxyribonucleic acid
DSP	Digital signal processor
ECG	Electrocardiogram
EDC	1-Ethyl-3-[3-dimethylaminopropyl]carbodiimide hydrochloride
EEPROM	Electrically erasable read-only memory
EIS	Electrochemical impedance spectroscopy
EIT	Electrical impedance tomography
ELISA	Enzyme-Linked Immuno Sorbent Assay
ELPHYC	Electrical and physical characterization
FCS	Fetal calf serum
FFT	Fast Fourier transformation
FTDI	Futrure technology devices international
GF	Gain factor
HCl	Hydrochloric acid
HEK	Human embryonic kidney cell
HRP	Horseradish peroxidase
I^2C	Inter-integrated circuit bus

IC	Integrated circuit
ICG	Impedance cardiography
Im	Imaginary
KCl	Potassium chloride
KH_2PO_4	Monopotassium phosphate
L	Inductor
LAN	Local area network
LMA	Levenberg Marquardt algorithm
LPS	Lipopolysaccharide
MINO	Minocycline
MIP	Molecularly imprinted polymer
Na_2HPO_4	Disodium phosphate
NaOH	Sodium hydroxide
NCD	Nano crystalline diamond
NIP	Non-imprinted polymer
PMA	Para-Methoxyamphetamine
O	Finite Warburg
OPAMP	Operational amplifier
PBS	Phosphate buffered saline
PCB	Printed circuit board
Q	CPE
θ	Phase angle
QCM	Quartz crystal microbalance
R	Resistor
R_e	Real
RF	Radio frequent
R_l	liquid resistance
R_p	Polarization resistance
R_{ct}	Charge transfer resistance
RTD	Resistive thermal device
SAM	Self-assembled monolayer
SD	Secure digital
SEM	Scanning electron microscope
SMD	Surface mount device
SNP	Single nucleotide mismatch
TRIS	Tris(2,3-dibromopropyl) phosphate
UART	Universal asynchronous receiver/transmitter
USB	Universal serial bus
W	Infinite Warburg
WIFI	Wireless local area network
|Z|	Impedance magnitude

List of figures and tables

Figures

Tables